UNIVERSITÀ DEGLI STUDI DI TRIESTE

XXVIII CICLO DEL DOTTORATO DI RICERCA IN SCIENZE E TECNOLOGIE CHIMICHE E FARMACEUTICHE

CONVENIENT COVALENT FUNCTIONALIZATION OF CARBON NANOTUBES FOR RADIOACTIVITY DELIVERY

Settore scientifico-disciplinare: CHIM/08

DOTTORANDA
AGNIESZKA GAJEWSKA

COORDINATORE
PROF. MAURO STENER

SUPERVISORE DI TESI
PROF. TATIANA DA ROS

ANNO ACCADEMICO 2014 / 2015

UNIVERSITÀ DEGLI STUDI DI TRIESTE

XXVIII CICLO DEL DOTTORATO DI RICERCA IN SCIENZE E TECNOLOGIE CHIMICHE E FARMACEUTICHE

CONVENIENT COVALENT FUNCTIONALIZATION OF CARBON NANOTUBES FOR RADIOACTIVITY DELIVERY

Settore scientifico-disciplinare: CHIM/08

DOTTORANDA
AGNIESZKA GAJEWSKA

COORDINATORE
PROF. MAURO STENER

SUPERVISORE DI TESI
PROF. TATIANA DA ROS

ANNO ACCADEMICO 2014 / 2015

Acknowledgements

Luckily, after three years of the unconditional support I would like to thank to:

My supervisor Prof. Tatiana Da Ros for giving me this great chance to develop my Ph.D. thesis at University of Trieste. Also for the patience, for many essential advices and having door open in a case of any doubts.

Prof. Maurizio Prato for the opportunity to work in his group in Trieste. For collaboration in the frame of the project.

I would like to thank the jury members Prof. Ester Vazquez Fernandez-Pacheco, Prof. Sonia Merino, Prof. Enzo Menna and Prof. Silvia Marchesan for accepting to read and judge my work.

Special word of thanks goes to Claudio Gamboz for his useful help with TEM.

Prof. Benjamin G. Davis, for having accepted me in his wonderful group in Oxford. To Sonia, Reida and Christopher for such a good care and hospitality, and to all, canal punting team for great time and kind treatment.

Dr. Khuloud Al-Jamal for the opportunity of all biological test. For the great help and assistants, as well for high climbing goals to Rebecca, Julie, Cinzia, Maxime and Houmam and all group who was so helpful to the chemist in biolab.

All Raddel group: Anne, Ana, Sandra, Adem, Aritz, Martin, Robert for such a lovely integration and multicultural experience which we could expand in our network.

Cinzia, for being the best hotelmate and tripadvisor in one.

Magdalena, Elzbieta and Markus - almost Polish team - thank you for your Radler support and collaboration almost on every level.

I've been fortunate to work with great colleagues from Prato Group. In particular I would like to thank you to:

Adrian, for help at the beginning of my PhD adventure.

Caroline, "mother of all doctoral students" for helping, listening and making things possible.

Michela, Sussana, Nuria, Davide, Angela, Dani, Eleonora, Francesco, Cristina, Maribel, Andrea, Mimmo, Michele, Akcan, Anirban. "So far and yet so near" - for Pharmacy - C11 integration.

Maria, Ana and Arturito for many nice moments, chats, Spanish lessons, and other entertaining contributions in our daily coffee/chocolate brioche/tee time.

Jenni and Manu, you are the best Galician ever, hay parfavar don't grow up!

The new and old batches of master students: Lor enzo, Alexa, Jacopo, Silvia, Federico for a pleasant fresh wind in the long PhD's live, for excellent atmosphere in the lab and the sunny lunches.

Zois, my big, Greek friend, thank you for all advices, chemistry discussions and smart suggestions, also in the life!

*Valentina, for infinite, Roman energy which turns the Earth and lights the Sun.*

Giuly, for understanding, simplifying all complicated world to few eloquent emoticons and being always in the right time and place when I needed you.

Tanja, fortunately, there were also the moments of relaxation, long conversation, kebeb, Lasko beer and future planning... Thank you!

All my friends from Poland Sylwia, Wiola, Tetyana, Justyna, Iza for being, knowing my complicated character and loving me as I am.

Dziękuję moim rodzicom, Jakubowi i Ewelinie, Karolowi i Martynie, Joannie i Tadeuszowi, którzy przez te trzy lata dzielnie znosili rozłąkę i zawsze pomagali w trudnych chwilach.

Finally, a thousand thanks for all this constant support and understanding during these last years I would like to dedicate to my husband Piotr. Thank you for always believing in me!
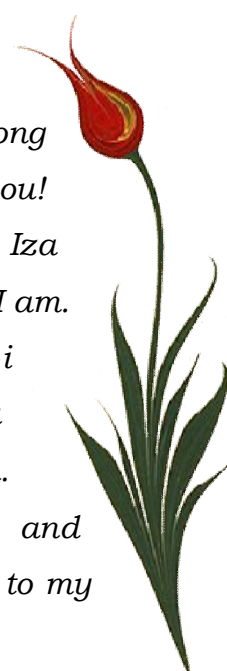
LIST OF ABBREVIATIONS

Boc	*t*-butyloxycarbonyl
Boc$_2$O	Di-*t*-butyl dicarbonate
CNTs	Carbon Nanotubes
DCM	Dichloromethane
DIEA	Diisopropylethiylamine
DMF	Dimethylformamide
EI	Electron impact mass spectrometer
ESI	Electrospray ionization mass spectrometer
Et$_2$O	Diethyl ether
HiPCO	High-pressure carbon monoxide
HR-TEM	High Resolution Transmission Electron Microscopy
HOMO	Highest occupied molecular orbital
LUMO	Lowest unoccupied molecular orbital
MW	Microwave
MWCNTs	Multi-Wall Carbon Nanotubes
NMP	N-Methyl-2-pyrrolidone
NMR	Nuclear Magnetic Resonance
o-DCB	1,2-Dichlorobenzene
oxSWCNTs	Oxidized SWCNTs
PEG	Polyethyleneglycol
Pht	Phthalimide group
RBM	Radial breathing mode
RGD	Arginine-glycine-aspartic acid peptide
ROS	Reactive Oxygen Species
SPECT	Single-photon emission computed tomography
SWCNTs	Single Wall Carbon Nanotube
TEA	Triethylamine
TEG	Triethylene glycol
TEM	Transmission Electronic Microscopy
TFA	Trifluoroacetic Acid
TGA	Thermogravimetric Analysis
THF	Tetrahydrofuran
TLC	Thin Layer Chromatography
tR	Retention time
UV-Vis	Ultra Violet - Visible
X@CNTs	Carbon nanotubes filled with X
XPS	X-Ray Photoemission Spectroscopy

ABSTRACT

The attachment of radioactive metal ions on the external surface of carbon nanotubes allows the labeling and tracking of CNTs with good sensitivity the same result can be achieved by encapsulating emitting elements into the CNT cavities. This feature could be perfect to explore in biomedical applications including imaging and therapy, depending on radionuclide.

Both methods have their advantages but in this thesis the direct labeling by creation of nanocapsules was chosen as easier to control and more suitable for the external attachment of biologically active molecules.

The first part of the presented work, described in *Chapter II,* has been dedicated to new functionalization pathway of CNTs. The main attention has been given, to design reaction which 1) will work on SWCNTs and MWCNTs with a high degree of functionalization; 2) will not cause damages of the tubes leading to leakage of filled materials; 3) can be applied in a large scale and 4) will be fast enough for functionalization of CNTs filled with short life-time isotopes. The cycloaddition of 1,3-dipoles on CNTs was performed using various approaches but none of them was enough efficient to provide an easy setup for further exploration on filled CNTs. To accomplish the goal we have used arylation reaction, already described in literature. To fit to the requirements for biological application we have synthesized a linker which would provide high solubility and amine functions for further binding with biological molecules. The direct functionalization by arylation method of several filled nanotubes was the subject of *Chapter III* and on some of those compounds biological tests have been performed as reported in *Chapter IV.* The cytotoxicity of filled and functionalized SWCNTs and MWCNTs was examined. The biodistribution study

was performed on mice using MWCNTs filled with the radioisotope of samarium-153 (^{153}Sm) and functionalized with previously synthesized linker.

Our results suggest that application of diazonium-based arylation of filled CNTs can be generally adopt as an efficient and convenient technique for functionalization, without breaking and opening the tubes.

The functionalized nanocapsules filled with ^{153}Sm can be used for *in vivo* delivery coupled with long-term tracing studies.

RIASSUNTO

L'introduzione di elementi radioattivi sulla superficie esterna di nanotubi di carbonio (CNTs) permette di tracciare i CNTs con una buona sensibilità e lo stesso risultato può essere ottenuto incapsulando i radioisotopi nella cavità interna dei nanotubi stessi. Questa metodologia potrebbe essere perfetta per diverse applicazioni biomediche, tra cui l'*imaging* e la terapia radiativa, a seconda del radionuclide presente.

Entrambe le metodologie presentano dei vantaggi, ma nell'ambito di questo lavoro di ricerca si è scelto di lavorare con sistemi che presentavano derivati all'interno della loro struttura, con la creazione di nanocapsule essendo queste più adatte a legare sulla superficie esterna molecole biologicamente attive.

La prima parte del presente lavoro, descritta nel *Capitolo II*, è stata dedicata allo studio di nuove metodologie di funzionalizzazione dei CNTs, con particolare attenzione ad approcci:1) in grado di funzionalizzare riccamente sia SWCNTs che MWCNTs; 2) che non danneggino la superficie dei nanotubicon possibilità di fuoriuscite dei materiali incapsulati; 3) che possano essere applicati su scala relativamente larga e 4) che siano abbastanza rapidi da consentire un'efficiente funzionalizzazione di CNTs con isotopi con breve tempo di emivita. La cicloaddizione di diversi 1,3-dipoli su nanotubi di carbonio è stata effettuata utilizzando vari approcci, ma nessuno di essi ha dato risultati così soddisfacenti da impiegare le nuove procedure studiate per la funzionalizzazione delle nanocapsule.

Per raggiungere l'obiettivo abbiamo utilizzato un'altra reazione già descritta in letteratura e a tale scopo è stato sintetizzato un *linker* che fornisse

una buona solubilità al sistema e presentasse gruppi amminici terminali da poter sfruttare per la successiva introduzione di molecole biologicamente attive. La funzionalizzazione mediante arilazione di diversi nanotubi riempiti con sali di Gadolinio, Samario, Iodio e Lutezio è stata oggetto di studio (*Capitolo III*). La citotossicità di SWCNTs e MWCNTs con incapsulato il samario cloruro è stata studiata,come riportato nel *Capitolo IV,* e grazie alla presenza di materiale radiativo (^{153}Sm) è stato possibile effettuare un'analisi di biodistribuzione nei topi.

I nostri risultati suggeriscono che l'applicazione della reazione di arilazione può essere generalmente adottata quale tecnica efficace e conveniente per funzionalizzazione di CNTs che presentano materiale incapsulato al loro interno, senza che la struttura esterna venga danneggiata e vi sia rilascio del materiale radiativo. Le nanocapsule a base di ^{153}Sm potrebbero quindi trovare utilizzo in teranostica.

TABLE OF CONTENTS

I. Introduction

The vision of tiny, active robots which manufacture various substances to eliminate damages in the body after injection to the bloodstream was proposed in 1959 by physicist, future Nobel Prize laureate, Richard Feynman in his work "There's Plenty of Room at the Bottom". Nowadays, nanotechnology, a relatively young scientific discipline, gives the possibility to manipulate the matter on atomic, molecular, and supramolecular scale and it is applied across all fields of science, such as chemistry, biology, physics, materials science and engineering.

Medical application of nanoscale materials, which by definition are in range of 1-100 nm, is a topic of interest for many researches around the world. Nowadays, different nanotherapeutics have been already used for early diagnosis of cancer, accurate cancer imaging, cancer therapy and targeted drug delivery. Furthermore, it is generally unquestionable that these materials will significantly contribute to the next generation of health care technologies in treating various diseases.

Carbon nanotubes (CNTs) are particularly interesting nanomaterial, as they exhibit an amazing model of a one-dimensional system with fascinating physical and chemical properties. Since their discovery by Iijima in 1991

nanotubes were an object of intense research all around the world.[1] At first, carbon nanotubes were applied to different purposes, i.e. for electronics, optics, plastics, and other materials of the nanotechnology fields. Since the beginning of XXI century, they started to be studied in pharmacy and medicine for theranostic uses. Due to their high surface area, excellent chemical stability and rich electronic structure, CNTs are able to conjugate and interact with numerous therapeutic molecules i.e. drugs, proteins, antibodies, DNA, enzymes. It was demonstrated that carbon nanotubes are an excellent transporter medium, which penetrate into cells, without damaging them.[2,3] Many studies have shown that, when bonded to CNTs, therapeutic molecules were delivered more effectively and safely into cells compared to traditional methods.[4] This excellent breakthrough had a positive input on traditional concepts of pharmacology.[5,6] Recently also other biomolecules (i.e. genes, radioisotopes, vaccines) were successfully transported by means of CNTs to achieve gene therapy, radiotherapy, immunotherapy, tissue regeneration and diagnosis of various diseases.[7] For this reason, despites novelty of those findings, in a very short time, many scientists from a wide variety of disciplines, have focused their attention towards carbon nanotubes.[8]

The research described within this PhD thesis is focused on the modification of carbon nanotubes for biomedical applications. The main aim was the sidewall functionalization of the CNTs already filled with radioactive isotopes, which can be applied for cancer imaging and/or treatment. The main part of the research activity was devoted to improve dispersibility of CNTs in aqueous media by their direct, covalent functionalization and to shorten the reaction time of this transformation. Pharmacological studies on the new functionalized CNTs were performed and the perspectives of this promising material are commented in the conclusions.

I.1 Structure of carbon nanotubes

CNTs are entirely composed of carbon atoms and can be assigned to the fullerene family. CNTs are bounded in planar structure of sp^2 hybridization, creating hexagonal network of carbon atoms rolled up into hollow cylinders (Figure 1).
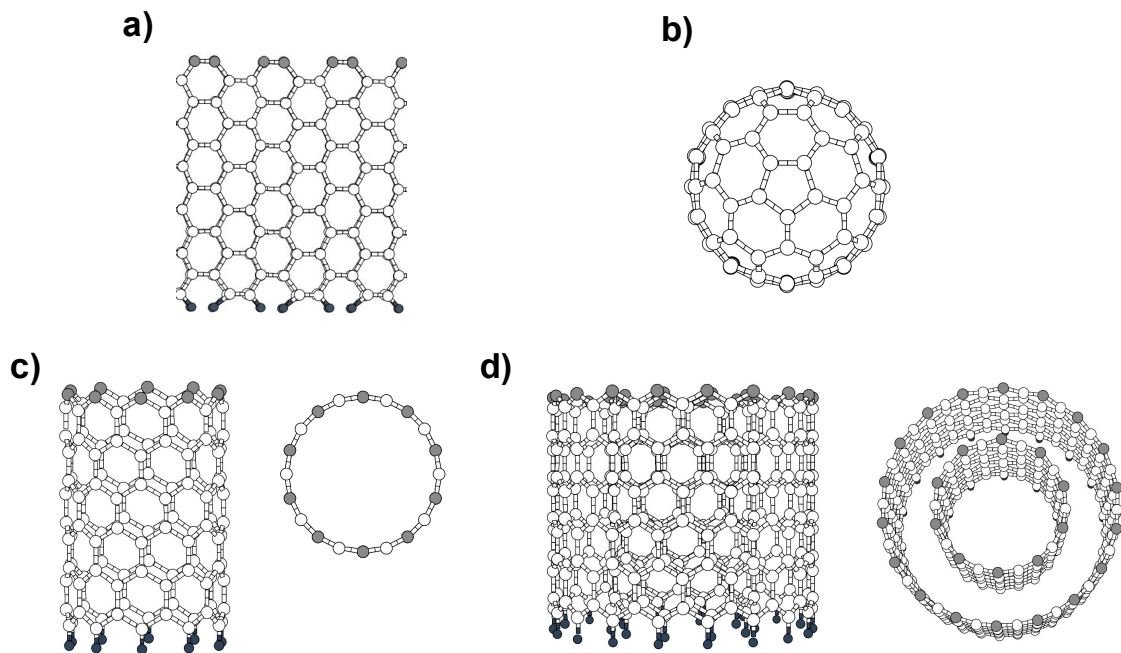
Figure 1. a) Monolayer of graphene sheet. b) Fullerene (C_{60}) with clearly visible pentagons and hexagons. c) Open-ended SWCNTs with the top view illustrating the cylindrical geometry. d) Side view of the open-ended double-walled carbon nanotubes with the top view of the same carbon system.[1]

Carbon nanotubes can be distinguished on the base of their structure:

a) **Single-walled carbon nanotubes (SWCNTs)** which are single cylinders of rolled graphene sheet with a diameter in the range of 1-5 nm and length up to several micrometers;

b) **Multi-walled carbon nanotubes (MWCNTs)** which cylinders of rolled graphene sheet are concentric. In this case the inner diameter is about 5-10 nm, and the outer 30-40 nm. The interlayer spacing in MWCNTs is larger than in graphite (0.34 nm).

It was discovered that both types of CNTs can spontaneously close their ends by forming a graphitic dome, at high temperature or during synthesis experiments.[9]

The individual structures of CNTs can be characterized by two integers (**n**,**m**) that define both their diameter and chirality. The structure of a single-wall carbon nanotube can be defined by hexagonal lattice of graphitic plane and specified by two vectors (Figure 2). The vector ***T*** - lattice vector, corresponds to the section of the nanotube perpendicular to the nanotube's axis. The second vector ***C$_h$*** - chiral vector can be expressed by the real space unit vectors a_1 and a_2 of the hexagonal lattice defined in Equation 1.

$$\textbf{\textit{C}}_{\textbf{h}} = \textbf{n}a_1 + \textbf{m}a_2 \qquad \text{(Equation 1)}$$
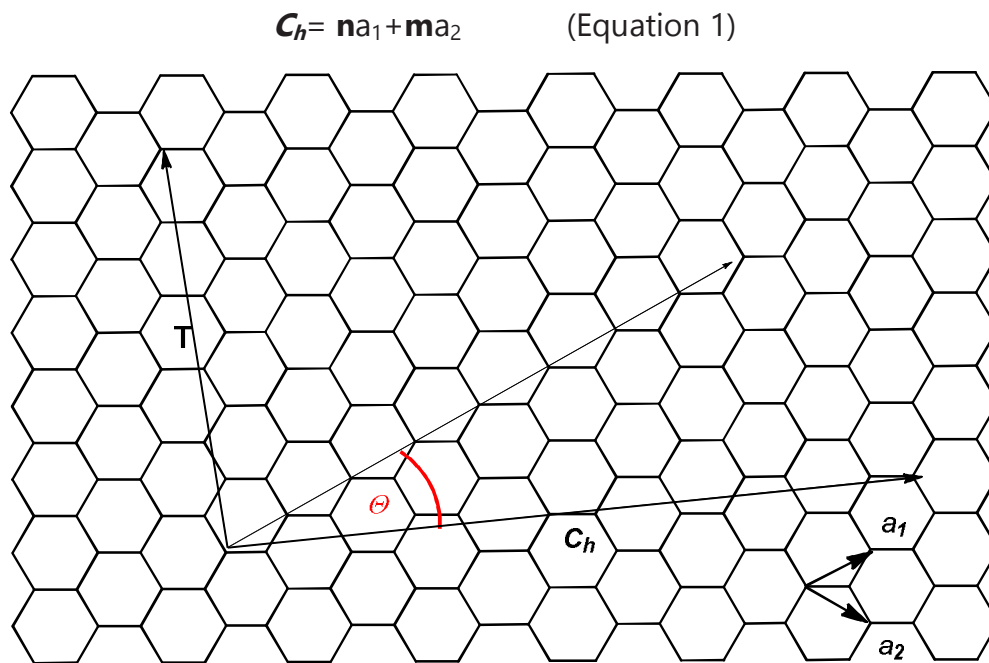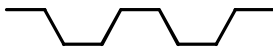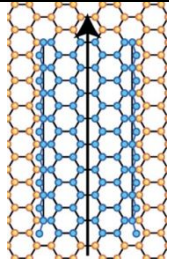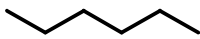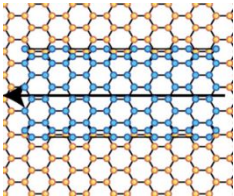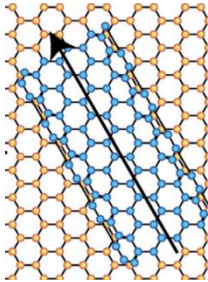
Figure 2. 2D graphene sheet with possible (n,m) and θ configuration.[10]

As depicted in Table 1, an armchair nanotube corresponds to the case of **n** = **m**, that ***C$_h$*** = (**n**,**n**), and a zig-zag nanotube corresponds to the case of **m** = 0, or ***C$_h$*** = (**n**,0). All other (**n**,**m**) chiral vectors correspond to chiral nanotubes. Because of the hexagonal symmetry of the honeycomb lattice, we need to consider only 0 < |**m**| < **n** in ***C$_h$*** = (**n**,**m**) for chiral nanotubes.

Table 1. Classification of carbon nanotubes.[11]

Type	$\theta^{a)}$	C_h	Shape of cross section	
armchair	30°	(n, n)	*cis*-type	
zig-zag	0°	(n, 0)	*trans*-type	
chiral	0°<|θ|<30°	(n, m)	mixture of *cis* and *trans*	

a) The chiral angle θ is defined by equation:

$$cos\ \theta = \frac{C_h \cdot a_1}{|C_h||a_1|} = \frac{2n+m}{2\sqrt{n^2+m^2+nm}} \qquad \text{(Equation 2)}$$

I.2 Properties of carbon nanotubes

Properties of CNTs significantly depend on their structure, in particularly on their chirality and number of graphitic sheets. These two factors can affect the tensile strength and the modulus of elasticity. They have also extremely low density ranging from 1.33 to 1.40 g/cm^3 and high specific strength, up to 50 GPa. CNTs present very high flexibility, which decreases for MWCNTs with high thickness. SWCNTs, for example, can twist, bent or be squeezed, without deformations and structural damages. During the deformation out of plane there are reversible changes of their sp^2 hybridization network: higher the deformation angle is, the stronger sp^3 character of the bonds occurs.

CNTs have also very interesting electronic properties. It is very fascinating that these structures, made entirely from only one element, may exhibit many different electronic behaviors. CNT's electronic conductivity, for example, sensitively depends on the tube diameter and the helicity of the tube lattice. Changes in those parameters cause a shift from a metallic to a semiconducting state. This relation is preserved for SWCNTs and also MWCNTs.[12] There are two estimated electronic band gaps: one has a defined value around 0.5–0.6 eV for semiconducting tubes, the other has significantly larger values of 1.7–2.0 eV for a metallic tubes.[13]

In the individual semiconducting SWCNT, the density of electronic states has a series of sharp peaks, named van Hove singularities (HVSs), with energies depending mainly on the tube diameter. The energy of the Fermi level is defined as zero, and energy levels above and below the Fermi level are conduction and valence bands, respectively. The optical transition occurs when an electron or a hole is excited from one energy level to another, denoted E_{pq}, with p and q representing the order of conduction and valence bands, respectively. Transition is allowed only when p = q (e.g., E_{11}, E_{22}, and E_{33}). The emission and absorption spectra in the first van Hove transition (E_{11}) are strikingly correspondent, so the fluorescence can be assigned to the E_{11} emission of semiconducting SWCNTs. It is proposed that the excitation of the semiconducting SWCNT in the second van Hove transition E_{22} is followed by fast electronic relaxation before fluorescence emission in the first van Hove transition, E_{11} (Figure 3).[14]
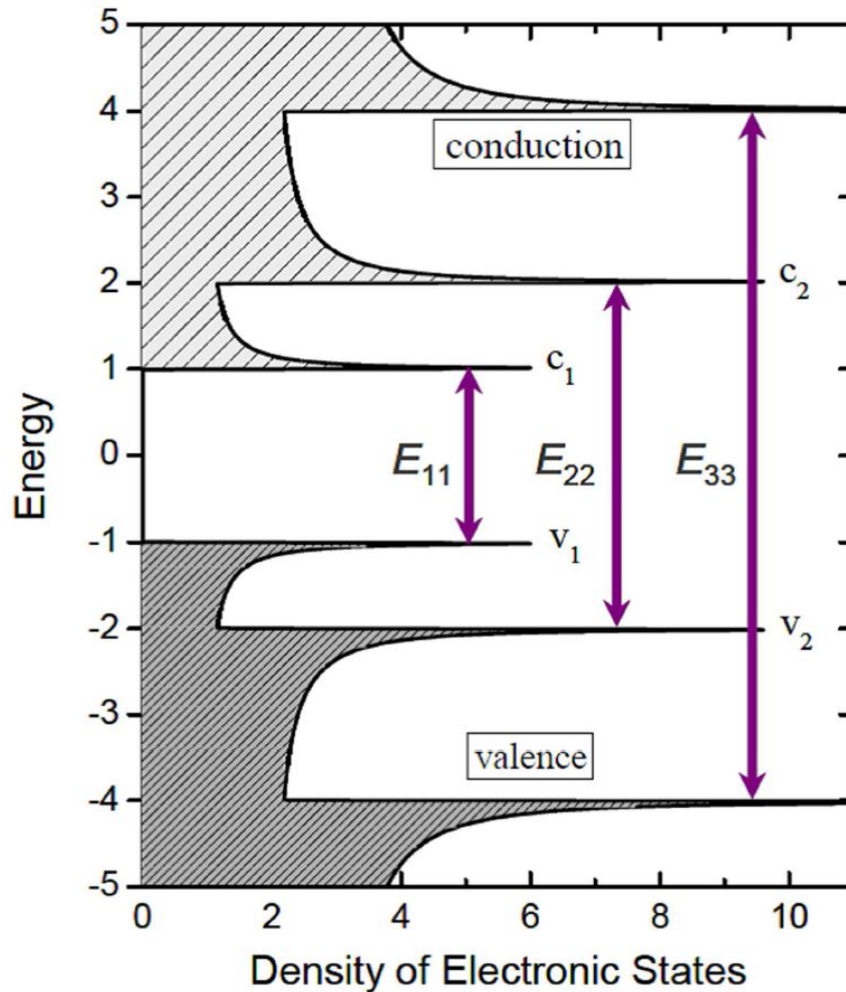
Figure 3. Density of electronic states for a single semiconducting nanotube structure.[15]

Narrow band gap allows for fluorescence emission in the near infrared (NIR) regions, including the classical NIR-I region (700–900 nm) and the newly defined NIR-II region (1100–1400 nm).

SWCNTs possess strong resonance in Raman scattering with extremely large scattering cross-section. Several vibrational modes can be distinguish, such as tangential mode of graphene (G-band) at ~1590 cm^{-1} and radial breathing modes (RBM) in the vicinity of 120–350 cm^{-1} for nanotubes between 0.7 and 2 nm in diameter, as well as intermediate frequency modes (IFM) which appear between the RBM and G peak regions. The unique Raman shifts of RBMs and IFMs are highly dependent on the nanotube graphitic species, allowing identification of the present of nanotube (n,m) species. The RBM frequencies, caused by the axial vibration of the nanotube circumference, related to

nanotube diameter with the relation $\omega_{RBM}=228/d_t+16$ cm^{-1}.[16] The IFMs have not been studied as extensively as the other modes, but certain modes with frequencies between 380 and 650 cm^{-1} have been assigned to nanotube (n,m) species or families of species. Some IFMs exhibit stepwise dispersion, changing in frequency upon excitation at different laser energies, while other modes are non-dispersive. Other information gained from carbon nanotube samples by Raman spectra includes the presence, in metallic nanotubes, the fano resonances. They are characterized by asymmetric line broadening expressed by the Breit-Wigner-Fano (BWF) line shape of the tangential mode. This phenomenon can be interpreted as the inference between the phonon and a continuum spectrum of electronic transitions near the band gap. The Raman spectra present also the sp^3 carbon defects via the 1297 cm^{-1} disorder mode (D-peak), and the presence of van der Waals contact in the RBMs. For instance, at 785 nm excitation, the (10,2) nanotube at 267 cm^{-1} comes into resonance upon such contact, denoting aggregation or "bundling".[17]

However, manipulation of CNTs is limited by several problems, such as:

1) formation of bundles due to π-π stacking and van der Waals interactions;

2) very low solubility in organic solvents and water;

3) low reactivity of pristine CNTs under many chemical reaction conditions, etc.

I.3 Synthesis of Carbon Nanotubes

Today's fabrication methods are focused on three main techniques:

1. <u>The arc-discharge method</u>, also used by Iijima, where two graphite electrodes are arced together in argon atmosphere, forming free carbon atoms which then condense as nanotubes on the container walls;

2. <u>Laser ablation</u>, where graphite is evaporated by an intense laser pulse and the carbon atoms condense as nanotubes.[1] These methods are well established in producing high-quality and nearly perfect nanotube

structures, despite large amounts of byproducts associated during the process;

3. <u>Chemical Vapor Deposition (CVD)</u>, where the flow of carbon rich gas (e.g. methane or acetylene) is heated to nearly 900 °C, which results in nanotube formation on metal catalyst nanoparticles, on a supporting substrate.

For SWCNTs, any of the three synthetic methods has yielded homogeneous diameters and chirality. Nonetheless, arc-discharge and laser ablation techniques are known for their impressively narrow diameter distributions, approximately 1.4 nm.[18]

I.4 Reactivity of Carbon Nanotubes

In principle, the chemical reactivity of carbon nanotubes can be compared with the reactivity of the other allotropes of carbon - graphite and fullerene. However, due to the unique structure of CNTs, there are differences with respect to what occur in other poly-aromatic carbon compounds. Compared to graphite, in the atomic structure of single layer of CNTs, there is a curvature of bonds between the sp^2 carbon atoms that leads to local bond stress.[19] Therefore, CNTs in general exhibit higher chemical reactivity than a flat layer of graphene. Due to the shape of closed ends of CNTs, the reactivity of these portions should be comparable to the fullerenes. The reactivity of a fullerene molecule is mainly due to the pyramidalization and the high tensions between carbon atoms (Figure 4a).[20] The pyramidalization angle in sp^2 hybridized carbon atoms is equal to $\theta_p=0°$ where sp^3 carbons exhibit $\theta_p=19.5°$. In the fullerene, the pyramidalization angle of all carbon atoms is equal to $\theta_p=11.6°$ and, as consequence, the reactivity is driven by release of pyramidalization strain energy. That is the explanation why fullerenes easier undergo the most of addition reactions.[21]
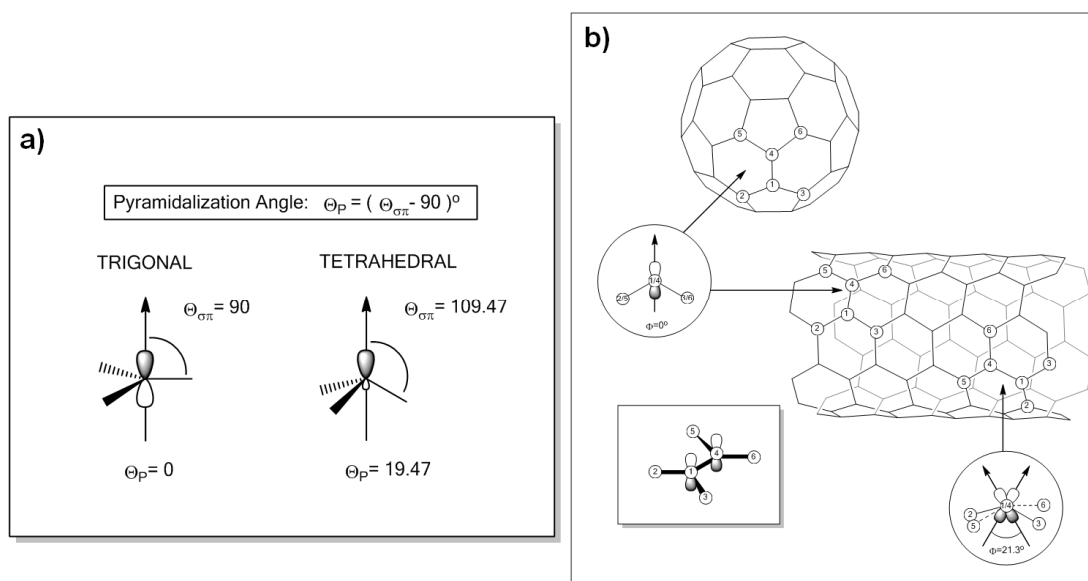
Figure 4. Diagrams of a) pyramidalization angle (θ_p); b) the π-orbital misalignment angles along the C1-C4 in SWCNT and fullerene C_{60}.[19,22]

The reactivity of CNTs is also dependent on a second factor, namely the π-orbital misalignment. The difference between C_{60} and CNTs is depicted in Figure 4b. The π-orbital alignments in fullerenes are nearly perfect and occur in almost all bonds with π-orbital misalignment angle $\phi = 0°$. Although all carbon atoms in CNTs are equivalent as well as in C_{60}, two types of bounds can be found. For example, at an armchair (5,5) SWCNTs, one runs parallel to the circumference (or perpendicular to the nanotube axis) with a π-orbital alignment angle of $\phi = 0°$ and the other set of bonds exhibits an angle to the circumference with a π-orbital misalignment angle of $\phi = 21.3°$. From calculations of torsional strain energies in CNTs, it can be concluded that the π-orbital misalignments are probably the major contribution of a binding force in CNTs aromatic lattice. Both factors, the π-orbital misalignment angle and the pyramidalization strain energy, have an important influence on the reactivity of the nanotubes.

Compared to SWCNTs, reactivity of multi-walled carbon nanotubes depends mainly on the diameter of the external tube. Considered that MWCNTs have a larger diameter, there is lower influence of pyramidalizationand π-orbital misalignment angles, with consequent lower reactivity. However, it must be

highlighted that there are many factors for the CNTs chemical reactivity and they are strongly connected with their structural cohesion. Since defects are formed directly during the manufacture it is hardly to say how they will affect the general reactivity of the tubes.

I.5 Functionalization of Carbon Nanotubes

The application of carbon nanotubes in any branch of nanotechnology strongly depends on their treatment and processability. The very low solubility in all organic solvents and water, strongly limits their applicability.[23] CNTs can be briefly held in solution only by sonication process. Another method to maintain CNTs in solution is the surface modification. In this way, depending on the attached functional groups, solubility in certain solvents can be increased. There are several methods for CNTs modification which allows applications of this material for hydrogen storage, biosensors, in medicine.[24,25,26]

There are many different approaches for the functionalization of carbon nanotubes, however they can be roughly divided into four classes:

1. Non-covalent functionalization;
2. Defect functionalization;
3. Endohedral functionalization;
4. Covalent sidewall functionalization.

I.5.1 Non-covalent functionalization

The non-covalent functionalization of carbon nanotubes is based on van der Waals, π-π stacking and current exchange effects between the extended π-system along the CNTs and the bounding molecules. These interactions are strong enough to break bundles of CNTs, but also debundling process has to be carried out under ultrasound irradiation. If the selected molecules are also

carrying charges, individualized CNTs are prevented by electrostatic repulsions from re-bundling. This approach is preferred for non-oxidative purification of CNTs. The big advantage over other methods is that the electronic structure of the nanotubes will not be changed and their outstanding electrical and physical properties remained unaffected.

For the non-covalent functionalization, several different surfactants can be applied. Selection depends on the charge their head group. They can be: cationic (with the head groups such as quaternary ammonium)[27] also anionic (with head group such as carboxylates, sulfonates), non-ionic (with the head group such as alcohols, sugars or carboxylic acids) (Figure 5) and zwitterionic (positively and negatively charged functional group).[28]

Figure 5. The schematic representation of how surfactants may adsorb onto the CNTs surface.[27]

The main disadvantage of this process is the fact that relatively high concentrations of surfactant in the solution are needed for an efficient separation of CNTs and it is moderately difficult to remove the excess. Moreover, immediately after the surfactant removal, CNTs lose their stability and re-agglomeration occurs again.

Specific examples for non-covalent interactions can be found between SWCNTs and amines, as aniline[29] and some alkylamines.[30] This phenomenon is explained by the significant affinity of amines for physisorption along the SWCNTs sidewalls. At elevated temperatures, CNTs and amines may form a charge-transfer complex in its ground state which affects drastically the

12

electrical properties of individual SWCNTs. Complex can be simply removed by washing with acetone.

An efficient coating of CNTs can be achieved with organic polymers[31,] where the polymer wraps individual CNTs within a bundle and leads to their separation.[32] Polymers such as poly(*p*-phenylenevinylene-co-2,5-dioctyloxy-*m*-phenylenevinylene) (PmPV-co-DOctOPV) have a typical selectivity for SWCNTs within a certain diameter range.[33] Thanks to the presence of polar portions of the polymer chains, derivatives as polyvinylpyrrolidone (PVP) or polystyrene sulfonate (PSS) are able to stabilize CNT-polymer complexes and prevent their agglomeration even in water.[34] Other non-covalent functionalizations are established in bio-medical field: a large number of biomolecules, such as sugars,[31] proteins and peptides, can be adsorbed onto CNTs surface.[35] A non-covalent binding of SWCNTs with DNA is also possible and leads to individualization of the CNTs in an aqueous medium. Different strong interactions between single-stranded DNA and CNTs were observed to be dependent on the diameter and the electronic properties of the CNTs.[36,37]

I.5.2 Defect groups functionalization

Carbon nanotubes, during the synthesis or the purification, or upon exposure to light and oxidation on air, can gain a certain number of defects. The most common types of defects with a carbon atom arrangement different than the hexagonal one in the SWCNTs lattice are shown schematically in Figure 6.[38,39] They includes Stone–Wales defects, obtained by a 90° rotation of a C-C bond creating a 5-7-7-5 ring pattern (Figure 6c), sp^3 defects saturated with hydrogen atoms, structural holes, dangling bonds and open tube ends terminated by carboxylic acid functionalities with sp^3 carbon hybridization. Furthermore, the formation of defects during the CNTs growth can lead to the production of branches (Y-junctions) of the tubes and even to the deformation of whole structure.[40]
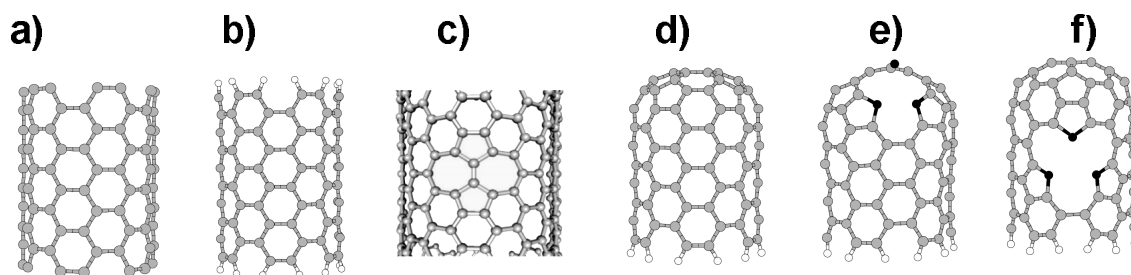
Figure 6. Defects on SWCNTs. (a) Infinite tube (periodic boundary conditions);(b) H-saturated open tube on both sides (used to characterize the saturation energy); (c)pentagon and heptagon defects on the sidewall; (d) closed tube; (e) oxidized hole obtained by removing a hexagon at the cap; (f) the same as at the wall.

The presence of defects can increase the chemical reactivity of the surroundings aromatic structure. By an oxidative treatment, e.g. during the purification of the row CNTs, the presence of the defect can initiate the oxidation process and deform the tube structure as consequence.[41] Oxidation of carbon nanotubes under strong conditions leads to several types of defects schematically shown in Figure 7. The presents of the defects can also affects other types of functionalization on CNTs (see next paragraph) and change the general reactivity of the tubes.
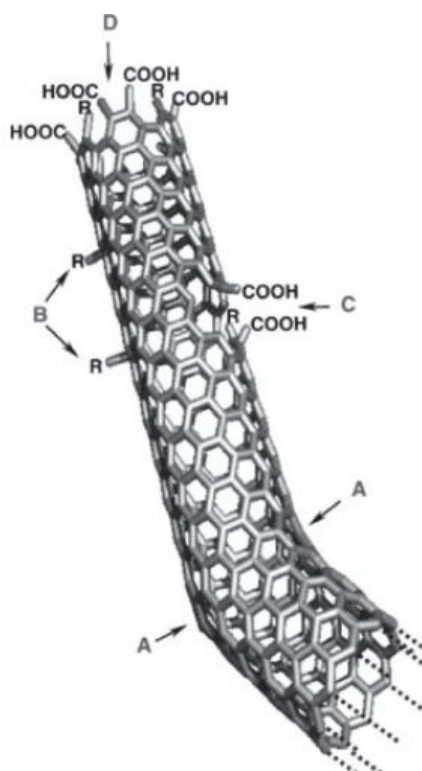

Figure 7. Typical defects in a SWCNT.A - deformed construction of SWCNT due to pentagon and hexagon structures. B - sp³-hybridized defects. C - carbon framework damaged by oxidative conditions, which leaves a hole lined with –COOH groups. D - open end of the SWCNT, terminated with COOH. Other terminal groups such as -NO₂, -OH, -H, and =O are possible.[42]

I.5.3 Endohedral functionalization

Endohedral functionalization of CNTs means that the inner cavity of the tube is filled with single atoms or small molecules. The new structure is described as X@CNT [hybrid nanotubes in which the inner cavity has been filled with foreign atoms] where X is the chemical symbol of the content of the tube. Endohedral modification is usually performed to create a new organization of several confined materials with controlled size, structure and shape, where the internal cavity of the tube serves as a template. Secondly, the new material can gain new physical, chemical and electronic properties depending on the type of CNTs and foreign material.

CNTs can be filled in one step, by *in situ* method, during the CNTs growth.[43] However in most of cases, filling is separated from synthesis, occurring *ex situ*, through the open tips. Several gases, molten or sublimated materials can be introduced,[44] as well as metal nanoparticles,[43] oxides,[45] salts,[46] organic compounds among which dyes such as beta-carotene[47] or porphyrines[48] and other carbon nanostructures such carbon nanoribbons[49] and C_{60}[50] (Figure 8).
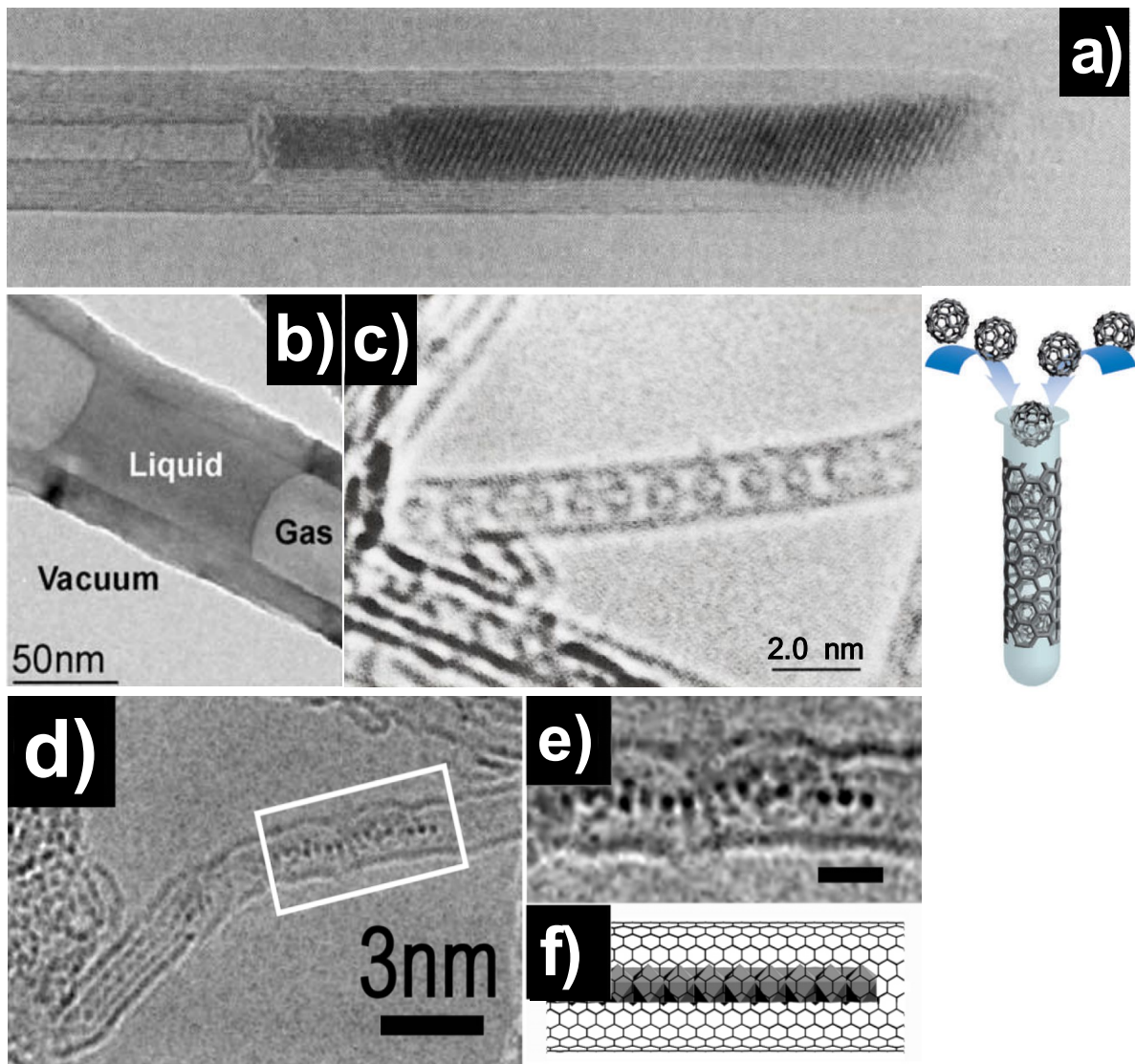
Figure 8. TEM image of filled CNTs. (a) Crystalline portion of lead in MWCNT[51]; (b) TEM micrographs showing a liquid plug in MWCNT[52]; (c) a SWCNT carbon nanotube containing a chain of C_{60} t50 to produce so-called peapod structures[53]; (d) HRTEM micrograph showing a twisted 1D chain of $GdCl_3$ formed within a (10,10) SWCNT; (e) enlargement of boxed region from (d)-(f) structural representation of a chain with $GdCl_3$.[54]

First, it has proved that liquids may fill open CNTs by capillary effect. It was found that the surface energies of the interaction between the liquid and the nanotube are crucial. Wetting is necessary for observing capillarity action, as can be understood from the Young–Laplace equation (Equation 3).[55]

$$\gamma_{SV} = \gamma_{SL} + \gamma_{LV}\cos\theta \quad \text{Equation 3}$$

It describes the relation between the interfacial tension between the solid and the gas - γ_{SV}, the interfacial tension between the solid and the liquid - γ_{SL}

and the interfacial tension between the liquid and the gas - γ_{LV}. If is larger than 90°, the contact angle will be non-wetting. If θ is smaller than 90°, the liquid will spontaneously enter into the empty cavities of CNTs (Figure 9).
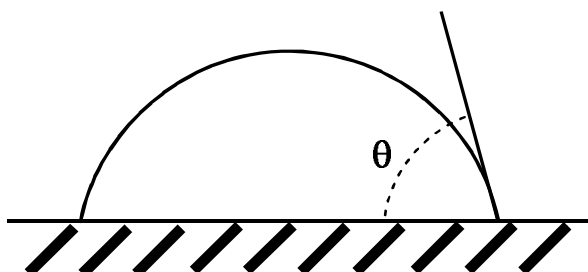

Figure 9. Contact angle - of a liquid on a solid surface.[55]

The surface tension is a key parameter for the successful filling process: the cut-off value of 200 mN/m is at the border between wetting and non wetting, water (72 mN/m), nitric acid (43 mN/m) or organic solvents (from 26 up to 47 mN/m) should wet nanotubes and a slow surface tension media could be used. Ethanol, some oxides with low surface tension (PbO, V_2O_5) and some solids with low melting points (S, Cs, Rb, Se) were found to easily fill the inner cavities of CNTs with large diameters. Pure metals or metal compounds with high surface tension can possibly fill the CNT only in oxidizing atmosphere due to the fact that low surface tension oxides are formed. Taking into account all types of filling, the highest rates of endohedral functionalization can be achieved from the gas phase, even up to 100%. Molten phase methods were found to provide maximum filling yield in the range of 20–50%, while filling from solution phase did not go beyond 25–30%. High filling rates have not been achieved yet for solid phase materials with the exception of C_{60}.

The proper characterization of the obtained material is one of the major issues in the synthesis of hybrid CNTs. Once the hybrid nanotube is synthesized, it is essential to identify by nano-probe spectroscopic methods where foreign material is presented to understand if it is really encapsulated or intercalated in the tube ropes. A first method, sufficiently convincing, is transmission electron

microscopy (TEM). On TEM images it is possible to observe separated or bundled tubes where the foreign material is visible by differences in contrast. The crucial problem of this technique is that it is based on local observations, where the hybrid nanotubes have to be well separated. For a full characterization, numerous images are necessary to have representative image of the sample. Where the filling is crystallized inside the inert cavities, the high-resolution microscope can revealed specific lattice distances of the inserted material. It also might not be sufficient to use nano-probe energy-dispersive X-ray spectroscopy (X-EDS) for exact identification of the filling materials due to intrinsic spectroscopy limitations. X-EDS is hardly quantitative, and provides chemical information on which elements are present in a chosen area of the sample. Electron energy loss spectroscopy (EELS) might be a better choice, since it is potentially able to provide both qualitative and quantitative chemical data about atom identification, oxidation state, band structure, etc., but fine structure EELS work is necessary, which is not a routine-based procedure. Anyway, if such accurate methods are not used, it is quite risky to deduce the chemical identification of the filling materials from just considering the expected chemical reactions involved during the filling process.

Another method of chemical analysis is atomic emission spectroscopy (AES). This technique employs the intensity of light emitted from a flame, plasma, arc, or spark at a particular wavelength to determine the quantity of an element in a sample. The wavelength of the atomic spectral line gives the identity of the element, while the intensity of the emitted light is proportional to the number of atoms of the element itself. The limitation of this method is that there is no distinction between the inside and the outside of CNT so it is not possible to differentiate among filled material and compound deposited on the external surface of the tubes. Values reported in the literature should thus often be considered only as rough evaluation.

The work of Ballesteros *et al.* reported the first methodology for the quantitative assessment of the amount of inorganic material encapsulated in carbon nanotubes.[56] The method is based on TGA in air, where analysis of the empty and filled nanotubes is needed for a calculation. During the TGA experiment of filled nanotubes in air, the filling material may react with oxygen to form a solid residue, normally an oxide and/or may sublime to form a gaseous oxide. In any case, the filling yield (FY) can be accurately determined by Equation 4, where percentage values for residues in air are R_1 for the empty carbon nanotubes, R_2 for clean filled nanotubes, and R_A bulk material

$$FY\ (wt\%) = \frac{100 \cdot (R_2 - R_1)}{R_A - R_1} \qquad \text{Equation 4}$$

In the calculation it was also taken into account that the encapsulated material can sublimate or react with oxygen to give a gaseous oxide: in this case the residue for the filled SWCNTs (R_2) will be lower than that for the empty SWCNTs (R_1).

If the filling material oxidizes to form a solid oxide, the residue of the TGA in air will be due to the catalyst impurity residue and compound B:

$$xA_{(s)} \xrightarrow{\text{air, } \Delta T} yB_{(s)}$$
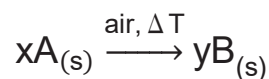
If the filling material oxidizes to form a solid R_A can be then calculated taking into account the stoichiometry of the oxidative reaction occurring during the TGA analysis. Thus the residue can be calculated according to Equation 5, where x and y are the reaction stoichiometric constants and MW_A and MW_B the molecular weights of A and B, respectively:

$$R_A = \frac{100 \cdot y \cdot MW_B}{x \cdot MW_A} \qquad \text{Equation 5}$$

I.5.4 Covalent Sidewall functionalization

Covalent sidewall functionalization provides a direct path for the introduction of molecules on the carbon nanotube sidewall. This leads to partial destruction of the conjugated sp^2 carbon lattice to give sp^3 hybridization. If the chosen reaction conditions are too harsh, the tubes loose the aromaticity by rehybridization, and an excess of sp^3 carbon is present. In recent years, many attempts were made to apply on aromatic, cylindrical lattice of CNTs chemical reactions, which were already known in the chemistry of fullerenes and other aromatic molecules. A general idea of the already used reactions is listed in Figure 10.
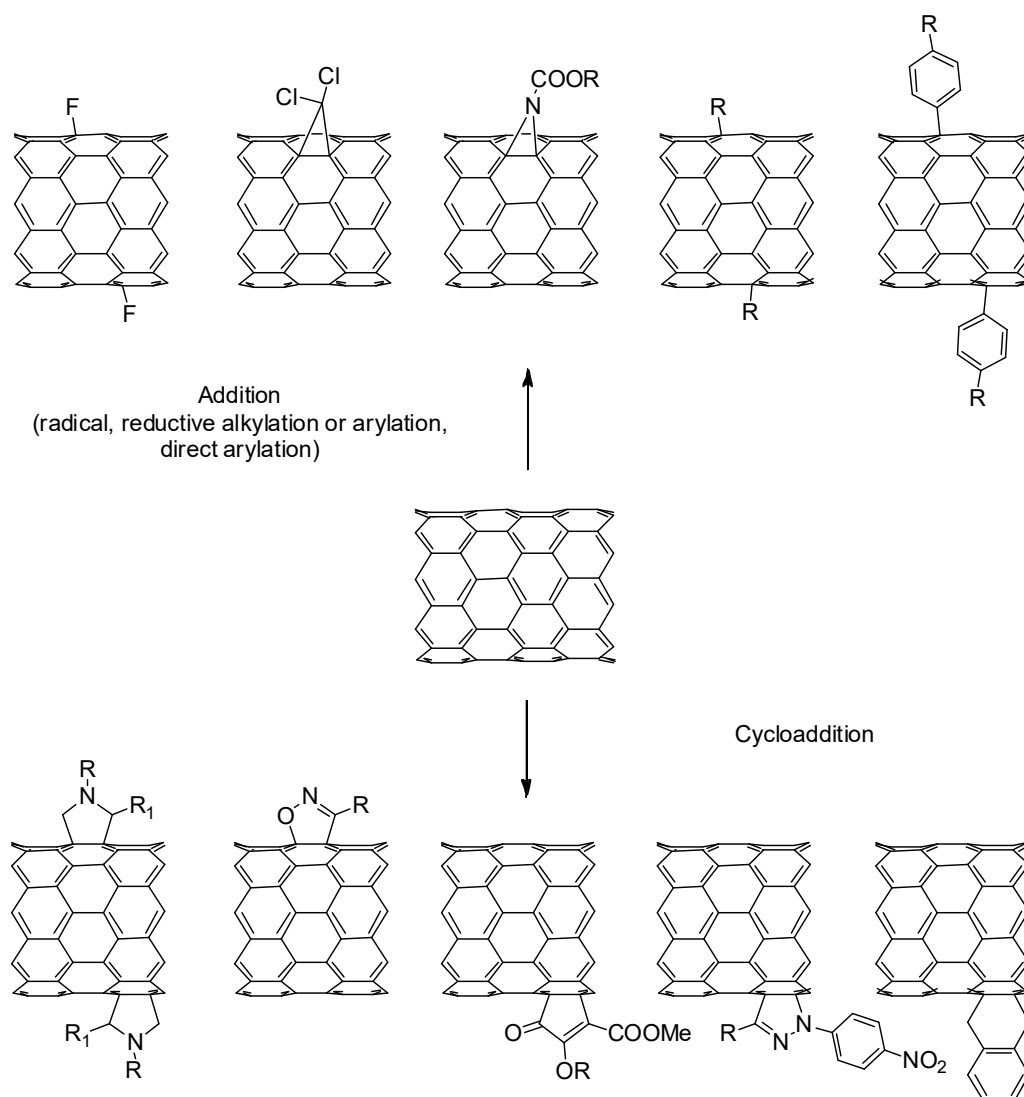

Figure 10. Covalent functionalizations of CNTs.

One of the first successful implementation of covalent reactions on carbon nanotubes was applied in 1996: the fluorination.[57,58] STM studies have shown that the reaction occurs where the fluorine atoms are adsorbed perpendicular to the axis. This can occur in two different addition patterns, namely 1,2-addition and 1,4-addition. Calculations have shown that isomer 1,4- should be more stable, but, due to the low energy barrier between the two substitution pathways, both isomers likely occur at the same time. After this discovery, a variety of different pathways were found for efficient fluorination of carbon nanotubes, including plasma-based functionalization.[59] Fluorinated nanotubes have been widely used as starting material for further chemical modifications, based on the nucleophilic substitution of fluorine atoms. For examples, the reactions of alkyl lithium and Grignard reagents lead to alkyl functionalization of sidewalls.[60] They can be de-halogenated under treatment with hydrazine or strong nucleophiles and functionalized in a second step.[61] Zhang *et al*. showed that fluorinated CNTs are even capable to react in Diels-Alder [4 + 2] reaction.[62] It is also possible that, by thermal oxidation, fluorinated or alkylated CNTs loose the side appendix and regenerate the original nanotubes.

A reaction of alkyl lithium compounds with non-fluorinated SWCNTs was reported in 2003 by Viswana *et al*.[63] The approach was developed to *in situ* composite synthesis by attachment of polystyrene (PS) chains to full-length pristine SWCNTs without disrupting the original structure, based on an established anionic polymerization. The reaction was performed by carbanion formation with *sec*-butyl lithium as an initial step for polymerization of styrene at the CNT sidewall. The reaction was performed also on MWCNTs with *n*-butyl lithium and chlorinated polypropylene.[64] A successful alkylation of CNTs was performed with *sec*-butyl lithium, and subsequent carboxylation with CO_2.[65] In the first reaction step, the nucleophilic addition of alkylcarbanionis used and then the second step is the addition of CO_2 as electrophile.

Another method is the reductive alkylation under the Birch conditions. The reaction is performed in liquid ammonia with alkali metals such as sodium, lithium or potassium to reduce SWCNTs and generate soluble CNT anions. It was shown that negatively charged single-wall and multiwall nanotubes can be derivatized by addition of alkyl halides.[66] The Birch method was extended to arylation, and besides the use of NH_3 as solvent, the reactions was performed with the radical anion salt of lithium naphthalenide in THF.[67] In 2007 Chattopadhyay *et al.* found that SWCNTs treated with lithium in liquid ammonia react also with aryl and alkyl sulfides by single electron transfer (SET).[68]

In 2001 Tour proposed an electrochemical reduction of aryl diazonium salts to provide reactive radicals that can covalently react with CNTs.[61] It was postulated that an electron from the CNTs is transfer on to diazonium salt, and then, after elimination of nitrogen, a reactive aryl radical is formed. By varying the aryl diazonium salt, SWCNTs can be functionalized to obtain well-soluble products. Soon the reaction was extended to a solvent-based thermally induced reaction, where diazonium compound were generated *in situ* by reacting aniline derivatives with isopentyl nitrite (Figure 11).[69] If the reaction is performed under controlled conditions, functionalization occurs preferentially on metallic SWCNTs.[70] The arylation on SWCNTs is described in details in following chapter.
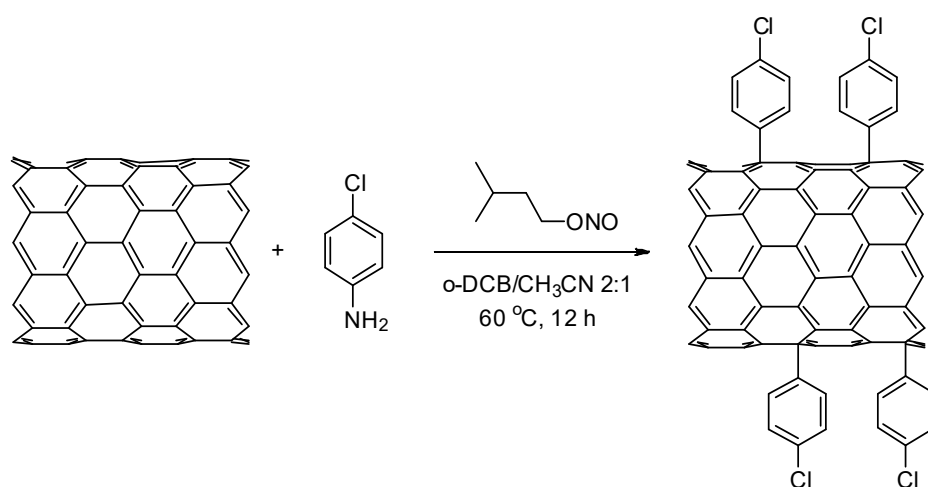

Figure 11. CNTs arylation.

Following the idea of radical additions to CNTs, organic xanthates and peroxides are also suitable for covalent functionalization.[71] Pennetreau *et al.* stated that the reactivity of dilauroyl peroxide moieties onto the CNT surface along with xanthate-derived radicals are inversely proportional to the stability of the radical that is formed during the reaction.

A different example of reaction is nucleophilic cyclopropanation *via* Bingel reaction. This reaction is commonly used in fullerene chemistry. On carbon nanotubes, it proceeds by an addition reaction of the bromomalonate generated *in situ*, followed by intramolecular nucleophilic substitution to generate the cyclopropane ring. Coleman *et al.* reported diethylmalonate attachment on SWCNTs walls under the Bingel reaction conditions and the detection of the functional groups using chemical markers for AFM visualization.[72] Umeyama *et al.* introduced on the SWCNTs surface benzyl 2-ethylhexylmalonate.[73] They emphasized the necessity of a pretreatment procedure, which includes the oxidation and the formation amide functionality on sidewalls, followed by Bingel modification to increase the reactivity.
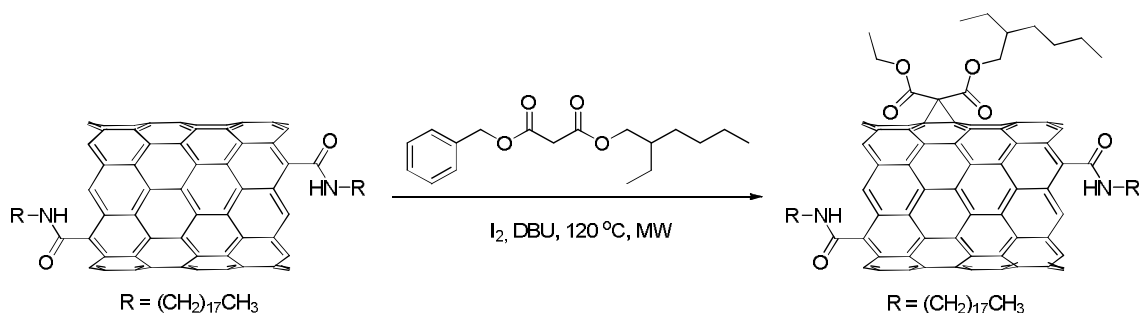

Figure 12. Bingel reaction on CNTs.

Another important reaction on CNTs was firstly reported in 1998: the cycloaddition of dichlorocarbene.[74] Dichlorocarbene was generated *in situ* from chloroform with potassium hydroxide or from phenyl (bromodichloromethyl)mercury for covalent attachment to SWCNTs. The electrophilic carbene addition led to a low functionalization degree of about 2%.

The functionalization was more efficient for small diameter tubes and caused great enhancement of charge transfer on semiconducting tubes.

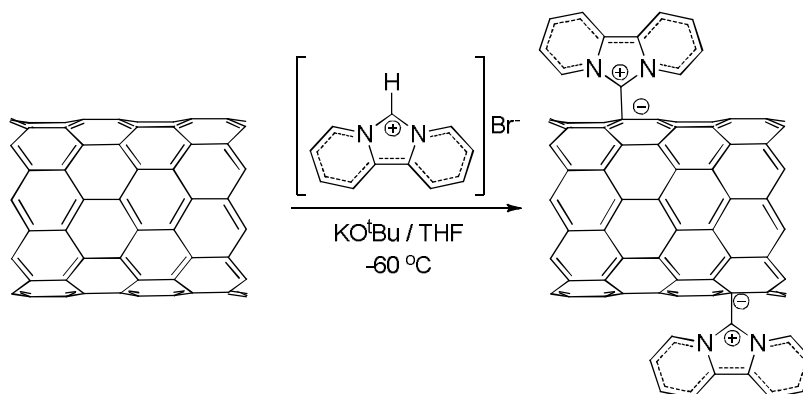In an early study, Hirsch group reported that the SWCNTs sidewalls can also be attacked by nucleophilic carbenes.[60]

Figure 13. Carbene addition on CNTs.

A very efficient method of covalently functionalized CNT by cycloaddition was developed by Prato and co-workers. SWCNTs or MWCNTs were treated with an azomethine ylide generated from aldehyde and *N*-substituted glycine derivative to obtain pyrrolidine rings at the nanotubes sidewall.[75] This method of functionalization of CNTs is very efficient especially for oxidized CNTs.[76] Taking advantage of easy derivatization of α-amino acids, several biocompatible systems can be build at the sidewall of CNTs. The 1,3-dipolar cycloaddition is described in details in following chapter.

Overall, there are several reactions for the covalent functionalization of CNTs. The main advantage of the functionalization is the possibility of derivatization of CNTs according to the purpose, for example to improve their solubility in organic solvents, to make them suitable for incorporation into polymer composite materials, or to create the flexible platform for derivatization with biological molecules.

I.6 Biomedical application of carbon nanotubes

The properties of CNTs allow to envision application in many biomedical areas by offering unique alternatives to present technologies, from tissue scaffolds to drug delivery vehicles.

I.6.1 Carbon nanotubes as cell substrates

One of the very promising and important implementation of CNTs is connected with their topological and chemical structure. It is well established that topographies and patterns can influence the cellular behaviors. By controlling the nanoscale topography of cellular substrates, the implantation of medical devices facilitate new biological processes, including embryogenesis, angiogenesis, and pathological conditions.

CNTs as nanoparticles are inherently appropriate for surface modifications by simple incorporation or deposition on their surface. They have a fibrillar shape and versatile optical, electrical, and mechanical characteristics for applications as a cellular substrate. Many groups have successfully utilized CNTs for cellular growth surfaces to provide structural support or present novel properties.[77] For instance, a range of cell phenotypes were presented to have high binding affinities for CNTs surfaces, demonstrating the CNTs may be used for a variety of tissue implantation devices or novel substrates.[78,79]
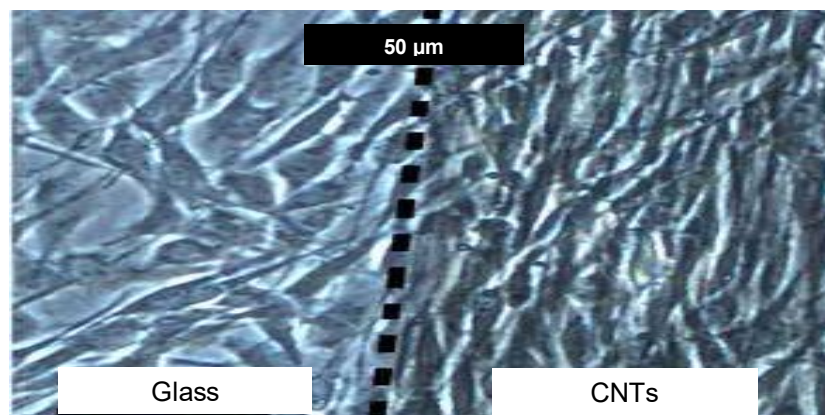

Figure 14. Human skin fibroblasts growing isotropically on glass and aligned in one direction on well-aligned MCWNT arrays.[80]

Several papers have presented CNTs as conducive to neuronal adhesion and safe for neural processes outgrowth, suggesting that CNTs are biocompatible with neurons. Cellot *at al.* reported CNTs to provide shortcut for the electrical signaling connecting tight junctions adhered onto the nanotube surface at proximal and distal portions of the neuron.[81] Mature neuronal cells have also been derived directly from human embryonic stem cells (hESCs) using polymer-grafted CNTs thin film scaffolds.[82] Malarkey and co-workers, by modulating the thickness and the conductivity of a CNTs film, were able to change neuron morphology, neurite outgrowth, and the number of growth cones.[83] Even if till now neuronal interfacing has no direct clinical benefits, research developments in this area may help to explain biological mechanisms and neural interactions relevant to injury and disease. Preferential interactions of neural cells and CNTs permit the study of axonal outgrowth and connection between neural clusters and patterned CNTs. Also the directed growth and migration along CNT surface architectures allowed the study to prevent and repair of nerve injuries, such as spinal cord injury or stroke.[84]

Lee *et al.* pretreated rats with amine-modified SWCNTs to protect neurons and to improve the recovery of behavioral functions in rats with induced stroke. Authors suggest that CNTs with positive charges may have contributed to a favorable environment for neurons.[85] Roman *et al.* investigated the administration of PEGylated SWCNTs after traumatic neural cord injury, which could promote regeneration of axons into the lesion cavity and functional recovery of the hindlimbs.[86] They found that, after a spinal cord injury (SPI), neurofilament-positive fibers of SWCNT-PEG induced a modest improvement in hindlimb locomotor recovery without inducing hyper algesia. These data suggest that SWCNT-PEG may be an effective material to promote axonal repair and regeneration after SPI.

I.6.2 Carbon nanotube for delivery of drugs

The high biocompatibility of CNTs and their possibility to penetrate the cells provide the excellent intracellular vehicle to interact with mammalian cells. In 2004 Pantarotto *et al.* demonstrated the translocation of CNTs in cellular membranes and proposed uptake mechanism, intracellular distribution, elimination from cells and possible adverse effects.[87] Two types of CNTs functionalization were reported: SWCNTs FITC-labeled and peptide–SWCNTs conjugated. Generally, these compounds were able to pass the cell membrane and the peptide-SWCNTs were found to accumulate in the nuclei of the cells, whereas the FITC-labeled SWCNTs were distributed in the cytoplasm. The internalization was not affected by the temperature or the presence of endocytosis inhibitors. So it was possible to claim that the uptake mechanism was endocytosis-independent and it was hypothesized that the cylindrical shape and high aspect ratio of functionalized CNTs allowed their penetration through the plasma membrane in a needle-like uptake. Kam *et al.* also studied the cellular uptake of fluorescent-labeled SWCNTs and fluorescent peptide–SWCNTs conjugate.[88] Their results suggested an uptake by endocytosis because it was inhibited at low temperatures. Nanotubes were localized in the endosomes and in the cytoplasm, but not into the nucleus.

These contrast results are ascribed to the different physical and chemical properties of used nanotubes, as well the type of functionalization.
In particularly the uptake mechanism is very important for delivery application. In the case of endocytic uptake, CNTs are initially covered by intracellular vesicles, called endosomes, with mild acidic pH. Next there is the fusion of the endosomes with lysosomes and pH reaches 5.5 for hydrolytic enzymes. Unfortunately in such conditions drugs and nucleic acids can degrade. Thus, in same case it is preferable that CNTs escape lysosomes. The needle-like uptake pathway transports the nanotube directly into the cytoplasm and there are more chances to avoid the lysosomal degradation.

CNTs can be combined with the drug in two ways: linked to the outer walls or by internal filling. In the case of external functionalization, this can be non-covalent or covalent. The non-covalent way is simply based on the interaction of CNTs and drugs after mixing. However, the stability of the produced system depends on environmental factors. This approach can find a convenient application when the drug can be released from complex in slightly acidic microenvironment of endosomes and lysosomes, as for CNT-doxorubicin couple, which is bound via π-π interactions. At physiological pH the amino group of the doxorubicin sugar moiety is deprotonated, promoting strong hydrophobic interactions with the nanotubes sidewalls and conferring low solubility in water. In contrast, at lower pH as in cancer cells or lysosomes, the amino group becomes protonated, increasing the solubility in water and resulting in the release of the drug from the nanotubes.[89] Other examples of non-covalent binding to CNTs include paclitaxel[90] and camptothecin.[91]

The covalent binding between CNTs and drugs is usually based on cleavable bonds like disulfides[92], esters[93], carbamates[94]. In these cases, the drugs are bound not directly to the nanotube but to the linkers which have been introduced to increase the solubility and biocompatibility of the carbon scaffold. The most common linkers are so far poly(ethylene glycol) (PEG) and linear polymers, such aspoly(vinyl alcohol)[95]. In recent years, branched polymers have become more popular, among these dendrimers[96] and dendrons.[97]

When a drug is delivered inside the cavities of the tubes, it can be transferred with high protection and released in a controlled way. Hampel *et al.* have filled MWCNTs with carboplatin; they used wet chemistry approach to reach approximately 30 wt% of filling yield.[98] The complex displays a cytotoxic effect depending on the concentration reached inhuman bladder cancer cells. The study was performed also with empty tubes, showing strong inhibition of the cells viability only in the case of carboplatin filled CNTs (Figure 15).
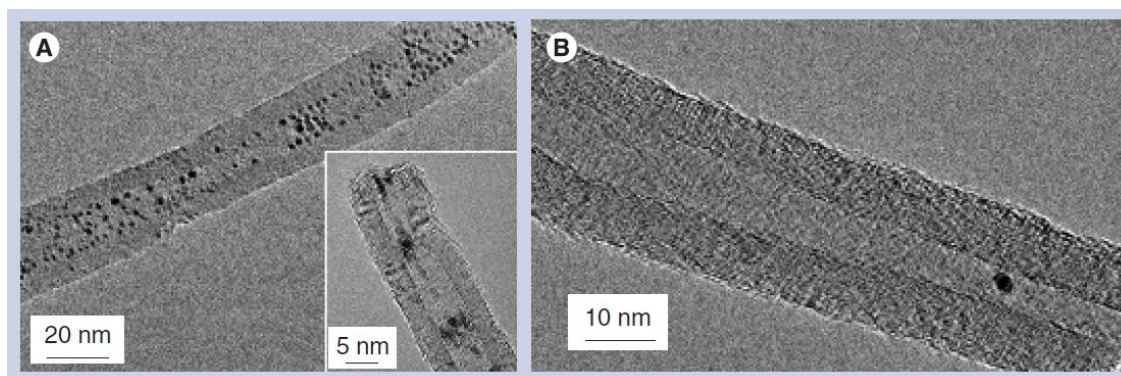
Figure 15. Carboplatin release from the nanocontainer. A) Filled nanotubes after incubation in the cells for 30 min. B) Carboplatin filled Nanotubes after 24 h incubation in cell culture medium.[98]

Targeting - a very important aspect of chemiotherapy - is the controlled distribution of the drug, which should reach a specific location. This can be achieved with two approaches: vector-based and nonvector-based systems. In the first case, CNTs used as carrier need the therapeutic agent and also the targeting molecule.[99] When the targeting molecule is omitted, the accumulation of the particles is based on the size and physical properties of the nonovector (passive targeting).

For the active targeting antibodies, aptamers, or ligands to cell surface receptors are used. For example cyclic arginine-glycine-aspartic acid (RGD) peptide recognizes the integrin $\alpha_v\beta_3$ receptors presented on solid tumors.[100] Also folic acid is widely used because its receptor is over-expressed in many human cancers.[101] Among others, the epidermal growth factor (EGF) is used as active targeting agent being the ligand to the epidermal growth factor receptor (EGFR) to selectively target squamous cancer cells.[102] McDevitt *et al.* designed antibody functionalized SWCNTs to target the CD20 epitope on human Burkitt lymphoma cells. The covalent attachment of antibodies to the CNT scaffold dramatically altered the kidney biodistribution and pharmacokinetics when comparing tumor bearing and healthy mice.[103] Aptamers could be also used as alternative targeting agent. They are synthetic, single-stranded nucleic acid molecules able to fold up into unique 3D structures, which give them molecular recognition

properties similar to antibodies. They are easily producible for variety of targets with little or no immunogenicity in therapeutic submissions. However, they usually have an inefficient cell uptake but Van der Bossche *et al.* have demonstrated that aptamers bound onto CNTs are translocated into the cytosol of different cell types independently of receptor-mediated uptake.[104]

I.6.3 Carbon nanotubes for imaging

By functionalization, CNTs can be conjugated with imaging agents, such as metallic nanoparticles, quantum dots, or isotopes to make possible imaging via conventional techniques. Chen *et al.* studied the conjugation of CNTs with super paramagnetic iron oxide nanoparticles (SPIO) and NIR fluorescent quantum dots CdTe.[105] The CNTs-SPIO-CdTe nanohybrids exhibited the superparamagnetic behavior of SPIO with a saturation magnetization of about 65 emug^{-1} at room temperature and strong emission band located at a near-infrared wavelength of 734 nm. Al-Faraj *et al.* and Vittorio *et al.* used magnetic resonance imaging (MRI) for visualizing CNTs in cells[106] or living organisms[107] taking advantage of the presence of iron oxide impurities.

The recent studies about application of CNTs for radiotherapy presented several examples of CNTs as a radioisotope carrier. In the case of encapsulation of the radionuclides, Hong *et al.*, presented single-walled CNTs filled with sodium iodide-125 (Auger and γ-emitter) for *in vitro* and *in vivo* study.[108] The material had a specific tissue accumulation (lung) and the leakage of the radionuclide was not observed.

I.7 Toxicity - physical determinants influencing the toxicity of carbon nanotubes

The biological application of CNTs strongly depends on all health hazards that the new material can cause. Since several years, *in vivo* and *in vitro* toxicological studies begun to determine the effect of this material in cells and tissues. However, it turned out that many parameters of CNTs, (as contaminants, surface chemistry, processing method, agglomerate state, length, diameter, and more others) can have various toxic effects.

I.7.1 Effect of purity on toxicity

As it was reported, the toxic effect of the CNTs can arise not directly from CNTs, but from the residues produced during the synthetic process as nickel, cobalt or iron nanoparticles, which can persevere in the CNTs and generate reactive oxygen species (ROS) in biological environment. It turns out that ROS cause inflammatory symptoms and induce mitochondrial membrane degradation, depletion of antioxidant agents, rise in inflammatory biomarkers, and decreases the cell viability. It has been demonstrated that 30% of iron in SWCNTs is able to generate free radicals within 15 min of exposure to epidermal keratinocytes in the presence of DMPO (5,5-dimethyl-1-pyrroline-1-oxide).[109] In a later study it was shown that higher amounts of catalyst generate higher concentrations of free radicals and increase inflammatory responses.[110] Additionally nickel alters the expression of the gene encoding the protein HIF1A, a factor of transcript involved in the regulation of inflammatory genes and apoptosis.[111] All studies on the toxicity of CNTs must than take into account the nature of the metallic catalyst and its percentage/quantity. It is difficult to obtain pure CNTs by removing all traces of catalysts and several methods can be employed to decrease residual catalysts including centrifugation, high-temperature annealing[112] and oxidation treatment by acid reflux.[113]

I.7.2 Effect of CNTs functionalization

Toxicity can be also influenced by the modification on CNTs surface. Only with the acid-treatment on CNTs surface, it is possible to introduce number of defect sites along the CNT surface (see above). Muller *et al*. changed the number of defect sites on MWCNTs by mechanical grinding and annealing at high temperature and demonstrated that acute pulmonary toxicity and genotoxicity increased after intratracheally administration of MWCNTs with a larger number of defect sites.[114] However, another study by Kagan *et al*. showed that oxidized SWCNTs can be biodegraded easier by myeloperoxidase enzyme, found in neutrophils and macrophages. The enzyme interacts with carboxylic sites on the nanotubes surface[115] and oxidized CNTs may be more biocompatible than pristine CNTs from this point of view. Following this pathway Sayes and co-workers examined cell viability in presence of oxidized and phenylated tubes. They discovered that the phenylated tubes exhibit lower toxicity, and this can be due to the hindering of the defect sides of the tubes.[116] Dumortier *at al*. have examined the toxicity of CNTs functionalized by 1,3-dipolar cycloaddition. They concluded that CNTs, fully soluble in aqueous culture media, did not modified primary immune cells viability *in vitro*.[117]

Also the CNTs surface area and their hydrophobic nature impact on the toxicity. The tubes, in fact, can potentially interact with numerous molecules like proteins, RNA, DNA, enzymes with toxic effects on the biological environment.[118] Dutta and co-workers found that the bovine or human serum albumin adsorption onto the CNT surface resulted in inflammatory responses after uptake by macrophage cells. Normally that effect occurs only when albumin adopts structurally changes or gets damaged.[119]

The effect of functionalization of the tubes highlights the importance of assessing toxicity profile for every type of new CNTs modification.

I.7.3 The length of carbon nanotubes

Finally, the CNTs length cannot be ignored. CNT sizes have an important effect on clearance. The length can range from nanometers up to millimeters. The exposure to long fiber-like material can induce dangerous damages in DNA and genetic mutations over a period of exposure, causing an extremely malignant form of cancer, mesothelioma. Symptoms of these bio-persistent fibers are the granulomas, which are the signs of oxidative stress, causing excessive fibrous tissue.[120]

Macrophage are the cells responsible for the removal of foreign material like CNTs from living organism. Fibers with a length exceeding 20 µm are extremely resistant to phagocytosis[121] and Poland *et al.* shown that CNTs as spherical or stellate shaped agglomerates with less than 20 µm have no significant damaging reactions compared to samples with individualized MWCNTs, agglomerates, and ropes of MWCNTs with lengths exceeding 20 µm.[120]

In conclusion, CNTs should be used without the presence of metal catalysts, should have an appropriate functionalization for the planned purpose with low surface oxidation, should present covered surface to effectively escape biointeractions, and should be short to avoid long retention times.

Bibliography

[1] S. Iijima; *Nature* **1991**, *354*, 56–58.

[2] D. Pantarotto, J. P. Briand, M. Prato, A. Bianco; *Chem. Commun.* **2004**, *7*, 16–17.

[3] Y. Zhang, Y. Bai, B. Yan; *Drug Discovery Today* **2010**, *15*, 428–435.

[4] N. W. Kam, H. Dai; *J. Am. Chem. Soc.* **2005** *127*, 6021–6026.

[5] B. G. P. Singh, C. Baburao, V. Pispati, H. Pathipati, N. Muthy, S. R. V. Prassana, B. Ganesh Rathode; *International Journal of Research in Pharmacy and Chemistry* **2012**, *2*, 523–532.

[6] Z. Liu, S. Tabakman, K. Welsher, H. Dai; *Nano Research* **2009**, *2*, 85–120.

[7] G. Seeta Rama Raju, Leah Benton, E. Pavitra, Jae Su Yu; *Chem. Commun.* **2015**, *51*, 13248–13259.

[8] H. Gong, R. Peng, and Z. Liu; *Advanced Drug Delivery Reviews* **2013**, *65*, 1951–1963.

[9] J.–C. Charlier, X. Blase, A. De Vita, R. Car; *Appl. Phys. A* **1999**, *68*, 267–273.

[10] M. S. Dresselhaus, G. Dresselhaus, R. Saito, A. Jorio; *Physics Reports* **2005**, *409*, 47–99.

[11] L. Ortolani, F. Houdellier, M. Monthioux, V. Morandi; *Carbon* **2010**, *48*, 3050–3056.

[12] A. Thess, P. Nikolaev, H. Dai, C. Xu, A. G. Rinzler, D. T. Colbert, G. E. Scuseria, R. E. Smalley; *Science* **1996**, *273*, 483–487.

[13] J. W. G. Wildoer, L. C. Venema, A. G. Rinzler, R. E. Smalley, C. Dekker; *Nature* **1998**, *39*, 59–62.

[14] H. Huang, M. Zou, X. Xu, F. Liu, N. Li; *Trends in Analytical Chemistry* **2011**, *30*, 1109–1119.

[15] S. M. Bachilo, M. S. Strano, C. Kittrell, R. H. Hauge, R. E. Smalley, R. B. Weisman; *Science* **2002**, *298*, 2361–2366.

[16] Z. Luo, F. Papadimitrakopoulos, S. K. Doorn; *Phys. Rev. B.* **2007**, *75*, 205438.

[17] J. W. Kang, F. T. Nguyen, N. Lue, R. R. Dasari, D. A. Heller; *Nano Lett.* **2012**, *12*, 6170–6174.

[18] R. Andrews, D. Jacques, D. Qian, T. Rantell; *Acc. Chem. Res.* **2002**, *35*, 1008–1017.

[19] S. Niyogi, M. A. Hamon, H. Hu , B. Zhao, P. Bhowmik, R. Sen, M. E. Itkis, R. C. Haddon; *Acc. Chem. Res.* **2002**, *35*, 1105–1113.

[20] Mi. Sola, J. Mestres, M. Duran; *J. Phys. Chem.* **1995**, *99*, 10752–10758.

[21] A.V. Narlikar, Y.Y. Fu, Oxford Handbook of Nanoscience and Technology: Vol. 1: Basic Aspects, Oxford University Press, **2010**.

[22] A. Hirsch, O. Vostrowsky; *Top Curr. Chem.* **2005**, *245*, 193– 237.

[23] J. L. Bahr, E. T. Mickelson, M. J. Bronikowski, R. E. Smalley J. M. Tour; *Chem. Commun.* **2001**, 193–194.

[24] R. H.Baughman, A.A. Zakhidov, W. A. De Heer; *Science* **2002**, *297*, 787–792.

[25] K. Cho, X. Wang, S. Nie, Z. G. Chen, D. M. Shin; *Clinical Cancer Research* **2008**, *14*, 1310–1316.

[26] T. Dvir, B. P. Timko, D. S. Kohane, R. Langer; *Nature Nanotechnology* **2011**, *6*, 13–22.

[27] M. F. Islam, E. Rojas, D. M. Bergey, A. T. Johnson, A. G. Yodh; *Nano Lett.* **2003**, *3*, 269–273.

[28] H. Dodziuk, A. Ejchart, W. Anczewski, H. Ueda, E. Krinichnaya, Grygoriy Dolgonosa, W. Kutner; *Chem. Commun.* **2003**, 986–987.

[29] Y. Sun, S. R. Wilson, D. I. Schuster; *J. Am. Chem. Soc.* **2001**, *123*, 5348.

[30] D. Chattopadhyay, I. Galeska, F. Papadimitrakopoulos; *J. Am. Chem. Soc.* **2003**, *125*, 3370.

[31] T. Fujigaya, N. Nakashima; *Sci. Technol. Adv. Mater.* **2015**, *16*, 024802.

[32] A. Star, Y. Liu, K. Grant, L. Ridvan, J. F. Stoddart, D. W. Steuerman, M. R. Diehl, A. Boukai, J. R. Heath; *Macromolecules* **2003**, *36*, 553.

[33] A. B. Dalton, C. Stephan, J. N. Coleman, B. McCarthy, P. M. Ajayan, S. Lefrant, P. Bernier, W. J. Blau, H. J. Byrne; *J. Phys. Chem. B* **2000**, *104*, 10012.

[34] S. Park, H.-S. Yang, D. Kim, K. Job, S. Jon; *Chem. Commun.* **2008**, 2876–2878.

[35] S. S. Karajanagi, A. A. Vertegel, R. S. Kane, J. S. Dordick; *Langmuir* **2004**, *20*, 11594.

[36] M. Zheng, A. Jagota, M. S. Strano, A. P. Santos, P. Barone, S. G. Chou, B. A. Diner, M. S. Dresselhaus, R. S. McLean, G. B. Onoa, G. G. Samsonidze, E. D. Semke, M. Usrey, D. J. Walls; *Science* **2003**, *302*, 1545.

[37] Z. Mohammadi, S. F. Aghamiri, A. Zarrabi, M. Reza Talaie; *Chemical Physics Letters* **2015**, *642*, 22–28.

[38] M. S. C. Mazzoni, H. Chacham, P. Ordejon, D. Sanchez-Portal, J. M. Soler, E. Artacho; *Phys. Rev. B* **1999**, *60*, R2208.

[39] P. G. Collins, Defects and Disorder in Carbon Nanotubes, Oxford Handbook of Nanoscience and Technology: Frontiers and Advances. A. V. Narlikar, Y. Y. Fu, Eds., Oxford Univ. Press, Oxford, **2009.**

[40] M. F. Yu, O. Lourie, M. J. Dyer, K. Moloni, T. F. Kelly, R. S. Ruoff; *Nature*, **2006**, *442*, 282–286.

[41] J. Zhang, H. Zou, Q. Qing, Y. Yang, Q. Li, Z. Liu, X. Guo, Z. Du; *J. Phys. Chem. B* **2003**, *107*, 3712–3718.

[42] A. Hirsch; *Angew, Chem, Int.* **2002**, *41*, 1853–1859.

[43] P. Ajayan, S. Iijima; *Nature* **1993**, *361*, 333–334.

[44] F. Simon, H. Kuzmany, H. Rauf, T. Pichler, J. Bernardi, H. Peterlik, L. Korecz, F. Fulop, A. Janossy; *Chemical Physics Letters* **2004**, *383*, 362–367.

[45] S. Tsang, Y. Chen, P. Harris, M. Green; *Nature* **1994**, *372*, 159–162.

[46] M. V. Kharlamova, J. J. Niu; *Appl. Phys. A* **2012**, *109*, 25–29.

[47] K. Yanagi, Y. Miyata, H. Kataura; *Adv. Mater.* **2006**, *18*, 437–441.

[48] H. Kataura, Y. Maniwa, M. Abe, A. Fujiwara, T. Kodama, K. Kikuchi, H. Imahori, Y. Misaki, S. Suzuki, Y. Achiba; *Appl. Phys. A* **2002**, *74*, 349–354.

[49] A. I. Chernov, P. V. Fedotov, A. V. Talyzin, I. S. Lopez, I. V. Anoshkin, A. G. Nasibulin, E. I. Kauppinen, E. D. Obraztsova; *ACS Nano* **2013**, *7*, 6346–6353.

[50] B. W. Smith, M. Monthioux, D. E. Luzzi; *Nature* **1998**, *396*, 323–324.

[51] P. M. Ajayan, S. Lijima; *Nature* **1993**, *361*, 333–334.

[52] Y. Gogotsi, N. Naguib, J. A. Libera; *Chemical Physics Letters* **2002**, *365*, 354–360.

[53] M. Terrones; *Nat. Chem.* **2010**, *2*, 82–83.

[54] C. Xu, J. Sloan, G. Brown, S. Bailey, V. C. Williams, S. Friedrichs, K. S. Coleman, E. Flahaut, J. L. Hutchison, R. E. Dunin-Borkowski, M. L. H. Green; *Chem. Commun.* **2000**, 2427–2428.

[55] E. Dujardin, T. W. Ebbesen, H. Hiura, K. Tanigaki; *Science* **1997**, *265*, 1850–1852.

[56] B. Ballesteros, G. Tobias, M. A. H. Ward, M. L. H. Green; *J. Phys. Chem. C* **2009**, *113*, 2653–2656.

[57] T. Nakajima, S. Kasamatsu, Y. Matsuo; *Eur. J Solid. Inorg. Chem.* **1996**, *33*, 831–840.

[58] K. F. Kelly, I. W. Chiang, E. T. Mickelson, R. H. Hauge, J. L. Margrave, X. Wang, G. E. Scuseria, C. Radloff, N. J. Halas; *Chemical Physics Letters* **1999**, *313*, 445–450.

[59] L. Valentini, D. Puglia, I. Armentano, J. M. Kenny; *Chem. Phys. Lett.* **2005**, *403*, 385–389.

[60] M. Holzinger, O. Vostrowsky, A. Hirsch, F. Hennrich, M. Kappes, R. Weiss, F. Jellen; *Angew. Chem. Int. Ed.* **2001**, *40*, 4002–4005.

[61] J. L. Bahr, J. Yang, D. V. Kosynkin, M. J. Bronikowski, R. E. Smalley, J. M. Tour; *J. Am. Chem. Soc.* **2001**, *123*, 6536–6542.

[62] L. Zhang, J. Yang, C. L. Edwards, L. B. Alemany, V. N. Khabashesku, A. R. Barron; *Chem. Commun.* **2005**, 3265–3267.

[63] G. Viswanathan, N. Chakrapani, H. Yang, B. Wei, H. Chung, K. Cho, C. Y. Ryu, P. M. Ajayan; *J. Am. Chem. Soc.* **2003**, *125*, 9258–9259.

[64] R. Blake, Y. K. Gunko, J. Coleman, M. Cadek, A. Fonseca, J. B. Nagy, W. J. Blau; *J. Am. Chem. Soc.* **2004**, *126*, 10226.

[65] S. Chen, W. Shen, G. Wu, D. Chen, M. Jiang; *Chem. Phys. Lett.* **2005**, *402*, 312.

[66] I. W. Chiang, B. E. Brinson, R. E. Smalley, J. L. Margrave, R. H. Hauge; *J. Phys. Chem. B* **2001**, *105*, 7938.

[67] P. Papakonstantinou, R. Kern, L. Robinson, H. Murphy, J. Irvine, E. McAdams, J. McLaughlin; *Fuller. Nanotub. Carbon Nanostruct.* **2005**, *13*, 91–108.

[68] J. Chattopadhyay, S. Chakraborty, A. Mukherjee, R. Wang, P. S. Engel, W. E. Billups; *Phys. Chem. C* **2007**, *111*, 17928–17932.

[69] J. L. Bahr, J. M. Tour; *Chem. Mater.* **2001**, *13*, 3823–3824.

[70] C. A. Dyke, J. M. Tour; *Nano Lett.* **2003**, 3, 1215–1218.

[71] F. Pennetreau, C. Vriamont, B. Vanhorenbeke, O. Riant, S. Hermans; *Eur. J. Org. Chem.* **2015**, 1804–1810.

[72] K. S. Coleman, Sam R. Bailey, S. Fogden, M. L. H. Green; *J. Am. Chem. Soc.* **2003**, *125*, 8722–8723.

[73] T. Umeyama, N. Tezuka, M. Fujita, Y. Matano, N. Takeda, K. Murakoshi, K. Yoshida, S. Isoda, H. Imahori; *J. Phys. Chem. C* **2007**, *111*, 9734–9741.

[74] J. Chen, M. A. Hamon, H. Hu, Y. Chen, A. M. Rao, P. C. Eklund, R. C. Haddon; *Science* **1998**, *282*, 95–98.

[75] V. Georgakilas, K. Kordatos, M. Prato. D. M. Guldi, M. Holzinger, A. Hirsch; *J. Am. Chem. Soc.* **2002**, *124*, 760–761.

[76] D. Pantarotto, R. Singh, D. McCarthy, M. Erhardt, J. P. Briand, M. Prato, K. Kostarelos, A. Bianco; *Angew. Chem. Int. Ed.* **2004**, *43*, 5242 –5246.

[77] N. Saito, Y. Usui, K. Aoki, N. Narita, M. Shimizu, K. Hara, N. Ogiwara, K. Nakamura, N. Ishigaki, H. Kato, S. Taruta, M. M. Endo; *Chem. Soc. Rev.* **2009**, *38*, 1897–1903.

[78] J. Meng, L. Song, J. Meng, H. Kong, G. Zhu, C. Wang, L. Xu, S. Xie, H. Xu; *J. Biomed. Mater. Res. A* **2006**, *79A*, 298–306.

[79] A. O. Lobo, M. A. F. Corat, E. F. Antunes, M. B. S. Palma, C. Pacheco-Soares, E. E. Garcia, E. J. Corat; *Carbon* **2010**, *48*, 245–254.

[80] P. Galvan-Garcia, E. W. Keefer, F. Yang, M. Zhang, S. Fang, A. A. Zakhidov, R. H. Baughman, M. I Romero; *J. Biomater. Sci. Polym. Ed.* **2007**, *18*, 1245–1261.

[81] G. Cellot, E. Cilia, S. Cipollone, V. Rancic, A. Sucapane, S. Giordani, L. Gambazzi, H. Markram, M. Grandolfo, D. Scaini, F. Gelain, L. Casalis, M. Prato, M. Giugliano, L. Ballerini; *Nat. Nano* **2009**, *4*, 126–133.

[82] T.-I Chao, S. Xiang, J. F. Lipstate, C. Wang, J. Lu; *J. Adv. Mater.* **2010**, *22*, 3542–3547.

[83] E. B. Malarkey, R. C. Reyes, B. Zhao, R. C. Haddon, V. Parpura; *Nano Lett.* **2009**, *9*, 264–268.

[84] X. Zhang, S. Prasad, S. Niyogi, A. Morgan, M. Ozkan, C. S. Ozkan; *Sensors Actuators B* **2005**, *106*, 843–850.

[85] D. Rugar, H. J. Mamin, M. H. Sherwood, M. Kim, C. T. Rettner, K. Ohno, D. D. Awschalom; *Nat. Nanotechnol.* **2011**, *6*, 120–124.

[86] J. A. Roman, T. L. Niedzielko, R. C. Haddon, V. Parpura, C. L. Floyd; *J. Neurotrauma* **2011**, *28*, 2349–2362.

[87] D. Pantarotto, J.-P. Briand, M. Prato, A. Bianco; *Chem. Commun.* **2004**, 16–17.

[88] N. W. S. Kam , T. C. Jessop, P. A. Wender, H. Dai; *J. Am. Chem. Soc.* **2004**, *126*, 6850–6851.

[89] A.Di Crescenzo, D. Velluto, J. A. Hubbell, A. Fontana; *Nanoscale* **2011**, *3*, 925–928.

[90] C. L. Lay, H. Q. Liu, H. R. Tan, Y. Liu; *Nanotechnology* **2010**, *21*, 065101.

[91] J. Zhang, X.-J. Lv, X. Jia, Y.-L. Deng, H. Qing, H-Y Xie; *J. Nanosci. Nanotechnol.* **2011**, *11*, 953–958.

[92] N. Wong, S. Kam , Z. Liu, H. Dai; *J. Am. Chem. Soc.* **2005**, *127*, 12492–12493.

[93] C. Samorì, H. Ali-Boucetta, R. Sainz, C. Guo, F. M. Toma, C. Fabbro, T. da Ros, M. Prato, Kostas Kostarelos, A. Bianco; *Chem. Commun.* **2010**, *46*, 1494–1496.

[94] P. Chaudhuri, S. Soni, S. Sengupta; *Nanotechnology* **2010**, *21*, 025102.

[95] N. G. Sahoo, H. Bao, Y. Pan, M. Pal, M. Kakran, H. K. Feng Cheng, L. Li, L. Poh Tan; *Chem. Commun.* **2011**, *47*, 5235–5237.

[96] X. Shi, S. H. Wang, M. Shen, M.E. Antwerp, X. Chen, C. Li, E. J. Petersen, Q. Huang, W. J. Weber Jr., J. R. Baker Jr; *Biomacromolecules* **2009**, *10*, 1744–1750.

[97] Z. Sobhani, R. Dinarvand, F. Atyabi, M. Ghahremani, M. Adeli; *Int. J. Nanomedicine* **2011**, *6*, 705–719.

[98] S. Hampel, D. Kunze, D. Haase, K. Krämer, M. Rauschenbach, M. Ritschel, A. Leonhardt, J. Thomas, S. Oswald, V. Hoffmann, B. Büchner; *Nanomedicine* **2008**, *3*, 175–182.

[99] M. Ferrari; *Nat. Rev. Cancer* **2005**, *5*, 161–171.

[100] Z. Liu, X. Sun, N. Nakayama-Ratchford, H. Dai; *J. ACS Nano* **2007**, *1*, 50–56.

[101] J. M Tan, J. Biau Foo, S. Fakurazi, M. Z. Hussein; *Adv. Drug Delivery Rev.* **2011**, *63*, 1332–1339.

[102] A. A. Bhirde, V.h Patel, J. Gavard, G. Zhang, A. A. Sousa, A. Masedunskas, R. D. Leapman, R. Weigert, J. S. Gutkind, J. F. Rusling; *ACS Nano* **2009**, *3*, 307–316.

[103] M. R. McDevitt, D. Chattopadhyay, B. J. J. Kappel; *Nucl. Med.* **2007**, *48*, 1180–1189.

[104] J. Van den Bossche, W. T. Al-Jamal, B. Tian, A. Nunes, C. Fabbro, A. Bianco, M. Prato, K. Kostarelos; *Chem. Commun.* **2010**, *46*, 7379–7381.

[105] B. Chen, H. Zhang, C. Zhai, N. Du, C. Sun, J. Xue, D. Yang, H. Huang, B. Zhang, Q.J. Xie; *Mater. Chem.* **2010**, *20*, 9895–9902.

[106] O. Vittorio, S. L. Duce, A. Pietrabissa, A. Cuschieri; *Nanotechnology* **2011**, *22*, 095706.

[107] A. Al Faraj, K. Cieslar,G. Lacroix, S. Gaillard, E. Canet-Soulas, Y. Crémillieux; *Nano Lett.* **2009**, *9*, 1023–1027.

[108] S. Y. Hong, G. Tobias, K. T. Al-Jamal, B. Ballesteros, H. Ali-Boucetta, S. Lozano-Perez, P. D. Nellist, R. B. Sim, C. Finucane, S. J. Mather, M. L. H. Green, K. Kostarelos, B. G. Davis; *Nature materials* **2010**, *9*, 485–490.

[109] A. A. Shvedova, V. Castranova, E. R. Kisin, D. Schwegler-Berry, A. R. Murray, V. Z. Gandelsman, A. Maynard, P. Baron; *J. Toxicol. Environ. Health A* **2003**, *66*, 1909–1926.

[110] A. R. Murray, E. Kisin, S. S. Leonard, S. H. Young, C. Kommineni, V. E. Kagan, V. Castranova, A. A. Shvedova; *Toxicology* **2009**, *257*, 161–171.

[111] M. Kaczmarek, O. A. Timofeeva, A. Karaczyn, A. Malyguine, K. S. Kasprzak, K. Salnikow; *Free Radic. Biol. Med.* **2007**, *42*, 1246–1257.

[112] W. Huang, Y. Wang, G. Luo, F. Wei; *Carbon* **2003**, *41*, 2585–2590.

[113] Y. Li, X. Zhang, J. Luo, W. Huang, J. Cheng, Z. Luo, T. Li, F. Liu, G. Xu, X. Ke; *Nanotechnology* **2004**, *15*, 1645–1649.

[114] J. Muller, F. Huaux, A. Fonseca, J. B. Nagy, N. Moreau, M. Delos, E. Raymundo-Piñero, F. Béguin, M. Kirsch-Volders, I. Fenoglio, B. Fubini, D. Lison; *Chem. Res. Toxicol.* **2008**, *21*, 1698–1705.

[115] V. E. Kagan, N. V. Konduru, W. Feng, B. L. Allen, J. Conroy, Y. Volkov, I. I. Vlasova, N. A. Belikova, N. Yanamala, A. Kapralov, Y. Y. Tyurina, J. Shi, E. R. Kisin, A. R. Murray, J. Franks, D. Stolz, P. Gou, J. Klein-Seetharaman, B. Fadeel, A. Star, A.A. Shvedova; *Nat. Nanotechnol.* **2010**, *5*, 354–359.

[116] C. M. Sayes, F. Liang, J. L. Hudson, J. Mendez, W. Guo, J. M. Beach, V. C. Moore, C. D. Doyle, J. L. West, W. E. Billups, K. D. Ausman, V. L. Colvin; *Toxicol. Lett.* **2006**, *161*, 135–142.

[117] H. Dumortier, S. Lacotte, G. Pastorin, R. Marega, W. Wu, D. Bonifazi, J.-Paul Briand, M. Prato, S. Muller, A. Bianco; *Nano Lett.* **2006**, *6*, 1522–1528.

[118] D. B. Warheit, B. R. Laurence, K. L. Reed, D. H. Roach, G. A. M. Reynolds, T. R. Webb; *Toxicol. Sci.* **2004**, *77*, 117–125.

[119] D. Dutta, S. K. Sundaram, J. G. Teeguarden, B. J.Riley, L. S. Fifield, J. M.Jacobs, S. R. Addleman, G. A. Kaysen, B. M. Moudgil, T. J. Weber; *Toxicol. Sci.* **2007**, *100*, 303–315.

[120] C. A. Poland, R. Duffin, I. Kinloch, A. Maynard, W. A. H. Wallace, A. Seaton, V. Stone, S. Brown, W. MacNee, K. Donaldson; *Nat. Nanotechnol.* **2008**, *3*, 423–428.

[121] K. Kostarelos; *Nat. Biotechnol.* **2008**, *26*, 774–776.

II. Covalent functionalization of carbon nanotubes

II.1 Introduction

CNTs can be considered very attractive in various nanotechnological applications. However, these applications of CNTs are limited by poor solubility in many solvents and difficult manipulation. One of the method, to overcome these difficulties is covalent modification of CNTs. For an application in biological media as a nanocarrier for radioactive delivery, CNTs requires fast methodology for surface modification to enhance dispersibility and to create nontoxic platform for further modifications.

Up to now, there have been many approaches reported to modify the surface of CNTs (see Introduction, Covalent functionalization). Recently, CNTs for biomedical application were functionalized along their sidewalls using 1,3-dipolar cycloaddition. This chemical modification method has been well reported. Introduction on the sidewalls of ethylenglycolic chains ending with amine functions, provides anchoring sites on the nanotube surface, enhancing their biocompatibility and improving solubility in aqueous and organic solvents.[1] Nevertheless, the reaction usually requires harsh conditions and long reaction time.

It is an important challenge for us to find a reaction which 1) will work on SWCNTs and MWCNTs with a high degree of functionalization; 2) will not cause damages of the tube leading to leakage of internal material of filled tubes; 3) can be applied in a large scale and 4) will be fast to be convenient for functionalization of CNTs filled with short life time isotopes.

In this study, we reported a route to find the best reaction for functionalization of SWCNTs and MWCNTs to be conveniently used on filled CNTs.

By the presented attempts of functionalization we were testing several methodologies using 1,3-dipoles and aryl radicals to achieve the ultimate goal of fastest and most suitable functionalization.

II.2 Cycloaddition

CNTs structure limits the number of organic reactions that could be applied on their sidewall. A lot of efforts were put to functionalize this aromatic construction. The principle of covalent methods used for this purpose is generally based on diminishing their aromaticity. Some examples include oxidative dearomatization, reductions or Birch reduction as it was mentioned in the previous chapter. An alternative method for dearomatization process, would involve several cycloaddition reactions with 1,3-dipoles.

1,3-Dipoles consist of elements from main groups IV, V, and VI like nitrogen, carbon and oxygen to form limited number of structures. Two types of 1,3-dipoles can be obtained: allyl anion type which includes ozone, azomethine ylide, and nitrone. The second type is propargyl/allenyl anion type: nitrile ylide, nitrile imine, nitrile oxide, diazomethane and methyl azide (Scheme 1).
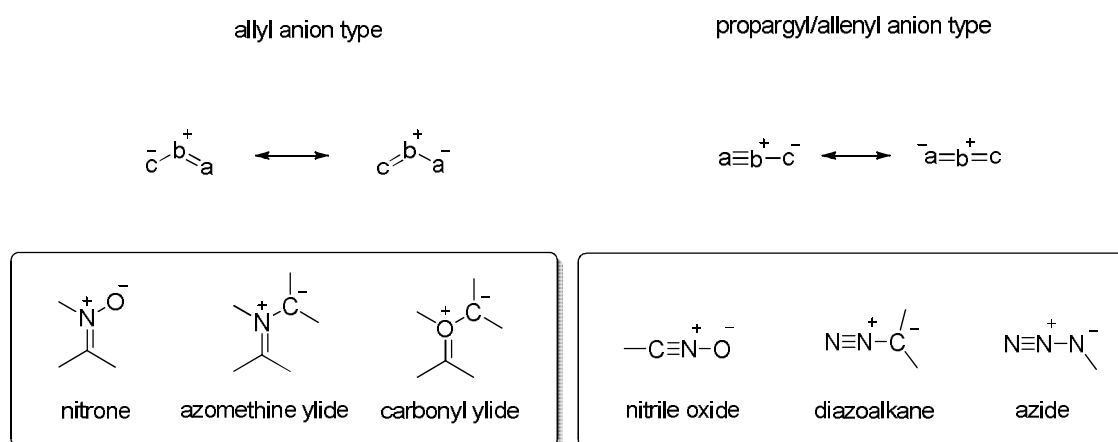
Scheme 1. Classification of 1,3-dipoles.

Most studies in the field of functionalization of CNTs were dedicated to azomethine ylide. Azomethine ylides are unstable and have to be prepared *in situ*. Several methods were developed for their synthesis, for example proton abstraction from imine derivatives of α-amino acids, thermolysis or photolysis of aziridines and dehydrohalogenation of immonium salts. Nitrile oxides represent the second type of 1,3-dipole used for CNTs functionalization, even if in a less

extent way, with only limited application in the synthesis of CNTs derivatives. They are easy available from aldoximes or primary nitro compounds, but most nitrile oxides must be prepared *in situ*, because of high reactivity and rapid dimerization. Even though, over last few years the first examples of application of this active species on CNTs have appeared in the literature.

A review of the literature associated with the 1,3-dipolar cycloaddition reactions of azomethine ylides and nitrile oxide on CNTs is presented here. Our research was devoted to develop the reaction which would be a fast and convenient method for effective functionalization of CNTs.

II.2.1 1,3-Dipolar cycloaddition of azomethine ylide

1,3-Dipolar cycloaddition to aromatic dipolarophile can be demonstrated by reaction of azomethine ylide with a benzenoid aromatic system that would give an pyrrolidine derivative (Scheme 2).
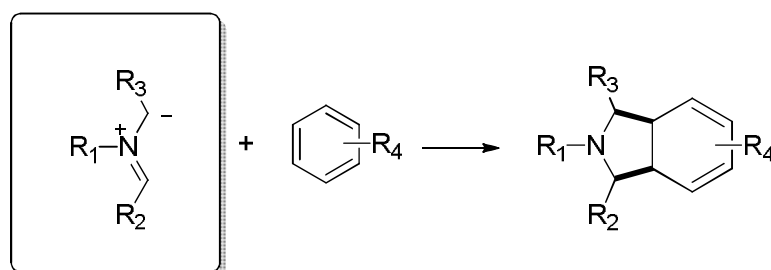
Scheme 2. 1,3-dipolar cycloaddition reaction of an azomethine ylide with a benzenoid aromatic system.

Azomethine ylide can be represented by four electrons distributed over three parallel π orbitals of a C-N-C group of 1,3-dipole. This dipole can appear in four resonance forms (Scheme 3):
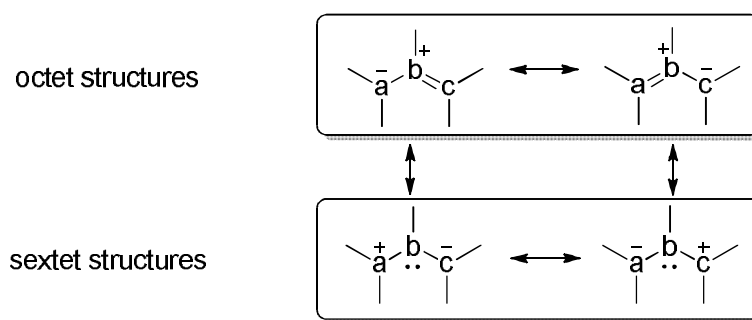
Scheme 3. Four electrons distributed over three parallel π orbitals of a C-N-C group of 1,3-dipole.

Calculations of energies of various orbitals revealed that azomethine ylides are electron-rich species characterized by relatively high-energy HOMOs and LUMOs, preferentially reacting with electron-deficient alkenes due to a narrow $HOMO_{dipole}$ - $LUMO_{dipolarophile}$ gap. HOMO-controlled reactions are accelerated by electron-releasing substituent in the dipole and electron-withdrawing groups in the dipolarophiles. The stereochemical outcome of the cycloaddition of azomethine ylides is dependent on the geometries of the dipoles as well as the dipolarophiles.

The ylides can be classified as stabilized or non-stabilized either by electron-withdrawing/electron-donating groups at the appropriate termini of the ylide or by *N*-metalation.[2] The stabilized azomethine ylide can be generated from several compounds (Scheme 4).
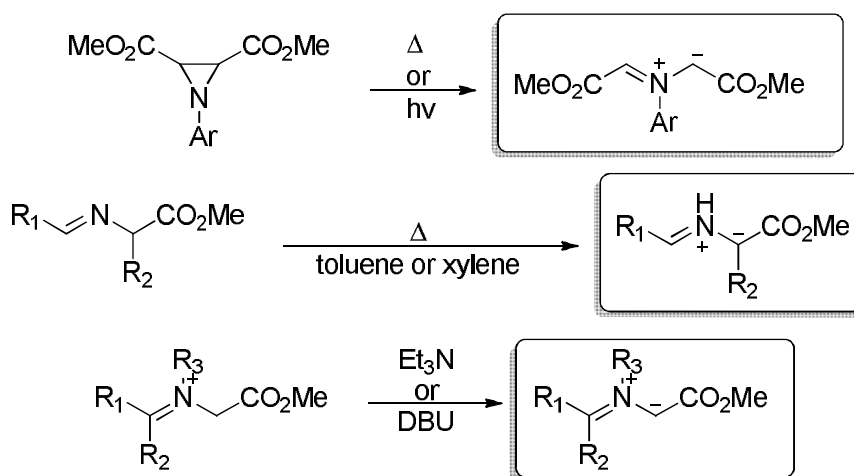
Scheme 4. Examples of stabilized azomethine ylides.

45

The heating of aziridine with an excess of phenanthrene at 100 °C for 24 h afforded a single cycloadduct (Scheme 5). The stereochemistry of product was taken as evidence that azomethine ylide was the reactive species. The cycloaddition reactions of linear polycyclic aromatic systems were also explored. The reaction of aziridine with an excess of anthracene in refluxing chlorobenzene for 24 h led to a *mono* adduct, isolated in 8% yield, and two *bis* adducts, isolated in 22% and 40% yield, respectively.[3]
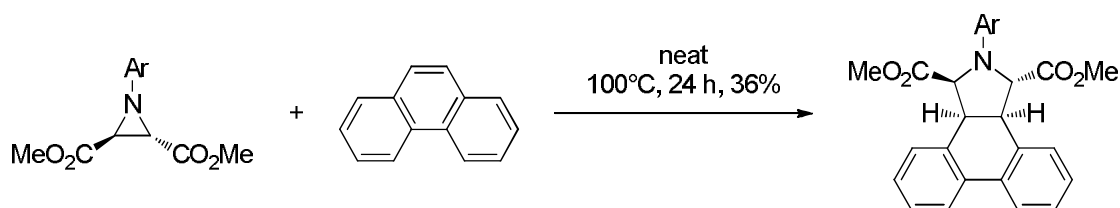
Scheme 5. Aziridine with an excess of anthracene in refluxing chlorobenzene.[3]

Considering the high reactivity of this dipole, reaction was applied also on single-wall carbon nanotubes (Scheme 6). Consider the strong microwave absorption of CNTs the irradiation in this range was applied to enhance the rate of reactions and improves product yields. In the reaction an excess of aziridine with respect to CNTs was used. The mixture was heated for 1 h under microwave irradiation, affording one functional group for about 76 carbon atoms.
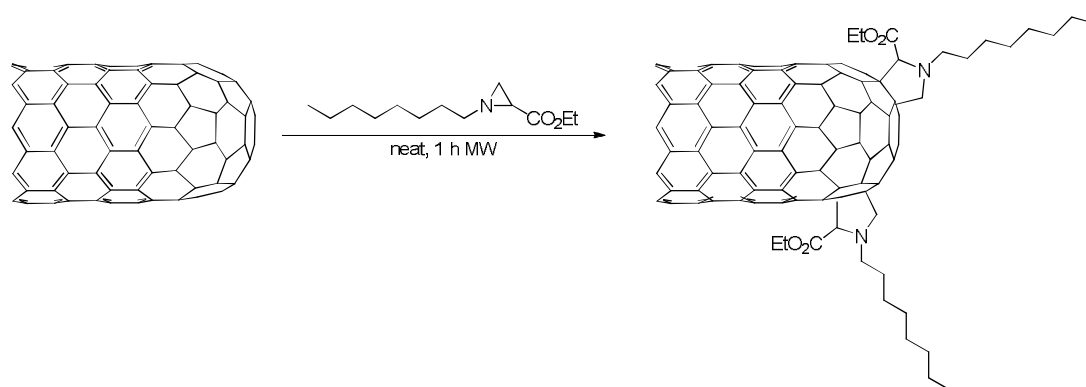
Scheme 6. Reaction of aziridine with CNTs under microwave.[4]

The 1,3-dipolar cycloaddition of non-stabilized azomethine ylides, generated by decarboxylative condensation of amino acids and formaldehyde is

perhaps the most straightforward, convergent approach to unsaturated system (Scheme 7).
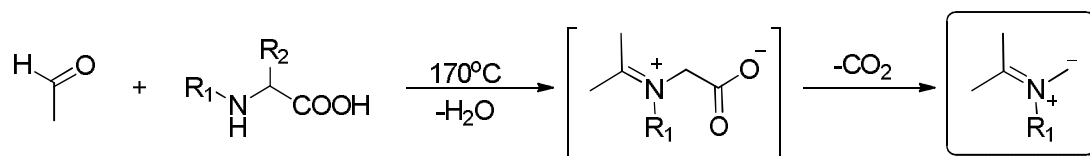
Scheme 7. Examples of non-stabilized azomethine ylides.

The cycloaddition of this 1,3-dipole with the indole as a dipolarophile is one of the example of the application of this reaction on unsaturated system (Scheme 8).[5] Although 3-nitroindoles with sarcosine or *N*-benzylglycine and formaldehyde afforded reasonable yields of the respective cycloadducts.
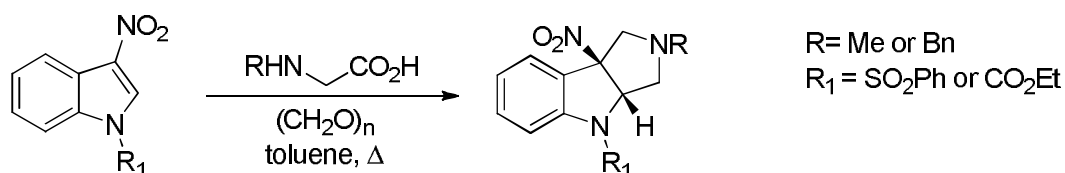
Scheme 8. The treatment of indole with the azomethine ylide generated in situ from sarcosine and paraformaldehyde in refluxing toluene.

No reaction was observed between the azomethine ylide from sarcosine and paraformaldehyde with 1-(phenylsulfonyl)indole, 3-cyano-1-(phenylsulfonyl)indole or 1-benzyl-3-nitroindole. A major conclusion is that the presence of the electron withdrawing nitro group and an electron withdrawing protecting group on the indole nitrogen can significantly increased the dipolarophilic reactivity of the indole to the azomethine ylide. The next aspect, which is very important, is that azomethine ylides generated from secondary amino acid derivatives are more effective as 1,3-dipoles then the primary one. The glycine and paraformaldehyde did not provided a cycloadduct.

The cycloaddition of non-stabilized azomethine ylide was successfully applied by Georgakilas *et al.* on polyaromatic structures such as CNTs in particular SWCNTs, oxidized SWCNTs and MWCNTs (Scheme 9).[6]

R \ R₁	$-H$	$\langle\rangle$—O	pyrene
(triethylene glycol chain)	✓	✓	✓
(alkyl chain)	✓	-	-
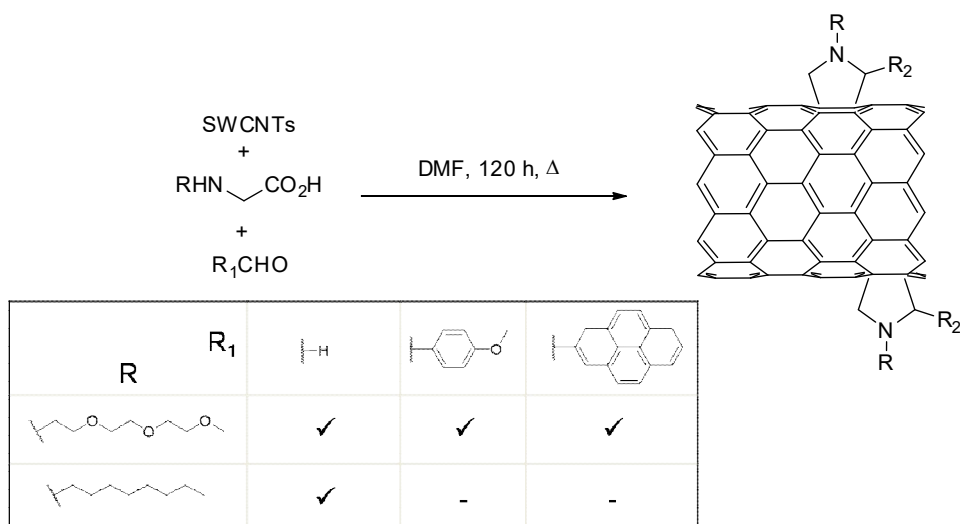
Scheme 9. 1,3-Dipolar cycloaddition of azomethine ylides, generated by condensation of an α-amino acid and an aldehyde.[6]

CNTs dispersed in DMF were treated for 5 days in the presence of an aldehyde and α-amino acid derivative. The reaction resulted in the formation of substituted pyrrolidine moieties on the sidewall. Using UV-Vis absorption and fluorescence experiments, it has been estimated that pyrrolidine moiety is introduced on the CNTs lattice.[6]

In order to reduce the reaction time to the order of minutes, an alternative microwave-induced reaction was proposed by Wang *et al.*[7] 1,3-Dipolar cycloaddition of SWCNTs was carried out under microwave conditions in three cycles for 5 minutes, with three additions of the α -amino acid. The microwave irradiation was also applied to functionalize MWNCTs by 1,3-dioplar cycloaddition. This heating method was found to be highly efficient for MWNCTs functionalized previously with solubilizing ester units, but was less useful for pristine MWNCTs.[8]

The azomethine-based functionalization sequence has become an important tool for CNTs sidewall functionalization due to its versatility. In principle, this method allows the attachment of any moiety to the carbon framework of the CNTs by a simple differentiation of the chemical structure of the staring material. We decided to explore an alternative methodology for

functionalization of CNTs. Among on the variety of the generation of non-stabilized azomethine ylides[9] involving the desilylation of appropriately substituted *N*-(silylmethyl)amine derivatives appeared particularly useful considering the ready availability of the starting material and the mild conditions required for the generation of the ylide.[10] As predicted by the principles of Frontier Molecular Orbital (IWO) theory these non-stabilized ylides readily react with electron efficient alkenes providing access to a wide array of pyrrolidines.

II.2.2 Results of cycloaddition of azomethine ylide

Our approach to develop the efficient method of functionalization of CNTs by non-stabilized azomethine ylides was inspired by the simplicity of the methodology already described for fullerenes.[11] In the reported reaction, *N*-benzyl azomethine ylide was used to functionalize C$_{60}$, giving C$_{60}$-fused *N*-benzylpyrrolidine in good yield. *N*-Benzyl azomethine ylide was generated *in situ* by the desilylation of *N*-benzyl-*N*-(methoxymethyl)-*N*-[(trimethylsilyl)methyl]amine catalyzed by trifluoroacetic acid.

As first, we used SWCNTs synthesized by HiPCO method[12] which were treated with concentrated HCl to remove any metal impurities.[13] The *N*-benzyl-*N*-(methoxymetyh)-*N*-[(trimethyl)methyl]amine is commercially available.
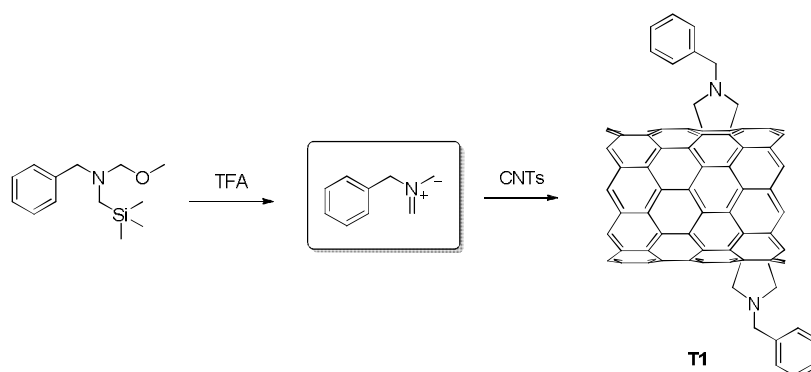
Scheme 10. The N-benzyl-N-(methoxymethyl)-N-[(trimethylsilyl)methyl]amine activated by trifluoroacetic.

Considering the previously reported functionalization on fullerenes in the first attempt we used excess (20 time in weight) of the amine respect to CNTs in dry, degassed DMF (Scheme 10). *N*-Benzyl azomethine ylide was generated *in situ* by desilylation of *N*-benzyl-*N*-(methoxymethyl)-*N*-[(trimethylsilyl)methyl]amine catalyzed by trifluoroacetic acid at 0 °C to room temperature. The reaction was carried out for 4 h at room temperature. We varied some reaction parameters in 15 experiments in total (Table 1). For the workup, the crude product was filtered through a 0.5 μm filter, and washed with several solvents to remove the unreacted impurities. The covalent functionalization was determined by TGA in nitrogen atmosphere, and Raman spectroscopy. The characterization of the pristine SWCNTs is presented in comparison to the functionalized material.

To find the best conditions for the reaction, temperature, time and solvents were investigated. Table 1 presents the best results obtained using *N*-benzyl-*N*-(methoxymethyl)-*N*-[(trimethylsilyl)methyl]amine.

Table 1. Results of functionalization of SWCNTs with azomethine ylide generated from of N-benzyl-N-(methoxymethyl)-N-[(trimethylsilyl)methyl]amine.[a]

Entry	Solvent	Time [h]	Temp [°C]	TGA Weight loss [%]	Functional group [μmol/g]	Raman $[I_D I_G^{-1} / I_{D0} I_{G0}^{-1}]$	Sample name
1	DMF	4	25	6.91	290	1.20	**T1**
2	*o*-DCB	4	25	8.45	404	1.15	**T2**
3	DMF	4	60	5.26	167	1.00	**T3**
4	*o*-DCB	4	60	5.70	200	1.00	**T4**
5	DMF	4	100	7.28	317	1.37	**T5**
6	*o*-DCB	4	100	6.32	246	1.20	**T6**
7	DMF	2	25	7.39	325	1.12	**T7**
8	*o*-DCB	2	25	7.49	333	1.07	**T8**
9	DMF	16	25	5.92	216	1.07	**T9**
10	*o*-DCB	16	25	5.84	210	1.07	**T10**
11	DMF	72	25	5.60	193	1.02	**T11**
12	*o*-DCB	72	25	6.78	280	1.02	**T12**
13	THF	4	25	8.41	401	1.08	**T13**
14	NMP	4	25	8.84	433	1.01	**T14**
15	DCM	4	25	7.35	322	1.16	**T15**

[**a**] Reaction conditions: **SWCNTs/amine** =1/20

Cycloaddition of azometine ylide is rather slow at room temperature. It drove us to conclude that the temperature of the reaction should be investigated. Two apriotic polar solvents were used in that investigation - anhydrous DMF and 1,2-Dichlorobenzene (*o*-DCB). We performed the experiments at three different temperatures: 25, 60 and 100 °C for 4 h. TGA of compounds **T1**-**6** presented a percent weight loss between 5.26-8.45% respectively (at 550 °C). Compared to 3% of the pristine SWCNTs, this corresponds to the presence of 167 - 404 µmol g^{-1} functional molecules on the surface (Figure 1).
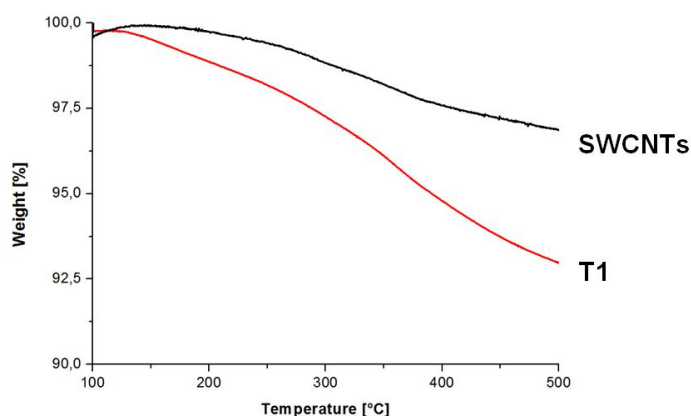
Figure 1. TGA analysis of pristine and functionalized SWCNTs (T1) with N-benzyl-N-(methoxymethyl)-N-[(trimethylsilyl)methyl]amine (nitrogen atmosphere).

Due to the functionalization the increase of the D-band was observed in the Raman spectra (Figure 2). While the spectrum of the starting material showed a small disorder mode at 1314 cm^{-1}, its intensity gradually increased with the number of sp^3 carbon atoms The highest ratio between functionalized and pristine material [$I_D I_G^{-1}$ / $I_{D0} I_{G0}^{-1}$] was achieved for **T1**, in which case the reaction was performed at room temperature for 4 h even though this is not in perfect agreement with the TGA data. Furthermore, for all samples, we observed small changes in radial breathing mode (RBM) in a spectral region below 400 cm^{-1}. Pristine SWCNTs and the one after functionalization have the same bands for both semiconducting nanotubes, above 230 cm^{-1}, and metallic nanotubes,

below this frequency. Although, some intensity variation can be observed, in particular, for metallic nanotubes which are probably the most reactive for this type of reaction.
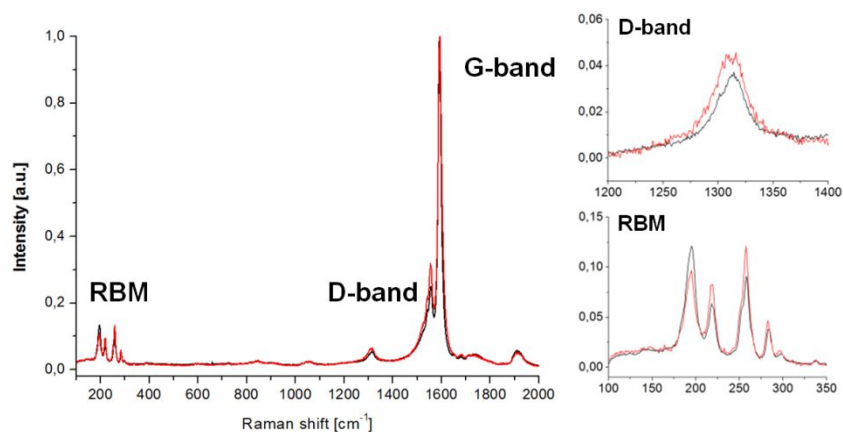
Figure 2. Raman spectra of SWCNTs (black-pristine SWCNTs; red-SWCNTs after functionalization T1). Laser excitation - 633 nm.

We examined also the time of reaction to understand if the reactivity of the ylide can be preserved with longer reaction times. We investigate 2, 4, 16 and 72 h in two solvents: DMF and o-DCB. TGA values at 550 °C were the highest for the shortest time (entries **7** and **8)** and similar to ones which were performed for 4 h (entries **1** and **2**) so prolonged time did not afford higher functionalization yield. We even observed that with longer reaction time, there was slightly decreased of functionalization. This fact could indicate the possibility of retrocycloaddition with time.

In the following experiments, the influence of solvent on the functionalization yield was examined. For this purpose we carried out the reactions for 4 h at room temperature with different anhydrous solvents like DMF (entry **1**), o-DCB (**2**), THF (**13**), N-Methyl-2-pyrrolidone (NMP) (**14**), DCM (**15**). Results from Table 1 demonstrate that the cycloaddition (Scheme 10) was achieved in all cases. Following the number of functional group on CNTs, calculated from TGA we can claimed that employment of DMF (entry **1**) and DCM (**15**) led to a negligible decrement of reaction's productivity, whereas all other solvents had a moderate high yield.

More recently it was established by Lee *et al.* that electron-withdrawing substituents have an important influence on the functionalization of polyaromatic structures.[14] The weaker electron-withdrawing ability of substituent, the lower reaction rates, and the longer reaction times.

To introduce an electron-withdrawing group on SWCNTs, we decided to oxidize them with acid treatment.[15] For the experiment, SWCNTs were suspended in a 3:1 mixture of concentrated H_2SO_4 and HNO_3 and stirred for 24 h. The resultant suspension was then diluted with deionized water and filtered to obtain **T16** (Scheme 11).
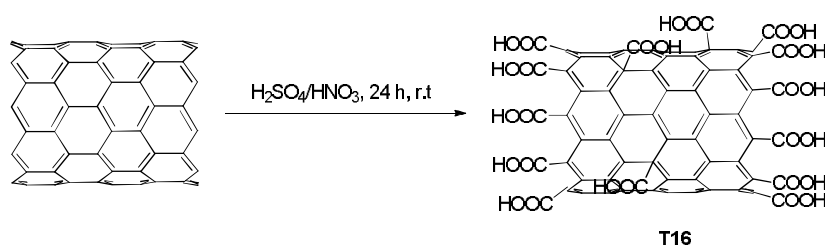
Scheme 11. Oxidation of SWCNTs.

By oxidation process, we introduced carboxylic groups which could increase their reactivity for cycloaddition of non-stabilized azomethine ylide generated from trimethylsilylmethylamine in presence of trifluoroacetic acid. For the reaction we used **T16** and commercially available *N*-benzyl-*N*-(methoxymethyl)-*N*-[(trimethylsilyl)methyl]amine. The reaction was carried out in DCM for 4 h at room temperature (Scheme 12).
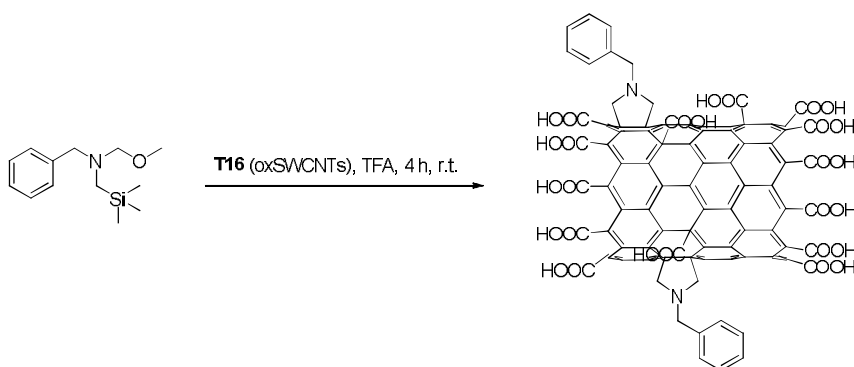
Scheme 12. The N-benzyl-N-(methoxymethyl)-N-[(trimethylsilyl)methyl]amine activated by trifluoroacetic.

The results of functionalization on oxSWCNTs **T16** were compared with the functionalized pristine SWCNTs (**T15**) and listed in Table 2.

Table 2. Results of functionalization of SWCNTs and oxSWCNTs with azomethine ylide generated from of N-benzyl-N-(methoxymethyl)-N-[(trimethylsilyl)methyl]amine.[a]

Entry	CNTs	Solv.	Time [h]	Temp [°C]	TGA Weight loss [%]	Functional group [μmol/g]	Raman [$I_D I_G^{-1}$ / $I_{D0} I_{G0}^{-1}$]	Sample name
1	SWCNTs	DCM	4	25	7.35	322	1.16	**T15**
2	oxSWCNTs (T16)	DCM	4	25	15.37	740	1.13	**T17**

[**a**] Reaction conditions: **SWCNTs**/**amine** =1/20

As expected, oxSWCNTs (**T16**), presenting carboxylic groups on their surface, were more reactive and good functionalization yield was obtained. The presented TGA curves showed the weight loss from 7 to 15% what is assign respectively to 544 to 740 μmol g^{-1}(Figure 3). From Raman spectra we could observe the increased ratio between D- and G-band of functionalized oxSWCNTs (T17) with respect to **T16** [$I_D I_G^{-1}$/$I_{D0} I_{G0}^{-1}$] to 1.22 (Figure 3).
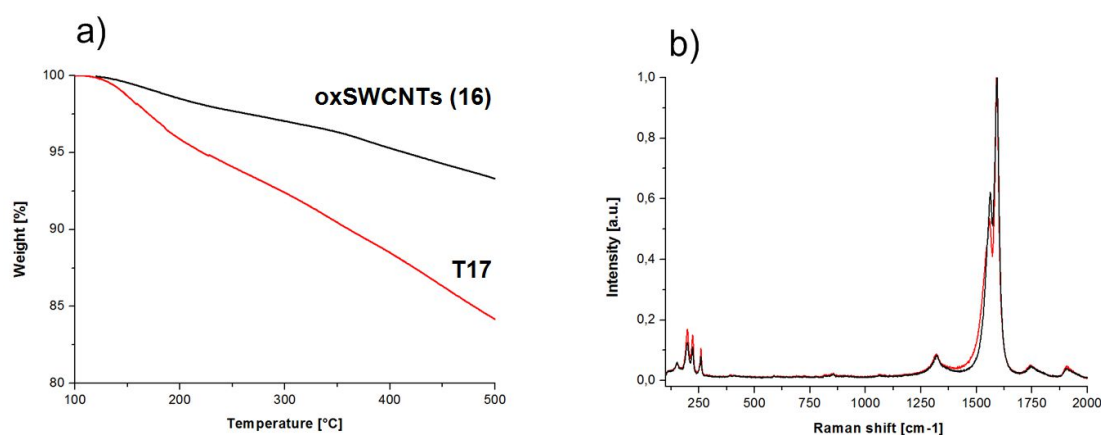
Figure 3. a) TGA analysis of oxSWCNTs (T16) and functionalized oxSWCNTs (T17) with azomethine ylide. Raman spectra of oxSWCNTs before and after functionalization (black-oxSWCNTs T16; red-T17).

As we could expect the presence of strongly electron-withdrawing groups on SWCNTs structure increased the reactivity. Nevertheless, the oxidation process was very harmful for SWCNTs and introduced high level of

damages on the CNTs structure. The comparison of Raman spectra presents the pristine SWCNTs and oxidized SWCNTs (Figure 4). The high level of oxidation and the number of defects, excluded this treatment from our further investigation and application of this reaction for filled nanotubes.
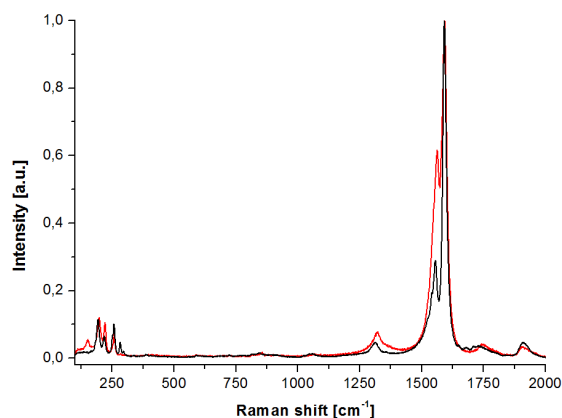
Figure 4. Raman spectra for SWCNTs before and after oxidation (black-SWCNTs; red-oxSWCNTs (T16)). Laser excitation - 633 nm.

Going on the exploration of reactivity of non-oxidized nanotubes (Table 1), we decided to apply the cycloaddition of non-stabilized azomethine ylide bearing an appendage, which would provide more possibilities for further derivatization. Following this idea, we synthesized the linker, which would increase solubility and present a terminal reactive group. The soluble derivative was based on 2,2-(ethylenedioxy)bis(ethylamine) (TEG) chain. One amine was protected with *tert*-butyloxycarbonyl group and the trimethylsilylmethyl chloride was allowed to react with the other free amine (Scheme 13). The azomethine ylide was then generated *in situ* from **P2** in the presence of formaldehyde and TFA.
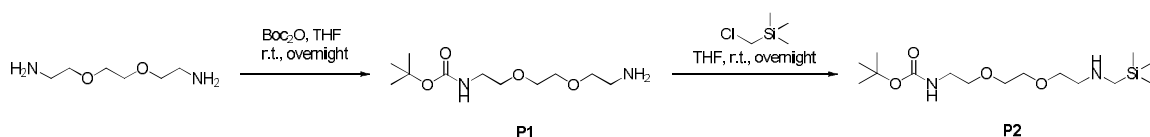
Scheme 13. Synthesis of trimethylsilylmethylamine P2.

The cycloaddition was performed with the conditions optimized for *N*-benzyl-*N*-(methoxymethyl)-*N*-[(trimethylsilyl)methyl]amine. For this experiment

we have used 10 mg of CNTs (HiPCO SWCNTs purified with HCl treatment, or MWCNTs), an excess of trimethylsilylmethylamine **P2** (26 times in weight) with respect to carbon nanotubes and catalytic amount of TFA (Scheme 14).
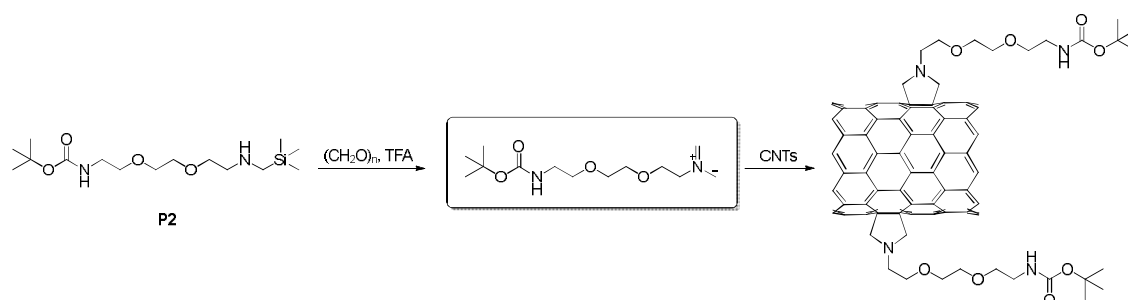
Scheme 14. 1,3-dipolar cycloaddition of azomethine ylide on CNTs, generated from trimethylsilylmethylamine.

Characterization of functionalized CNTs was performed by Raman spectroscopy, TGA and Kaiser test. The results are listed in Table 3.

Table 3. 1,3-dipolar cycloaddition of azomethine ylide generated from trimethylsilylmethylamine on SWCNTs and MWCNTs.[a]

Entry	CNTs	Solv.	TGA Weight loss [%]	Functional group [μmol/g]	Kaiser test [μmol/g]	Raman [$I_D I_G^{-1}$ / $I_{D0} I_{G0}^{-1}$]	Sample name
1	SWCNTs	DMF	11.00	289	15	1.15	**T19**
2	MWCNTs	DMF	6.69	190	10	1.04	**T20**

[**a**] Reaction conditions: **SWCNTs**/**amine** =1/26

To estimate the density of the covalently functionalized molecules on the sidewall we used TGA. A higher degree of functionalization was obtained for SWCNTs **T19** (Table 5a) when compared to functionalized MWCNTs **T20** (Table 5b) under the same reaction conditions. More specifically, the weight loss measured for the thermal decomposition of the chain on SWCNTs was 11% compared to 6.69% for functionalized MWCNTs. As expected, the reactivity of carbon nanostructures was found to depend on their structure and with higher curvature, SWCNTs proved to be more favorable for covalent chemical reactions than MWCNTs. However the content in carbon of MWCNTs is much higher than

in SWCNTs and this must also be taken into account. In summary, TGA measurements provided efficient tool to estimate the level of functional groups on 289 and 190 µmol g^{-1} respectively for SWCNTs and MWCNTs.
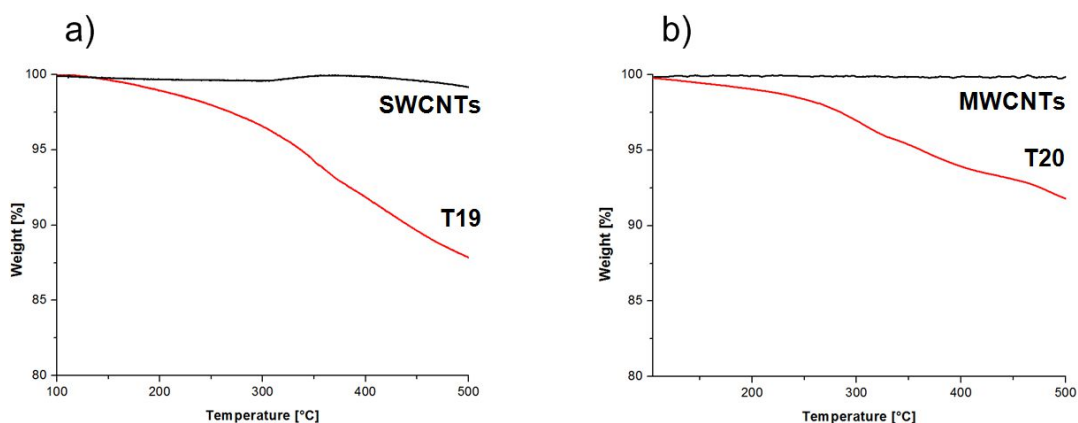
Figure 5. TGA of a) SWCNTs and b) MWCNTs functionalized with trimethylsilylmethylamine P2 (nitrogen atmosphere).

Raman spectroscopy revealed important chemical information about this surface functionalization of SWCNTs and MWCNTs (Table 6). Upon 633 nm excitation, SWCNTs present important signals the radial breathing mode bands (RBM) between 186 and 270 cm^{-1} suggesting the presence of both metallic and semiconducting SWCNTs. The small changes in radial breathing mode for metallic nanotubes were observed which are probably the most reactive for this type of reaction which is in agreement with previously reported results of cycloaddition of non-oxidized nanotubes. Secondly, the D-mode located between 1290 and 1315 cm^{-1} upon covalent functionalization slightly increased due to the rehybridization of carbon atoms from sp^2 to sp^3. The ratio of I_D/I_D between functionalized and pristine SWCNTs [$I_DI_G^{-1}$ / $I_{D0}I_{G0}^{-1}$] increased to 1.15. After the deprotection of the Boc functions we could evaluate the number of free amine groups by colorimetric Kaiser test (15 and 10 µmol g^{-1} respectively for SWCNTs and MWCNTs). However the same test performed before the deprotection gave a partial positive value (about 7 µmol g^{-1}) probably due to the partial deprotection of the amine group in presence of the catalytic amount of TFA used during the cycloaddition. In contrast to SWCNTs, the intensity ratio

between the D- and G- bands for MWCNTs increased only slightly from the pristine MWCNTs to functionalized MWCNTs, although the broader G- band included contributions from disorders, defects or intercalations between CNTs walls (Figure 6b).[16]
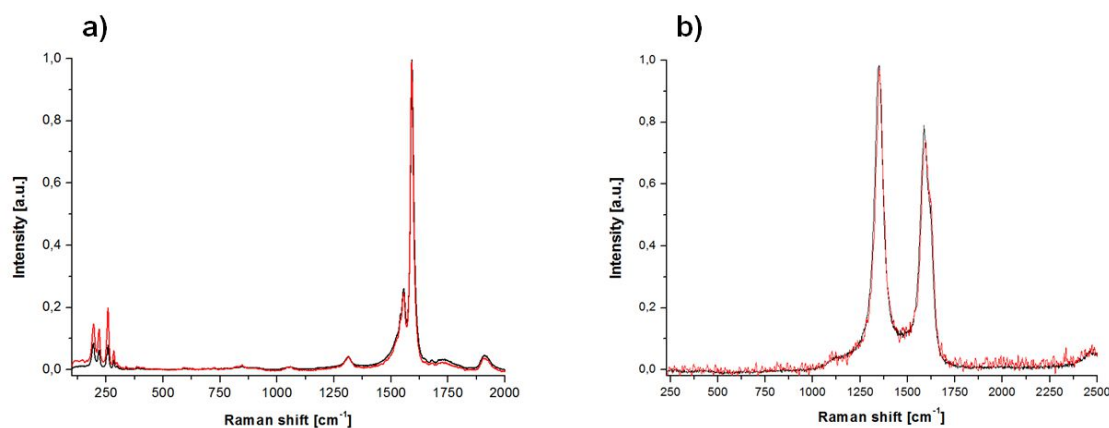
Figure 6. a) Raman spectroscopy for SWCNTs before and after functionalization (laser excitation - 633 nm); b) Raman spectroscopy for MWCNTs before and after functionalization (laser excitation - 532 nm); (black-before functionalization; red-after functionalization).

In summary, we presented here a comprehensive attempts for covalent functionalization of carbon nanotubes by 1,3-dipolar cycloaddition of non-stabilized azomethine ylide generated from the *N*-benzyl-*N*-(methoxymethyl)-*N*-[(trimethylsilyl)methyl]amine. The cycloaddition was performed on SWCNTs and time, temperature and solvent were examined in order to improve and optimize the functionalization yield. All samples were characterized by Raman spectroscopy and TGA. We found this reaction as efficient for functionalization of SWCNTs and SWCNTs after oxidation.

Furthermore, we applied also a trimethylsilylmethylamine with TEG chain terminated with -Boc protected amine. By this covalent method, we have functionalized SWCNTs and MWCNTs. For the characterization of the final material Raman spectroscopy, TGA and Kaiser test were applied. Using short time of reaction and mild conditions we could functionalize two types of CNTs in moderate yields in comparison to traditional 1,3-dipolar cycloaddition by

azomethine ylide generated by decarboxylative condensation of amino acids and formaldehyde.

II.2.3 Nitrile oxides

Nitrile oxides are one of the most commonly applied 1,3-dipoles for the synthesis of five-membered heterocyclic rings. They have highly polarized C-N and N-O bonds (Scheme 15). They are easy available from aldoximes or primary nitro compounds, but most nitrile oxides have to be prepared *in situ*, because of high reactivity and rapid dimerization. Main routes of nitrile oxides chemical transformations in absence of other reagents with multiple bonds are generalized in Scheme 15.
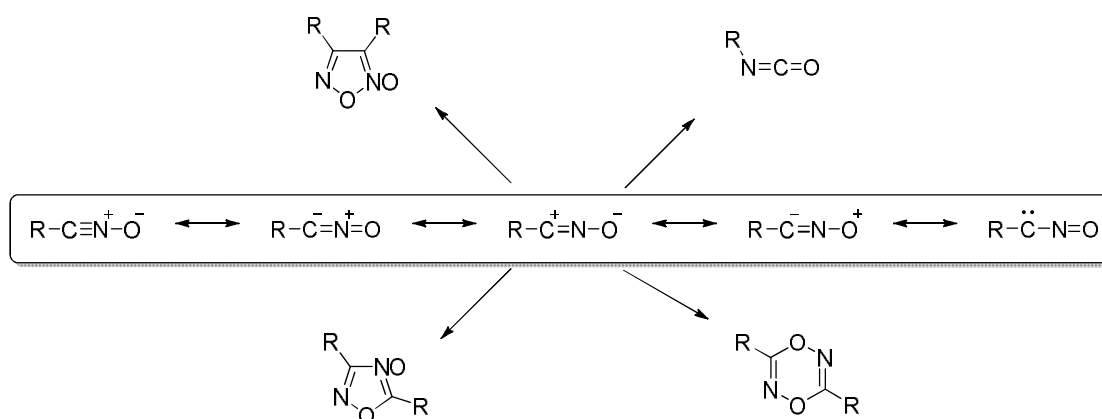
Scheme 15. Main routes of chemical transformations of nitrile oxides in absence of other reagents.

The conventional methods using nitrile oxides as dipoles in [3 + 2]-cycloadditions were studied extensively.[17] They undergo cycloaddition with alkenes and alkynes to provide isoxazolines and isoxazoles, respectively. These heterocyclic compounds are commonly occurring structural fragments in biologically active compounds.[18] Therefore, these heterocyclic systems are widely used and studied in modern drug discovery.[19]

Nitrile oxide as reactive dipole was applied onto polycyclic aromatic compounds such as phenanthrene and pyrene to give mono-cycloadducts (Scheme 16). In this particular example, mesitonitrile oxide was applied. The best conditions for the reaction were optimized using equimolecular amounts of the polyaromatic compound and the 1,3-dipole. The reaction was refluxed in benzene from three hours to one day, until the 1,3-dipole disappeared.

Experiments proved that phenanthrene is more reactive towards mesitonitrile oxide than pyrene. In dichloromethane at room temperature, the reaction of phenanthrene was very slow with an increased rate in boiling dichloromethane, whereas the cycloadduct was obtained after a long period of time (28 days). In both cases low yields were obtained, ranging from 8-15%. The increased yield was achieved by adding several small portions of mesitonitrile oxide. A moderate yield was obtained by using a large excess of mesitonitrile oxide.[20]
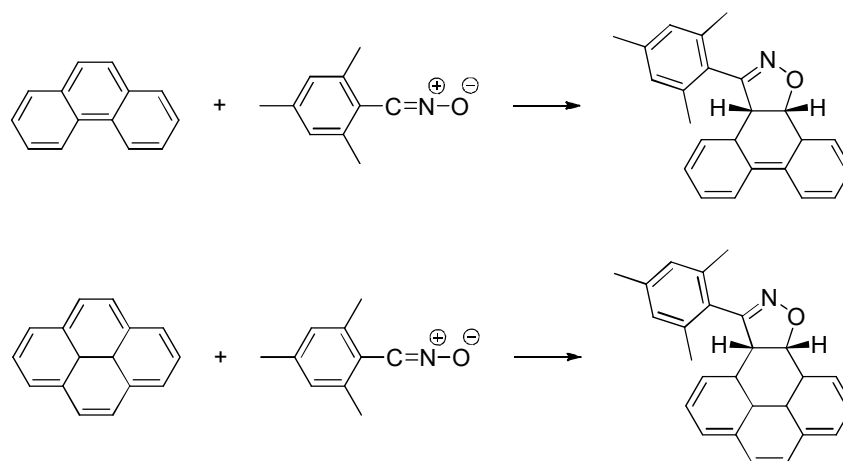
Scheme 16. Nitrile oxide cyclization onto polycyclic aromatic compounds.[20]

The application of nitrile oxide for polyaromatic system like CNTs was reported twice. The sidewall of CNTs was functionalized by nitrile oxide leading to pyridyl functionalities covalently attached to CNTs structure (Scheme 17). Echegoyen *et al.* used SWCNTs, which were functionalized at the end tips with pentyl esters to increase their dispersibility.[21] Then, nitrile oxide was generated *in situ* from 4-pyridylcarboxaldehyde oxime. The reaction was carried out in *o*-DCB under MW irradiation. This system was supramolecularly bound to porphyrin through the coordination of the nitrogen atom of the pyridyl unit to the zinc metal center of the porphyrin to create SWCNTs–porphyrin conjugate. Raman spectroscopy showed the expected peaks for the organic groups and confirmed the occurrence of a high degree of lateral functionalization. Moreover, the occurrence of this complex was clearly revealed by optical

spectroscopy and by the shifts in cyclic voltammetry potentials of Zn-porphyrin in the presence of SWCNTs.
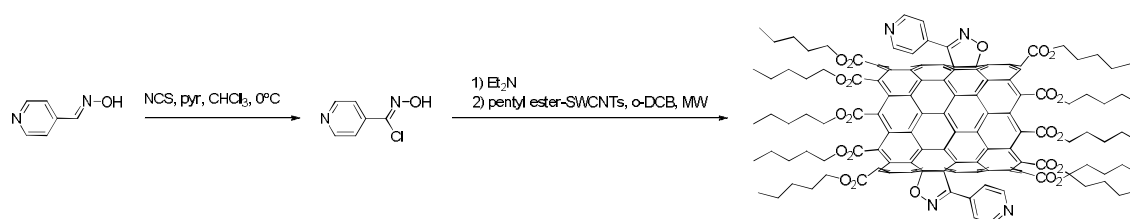
Scheme 17. Synthetic route for the functionalization of SWCNTs by nitrile oxide.

A similar example was published in 2010 by Popławska *et al.*[22] In their work, they reported the chemical modification of MWCNTs by 1,3-dipolar cycloaddition of nitrile oxide. The nitrile oxide was generated from 4-(dimethyloamino)benzaldehyde oxime with *N*-chlorosuccinimide (NCS) in chloroform. Triethylamine was introduced to the flask with MWCNTs solution in toluene (Scheme 18). A five - membered ring was formed on the external surface of MWCNTs after 4 h of sonication at r.t.
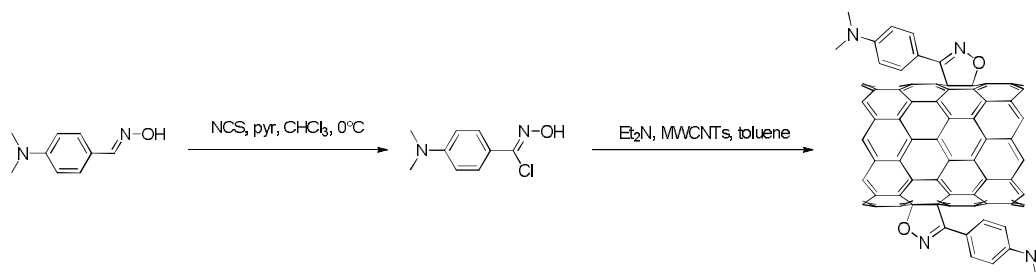
Scheme 18. Synthetic route for the functionalization of MWCNTs by nitrile oxide.

By TGA they quantitatively evaluated the degree of functionalization. The weight loss of functionalized MWCNTs was calculated between 200 °C and 500 °C. This was attributed to the decomposition of covalently bonded moieties and the mass loss was of 12% for modified MWCNTs. This showed that cycloaddition was achieved with high yields at very reasonable reaction times also on multi-wall carbon nanotubes.

The presented routes were reported as a fast, controllable, and occurred under mild conditions, provided high functionalization yields and resulted in

diverse surface composition. This encouraged us to use nitrile oxide for functionalization of CNTs and optimize the conditions to have the fast and efficient reaction suitable for application on filled CNTs.

II.2.4 Results of nitrile oxides cycloaddition
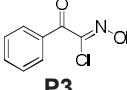
In the present work, we reported a 1,3-dipolar cycloaddition to CNTs using nitrile oxides. In the first trials nitrile oxide was generated from *N*-hydroxy-2-oxo-2-phenylacetimidoyl chloride (Scheme 19).
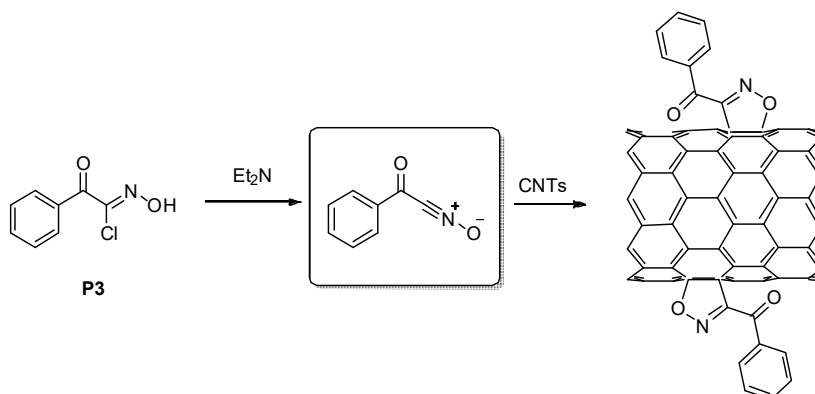
Scheme 19. Functionalization of SWCNTs with nitrile oxide.

The reaction was performed on two types of CNTs (SWCNTs and MWCNTs) in aprotic solvent. The functionalization was constructed in one steps operation. Compound **P3** was added to the dispersion of CNTs in DMF and cooled to 0 °C for the addition of triethylamine (TEA) and generation of nitrile oxide. Reaction with SWCNTs was carried out at room temperature for 16 h. The final product was purified by filtration and re-dispersion from several solvents. The resulted material was characterized by Raman spectroscopy and by TGA. The results are presented in Table 4.

Table 4. Results of functionalization of CNTs by nitrile oxide.[a]

Entry	Aldoxime chloride	CNTs	Time [h]	Solv	TGA Weight loss [%]	Functional group [μmol/g]	Raman [$I_D I_G^{-1}$ / $I_{D0} I_{G0}^{-1}$]	Sample name
1		SWCNTs	16	DMF	5.9	195	1.57	**T21**
2		SWCNTs	16	*o*-DCB	6.3	221	1.25	**T22**
3		MWCNTs	16	DMF	2.0	134	0.85	**T23**
4		MWCNTs	16	*o*-DCB	2.1	141	0.84	**T24**
5		MWCNTs	16	toluene	1.0	67	0.90	**T25**
6		MWCNTs	1	DMF	2.0	134	0.88	**T26**
7		MWCNTs	1	*o*-DCB	2.1	141	0.90	**T27**
8		MWCNTs	1	toluene	1.7	114	0.89	**T28**
9		MWCNTs	1	-	3.4	228	0.58	**T29**

[**a**] Reaction conditions: **CNTs/ Oxime** =1/10

Evidence of the sidewall functionalization was confirmed with TGA. The curve of thermal degradation of functionalized material was compared to the pristine SWCNTs. To make this comparison samples were treated with the same thermal program (carried out under N_2 atmosphere). The thermal decomposition of the organic functional groups present at the CNT sidewall occurred between 100-500 °C (Figure 7). For calculation, the weight loss of functionalized material was reduced by 3 % of the weight loss of pristine material as the weight difference between the TGA profiles. Such a weight loss difference has been attributed to the thermal decomposition and rearrangement of the cycloadduct moieties and was calculated as 195 and 221 μmol g^{-1} for **T21** and **T22**.
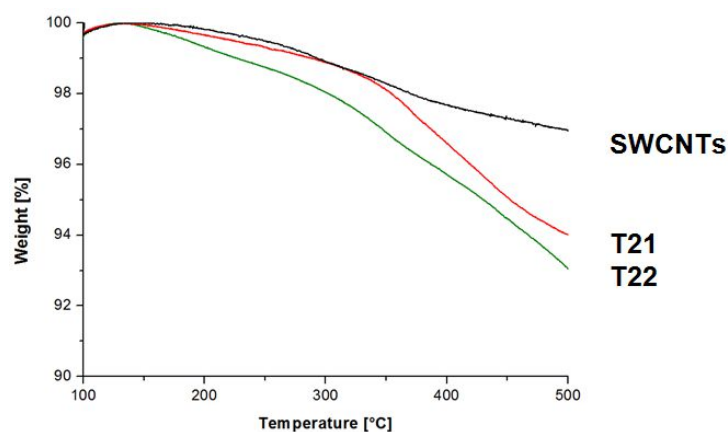
Figure 7. TGA of SWCNTs functionalized with aldoxime chloride P3.

The evidence for covalent sidewall functionalization was determined by Raman spectroscopy.[23] As shown in Figure 8 the Raman spectra of the SWCNTs exhibits all peaks typical for SWCNTs: a tangential mode (G-band) at 1590 cm^{-1} and a weak disorder mode at 1315 cm^{-1} (D-band). That peak arose after functionalization, in agreement with covalent attachment of the functional groups to the sidewalls of the SWCNTs in fact the ID/IG of functionalized material was compared to pristine material and the ratio was 1.57 for **T21** and 1.27 for **T22** (entry **1** and **2**, Table 4). The RBM observed at 266 cm^{-1} is attributed to bundling of in the pristine SWCNTs. The functionalized SWCNTs exhibit a substantially enhanced peak at 235 cm^{-1}. This emphasizes the partial debundling that is the result of functionalized SWCNTs for **T21** and **T22**.
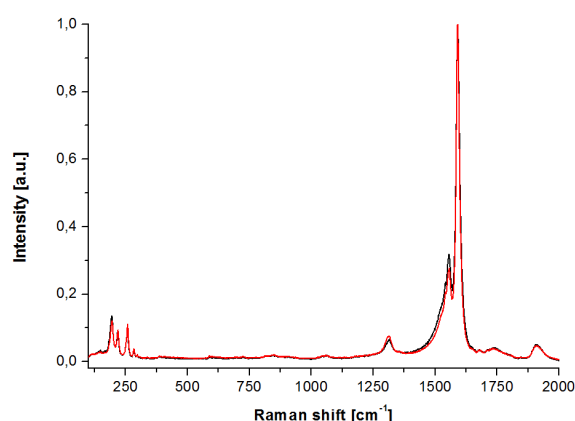
Figure 8. Raman of SWCNTs functionalized with aldoxime chloride P3 (black-pristine SWCNTs; red-T21).

We transferred the procedure on MWCNTs. The main reason why we wanted to do it was to check if less reactive MWCNTs can also undergo this reaction. The procedure was repeated in three different solvents: DMF, *o*-DCB, toluene (**T23**-**T25**).

The TGA results showed the highest % weight loss for **T23** and **T24** which where respectively performed in DMF (Figure 9, blue line) and *o*-DCB (Figure 9, redline). The MWCNTs functionalized in toluene (**T25**) had the smallest weight loss (Figure 9, green line).
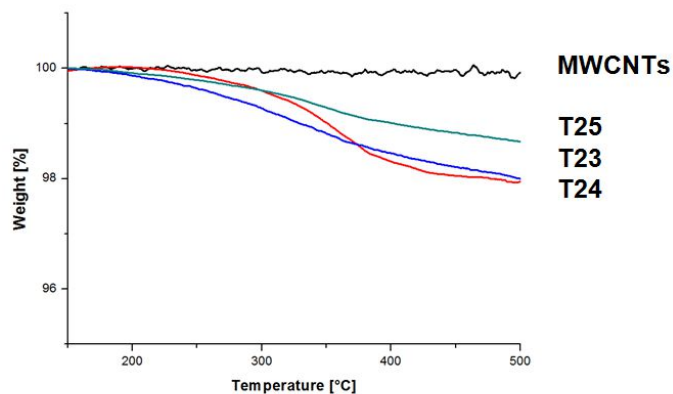
Figure 9. TGA for functionalized MWCNTs T23-T25 with aldoxime chloride P3.

The Raman for MWCNTs spectra of pristine and functionalized MWCNTs were recorded using the 532 nm laser (Figure 10). Typically, all spectra exhibit two main characteristic bands in the region between 1000 and 2000 cm^{-1} (D, and G modes), and their overtone and combination bands between 2400 and 3400 cm^{-1} (G_0= 2D). While the first-order G mode (E2 g symmetry) is attributed to a regular sp^2 graphitic network, the D and D_0 modes (A1 g symmetry) are due to the so-called double resonant Raman scattering from a nonzero-center phonon mode, and they are originated from disorder and defects in the carbon lattice.[24] From a closer examination of the spectra reported in Figure 10, it can be inferred that the functionalization process reduces the I_D/I_G intensity ratio, suggesting that a substantial modification occurs at the nanotube surface. As a matter of fact, the value of the intensity ratio observed in the pristine material (I_D/I_G = 1.26) was reduces in all functionalized MWCNTs (**T29** to 0.73) (Figure 10). These results suggest that the 1,3-dipolar cycloaddition of **P3** does not affect the crystal domain size of the sp^2 network, but it reduces the diffuse defects at the surface lattice.[25] The same results were found for cycloaddition on MWCNTs with cyclic nitrones[26] and nitrones.[27]
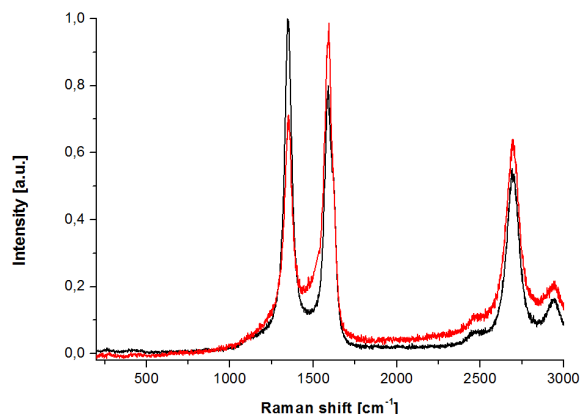
Figure 10. Raman spectra for functionalized MWCNTs T29 with aldoxime chloride P3 (black- pristine MWCNTs; red-T29).

For MWCNTs we have also examined the generation of nitrile oxide accelerated by MW irradiation. For this purpose the base was not present in the reaction medium and the nitrile oxide was generated *in situ* by thermal treatment (Scheme 20).
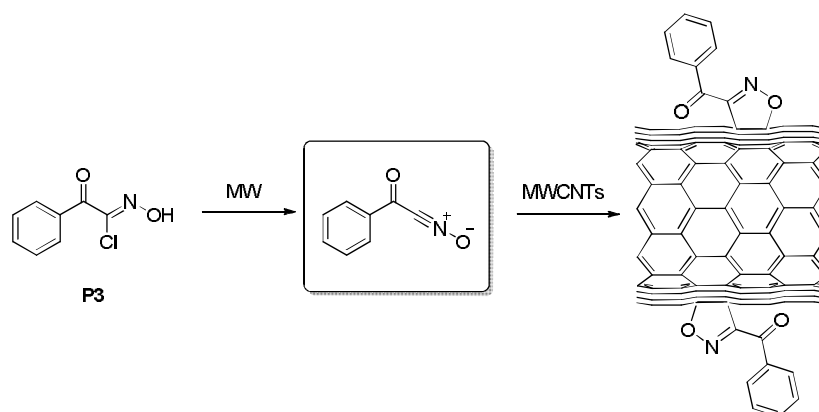
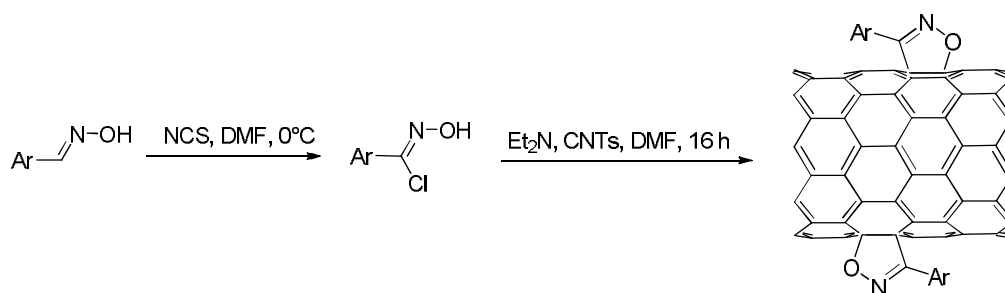**Scheme 20. Functionalization of MWCNT with nitrile oxide.**

The reaction was performed in three different solvents and also without in neat conditions. The MW was settled at 100 °C with 200 W of power. The reaction was carried out stirring for 1 h. The results were listed in Table 4. The application of MW slightly increased the functionalization yield and shortened the reaction time to one hour. The highest functionalization degree was obtained for nanotubes functionalized without the solvent medium (**T29**).

Therefore, we have started the next trials of 1,3-dipolar cycloaddition reactions of nitrile oxides on CNTs with the library of benzaldehyde oximes (precursors of

nitrile oxides) used in two different amount to understand if their high excess can increased the yield of functionalization. The oximes were prepared from corresponding aldehydes with hydroxylamine in presence of sodium hydrogen carbonate in EtOH/H_2O at 60°C (Scheme 21).
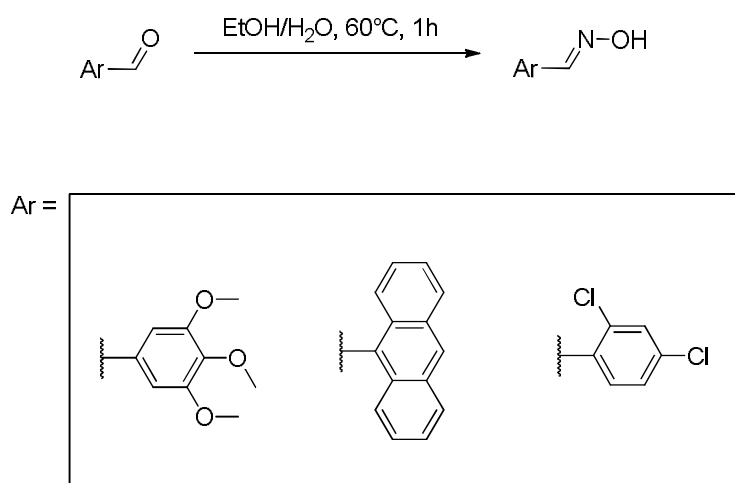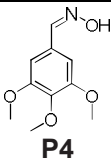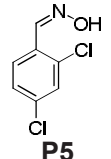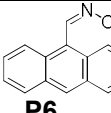

Scheme 21. Synthesis of corresponding oxime.

The functionalization took place in a two steps operation (Scheme 22). In first step the corresponding oxime was developed to corresponding benzohydroximinoyl chlorides by the addition NCS in the solution of DMF at 35 °C.[28] In the second step the dispersion of CNTs in DMF was added and then cooled to 0 °C for the addition of TEA and generation of nitrile oxide. Reaction was carried out at 70 °C for 16 h. The final product was purified by filtration and re-dispersion in several solvents. The resulted material was characterized by Raman spectroscopy and by TGA (Table 5).

Scheme 22. Functionalization of CNT with nitrile oxide.

Table 5. Results of functionalization of CNTs by nitrile oxide.

Entry	Oxime	CNTs	Excess [times in wt]	Solv.	TGAWeight loss [%]	Functional group [µmol/g]	Raman [$I_D I_G^{-1}$ / $I_{D0} I_{G0}^{-1}$]	Sample name
1		SWCNTs	15	DMF	7.8	227	1.27	**T30**
2		SWCNTs	100	DMF	10.7	331	1.74	**T31**
	P4							
3		SWCNTs	20	DMF	10.2	378	1.07	**T32**
4		SWCNTs	100	DMF	10.7	405	1.28	**T33**
	P5							
5		SWCNTs	20	DMF	8.1	224	1.04	**T34**
6		SWCNTs	100	DMF	9.2	278	1.23	**T35**
	P6							

TGA was employed to investigate the covalent chemical functionalization of SWCNTs. The thermodynamic stability of the SWCNTs and functionalized SWCNTs were investigated by TGA under a N_2 atmosphere (Figure 11). The TGA curve of the functionalized SWCNTs **T30** - **T35** reveals a weight loss of approximately 7 - 10 % in the temperature range 100–500 °C, which results primarily from the destruction of functional groups presented on the structure, but may also contain a contribution from loss of the organic and inorganic impurities. The number of the organic groups present in the derivatives was calculated by TGA for samples **T30** - **T35** taking into consideration the weight loss of pristine material.
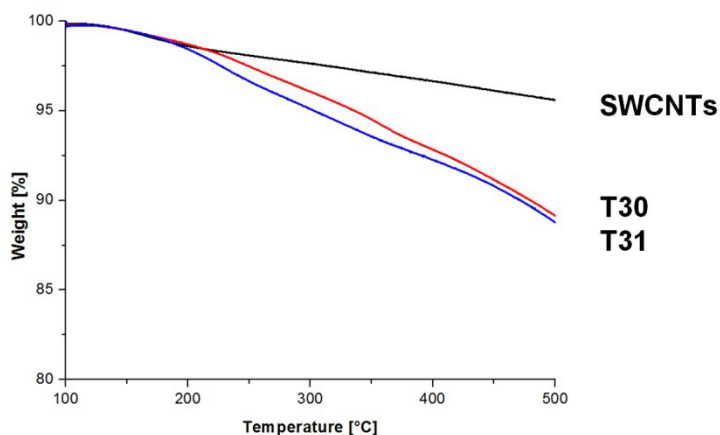
Figure 11. TGA analysis for the SWCNTs functionalized with oxime P4.

In Figure 12 we presented the Raman resonance spectra of pristine SWCNTs and SWCNTs after modification with **P4.** It is possible to confirm the occurrence of the reaction at the sidewalls and tips of the tubes by considering the increase of the disorder-induced mode (D-band) relative to the G-band.[29] In pristine SWCNTs, the D-band has a very low intensity at 1315 cm^{-1}. The Raman spectrum of SWCNTs functionalized by the 1,3-dipolar cycloaddition reaction shows a more intense D-band than pristine SWCNTs, but this is much lower when compared to that of SWCNTs functionalized by the higher excess of oxime used for the reaction. The higher D-band was also observed for the functionalization with large excess of **P5** and **P6**.
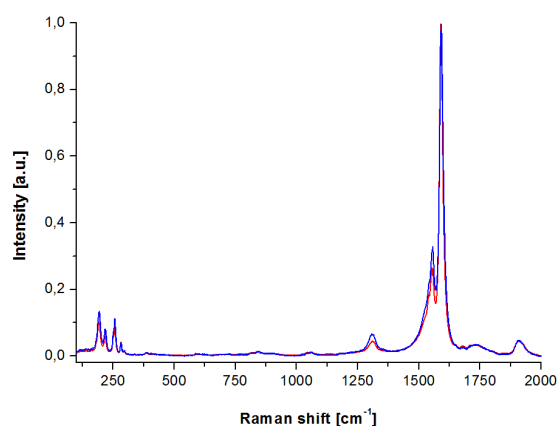
Figure 12. Raman spectra of functionalized SWCNTs (red-T30; blue-T31). Laser excitation - 633 nm.

The nitrile oxides used in this study lead to the production of moderate functionalized materials. The spectroscopic analysis of the functionalized materials for SWCNTs and MWCNTs led to the conclusion that the sidewall structural defects present on the pristine CNTs act as preferential reactive sites for the nitrile oxides in 1,3-dipolar cycloaddition. The proposed functionalization approach involves its non-damaging character; indeed, the preservation of the CNTs sidewall sp^2 network does not change the chemo-physical properties of the pristine materials. In this respect, the covalent functionalization of SWCNTs and MWCNTs can be a valuable alternative to the non-covalent bonding approaches for the generation of functionalized CNTs.

II.2.5 Conclusions

We have performed an experimental study to investigate the chemical reactivity of covalent functionalization of CNTs through the 1,3-dioplar cycloaddition reactions of two types of 1,3-dipoles with similar formula but different structures, bent allyl anion and linear propargyl/allenyl anion types of dipoles.

We found that azomethine ylide generated by desilation of trimethylsilylmethylamine and nitrile oxide are effective tools for 1,3-dipolar cycloaddition on SWCNTs. The reactivity of the nitrile oxide on MWCNTs was found very reactive for defect sides which is in agreement with literature for cycloaddition of polar dipoles on MWCNTs.[27] Moreover, chemical modification of the CNTs pirydyl frameworks allows for a modulation of the aromatic structure. The introduction of cyclic appendix represents a starting point for the development of further nanotubes derivatization approaches.

II.3 Diazonium-Based Functionalization

The diazonium-based functionalization of CNTs is a very useful method (described in Introduction). Since 2001, when Tour and coworkers discovered a convenient route to sidewall-functionalized carbon nanotubes by reacting aryl diazonium salts with SWCNTs in an electrochemical reaction,[30] a variety of the aryl diazonium salts was applied for covalent modification of CNT. The corresponding reactive aryl radicals can be generated from the diazonium salt by electrochemical one-electron reduction or *in situ* from the diazonium compound by reacting of aniline derivatives with isopentyl nitrite.[31] Another route was developed after the work of Tour and coworkers. The SWCNTs were functionalized for minutes at room temperature with aryl diazonium salts in the presence of ionic liquids and potassium carbonate.[32] The functionalized material was comparable to those derived from other processes using harsh reaction conditions. This functionalization was also performed in water as a solvent to reduce harmful wastes.[33] The range of solvents for this type of CNTs functionalization reaction was extended to Caro's acid, a mixture of 96% sulfuric acid and ammonium persulfate.[34] Lately, *in situ* generation of aryl diazonium salts in the presence of ammonium persulfate in a solvent-free medium was reported for the derivatization of MWCNTs, with high degree of functionalization.[35] Another comprehensive example on MWCNTs was published recently.[36] The covalent functionalization of MWCNTs was performed with the well-established procedure in water reported by Tour *et al.*[33]

As an alternative for aniline derivative, triazene compounds were used. This stable diazonium salt precursor was proposed for the functionalization of SWCNTs in aqueous media[37] and the authors claimed that is particularly useful for biological relevant molecules.

In literature there are also examples of application of MWs for the acceleration of the reaction.[38] The authors reported the results in comparison to

the functionalization with classical heating. In principle, under MW irradiation, the reaction leads to shorter reaction time and higher functionalization degrees.

Meanwhile, the diazonium-based functionalization became the most frequently used reaction to derivatized CNTs, for chemists and material scientists. For example short linkers like 4-aminobenzylamine, were covalently bind to CNTs sidewalls, by the diazonium route, and used for further modifications. Burghard *et al.* reported the attachment of gold nanoparticles to carbon nanotubes functionalized with 4-diazo-N,N-diethylaniline tetrafluoroborate for enhancing the Raman response.[39] Other nanoparticles - CdSe–ZnS quantum dots were conjugated to the sidewall functionalized SWCNTs templates for enhancing photophysical properties for light harvesting systems. [40]Diazonium-based functionalization was also used to bind nickel to the surface of the nanotube to direct the self-assembly of histidine-tagged proteins at controlled orientation.[41] This approach has application for metal interacting protein systems where the redox center of the protein is inaccessible through conventional means of directed assembly onto carbon nanotubes.

The presented examples, of the covalent functionalization of CNTs through aryl diazonium salts, were demonstrated as an easy and very efficient way to decorate carbon nanotubes. The fast and efficient way of functionalization with aniline derivatives gives a possibility for modification of sidewall of CNTs with versatile molecules. These encourage us to apply this reaction to develop the most suitable "bridge" between CNTs and biomedical application.

II.3.1 Results of Diazonium-Based Functionalization

Basing on the aim of the project, we decided to thoroughly investigate the functionalization of SWCNTs and MWCNTs with diazonium based aniline

derivatives, in order to understand the outcome of this methodology. In principle, it is accepted that the first step of the addition of diazonium salts to CNTs involves the reductive dissociation of the diazonium salt with loss of N_2, and formation of an aryl radical.[42] This in turn, may react with carbon–carbon double bonds[43] and lead to rehybridization of carbon atoms from sp^2 to sp^3.
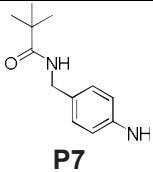
Our investigation of the functionalization CNTs with the aryl diazonium was started with the benchmark compound 4-[(*N*-Boc)aminomethyl]aniline, as shown in Scheme 23.
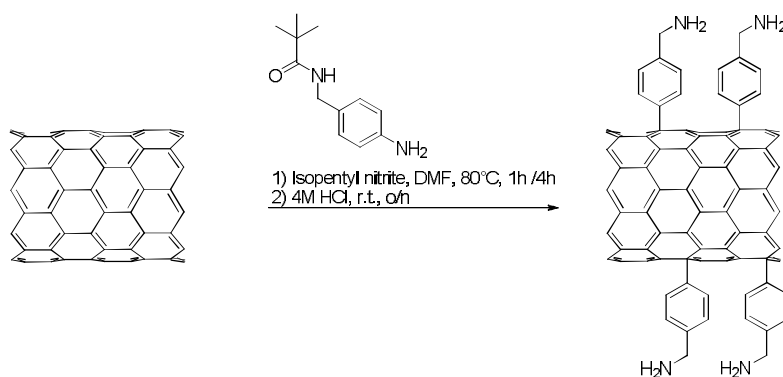
Scheme 23. Functionalization of SWCNTs with 4-[(N-Boc)aminomethyl]aniline.

In particularly we have started our research from time control experiments. The functionalization reactions were performed on SWCNTs produced by chemical vapor deposition from Thomas Swan & Co. Ltd (Elicarb®). The material was purified by steam treatment. In the experiments, DMF was used as a solvent and 10 fold excess in weight of amine was used for diazonium generation. The reaction was performed for two different time points: 1 h and 4 h. The product was purified by filtration/re-dispersion method from several solvents to remove the non-reacted material. Then the Boc protecting group was cleaved by acid treatment. The ready product was purified by filtration and dried under vacuum for complete removal of solvents and analyzed by TGA, Raman spectroscopy and Kaiser test. The comparison of the results is presented in Table 6.

Table 6. Functionalization of SWCNTS by arylation.

Entry	Aniline deriv.	Time [h]	TGA Weight loss [%]	Function al group [μmol/g]	Kaiser test [μmol/g]	Raman $[I_D I_G^{-1} / I_{D0} I_{G0}^{-1}]$	Sample name
1		1	9.5	445	260		**T36**
2	P7	4	9.2	429	196		**T37**

Interestingly, lower time of the reaction leads to higher functionalization yield. The curve of TGA in nitrogen presents the thermal stability of SWCNTs before and after functionalization (Figure 13). The TGA of functionalized nanotubes shows a weight loss in the 200 °C to 500 ° C region of about 9%. This value corresponding to a functionalization of 445 μmol g^{-1}. The presence of amine groups on the functionalized material, after cleavage of Boc group was estimated to be 260 and 196 μmol g^{-1} respectively for nanotubes **T36** and **T37** by Kaiser test.
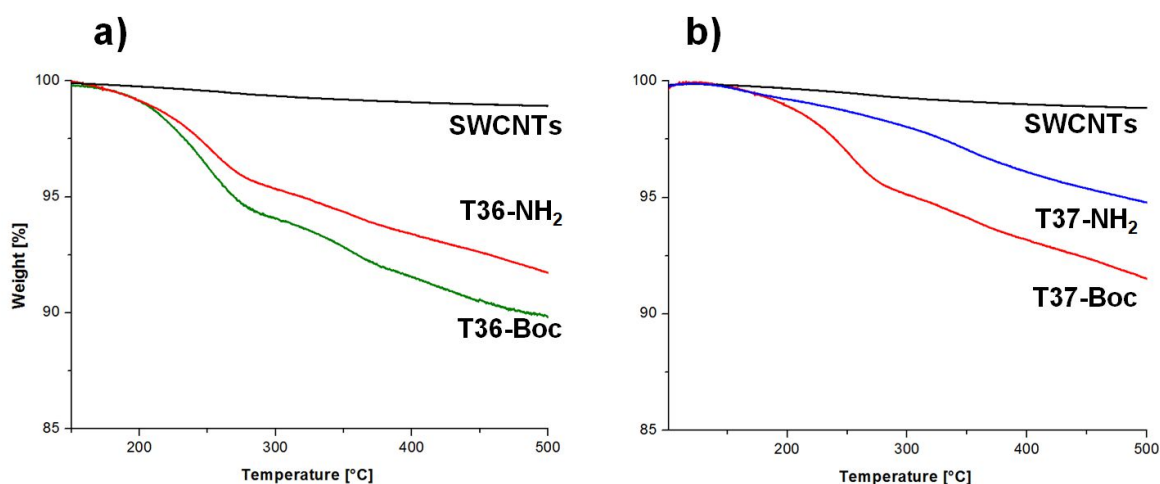
Figure 13. TGA of SWCNTs functionalized with 4-[(*N*-Boc)aminomethyl]aniline (nitrogen atmosphere).

The Raman spectra for both samples (Figure 14) represent the radial breathing (230 cm^{-1}) and tangential (1590 cm^{-1}) modes characteristic for SWCNTs, but the disorder D-mode (1315 cm^{-1}) in the spectra of compound **T36** and **T37** is enhanced with respect to pristine material.
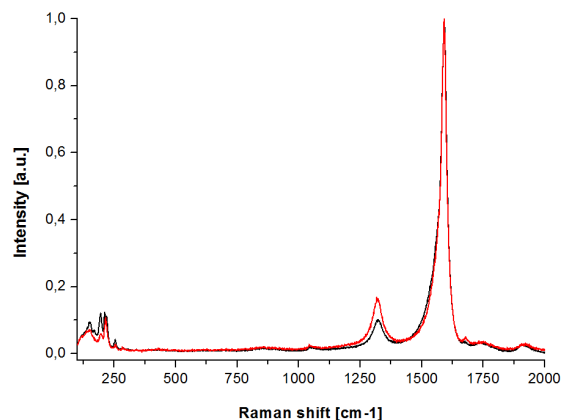
Figure 14. Raman spectra of functionalized SWCNTs (black- pristine SWCNTs; red-T36). Laser excitation - 633 nm.

With a view to perform the chemical modification of CNTs we introduced the same reaction also for functionalization of MWCNTs (Scheme 24). In the reaction the aniline **P7** was used in excess (10 times in weight) and, the reaction was carried out for 4 h in DMF. The TGA analysis of MWCNTs functionalized by 4-[(N-Boc)aminomethyl]aniline gave 8.1% weight loss what corresponds to 420 µmol g^{-1}, while the pristine MWCNTs gave no weight loss under identical TGA conditions (in nitrogen).
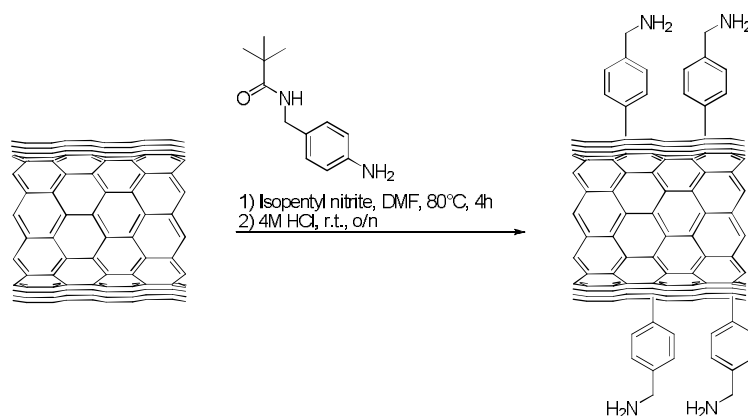
Scheme 24. Functionalization of MWCNTs with 4-[(N-Boc)aminomethyl]aniline.

In conclusion, this common approach of carbon nanotube derivatization meets our expectations. It is fast and provides the amine groups in high quantity, accessible for further binding.

Taking advantage of this method, we wanted to build a liker, which would be useful for biological application. The ideal one should 1) provide

higher dispersability and biocompatibility of functionalized tubes; 2) be sufficiently stable; 3) offer a protection to a free amine functionality, that could be used for further modifications.

Herein, we developed a simple and efficient method to obtain functional derivatives starting from the readily accessible triazine chemistry. Cyanuric chloride with formula $(NCCl)_3$ was used to introduce a branching point in the molecule. The three chlorine atoms of cyanuric chloride can be easily substituted by nucleophiles in a thermally controlled way. The first chlorine is substituted at 0°C or below, the second one at room temperature, while the third substitution requires temperatures higher than 60°C. In this way some notably one-one pot syntheses were accomplished. According to our intention we easily synthesized tri-substituted triazines by using hydrophilic monoprotected diamines and 4-aminobenzylamine for diazonium salt generation and binding to CNTs. By adding at 0°C the first amine and reacting at room temperature for overnight the di-substitution occurred, then the product was purified and the aniline was allowed to react 4 h at 80 °C (Scheme 25).
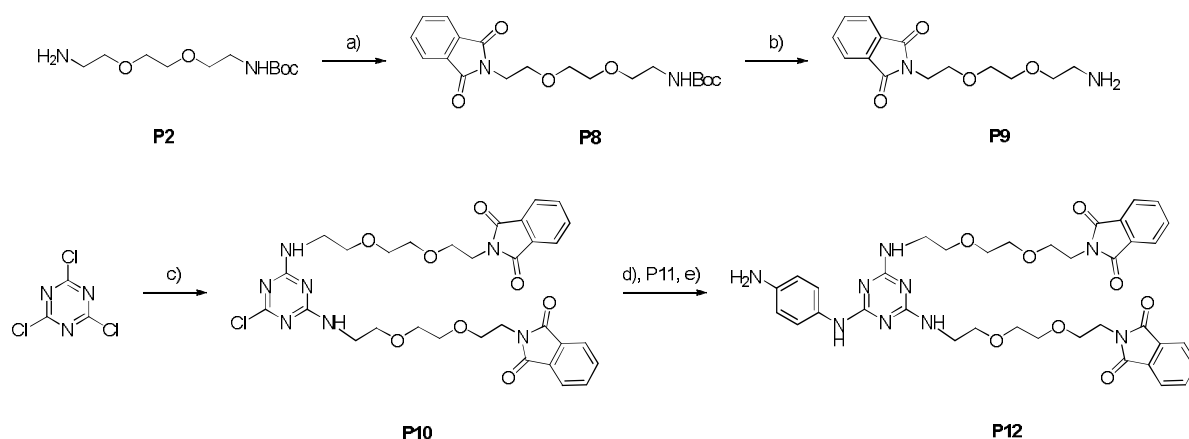
Scheme 25. General scheme for the preparation of compound P12. a) phthalic anhydrite, toluene, reflux, overnight, 92%; b) TFA, DCM, 4h, r.t., 98%; c) P9, DIEA, THF, 0 °C to r.t., 90%; d) N-Boc-p-phenylenediamine, THF, 80°C, 4h, 71%; e) TFA, DCM, 4h, r.t., 88%.

This linker offers the possibility of attachment to CNTs by generation of diazonium salt from the aniline function, and two hydrophilic chains present protected amine groups, which are cleavable by hydrazine treatment (Scheme 26).
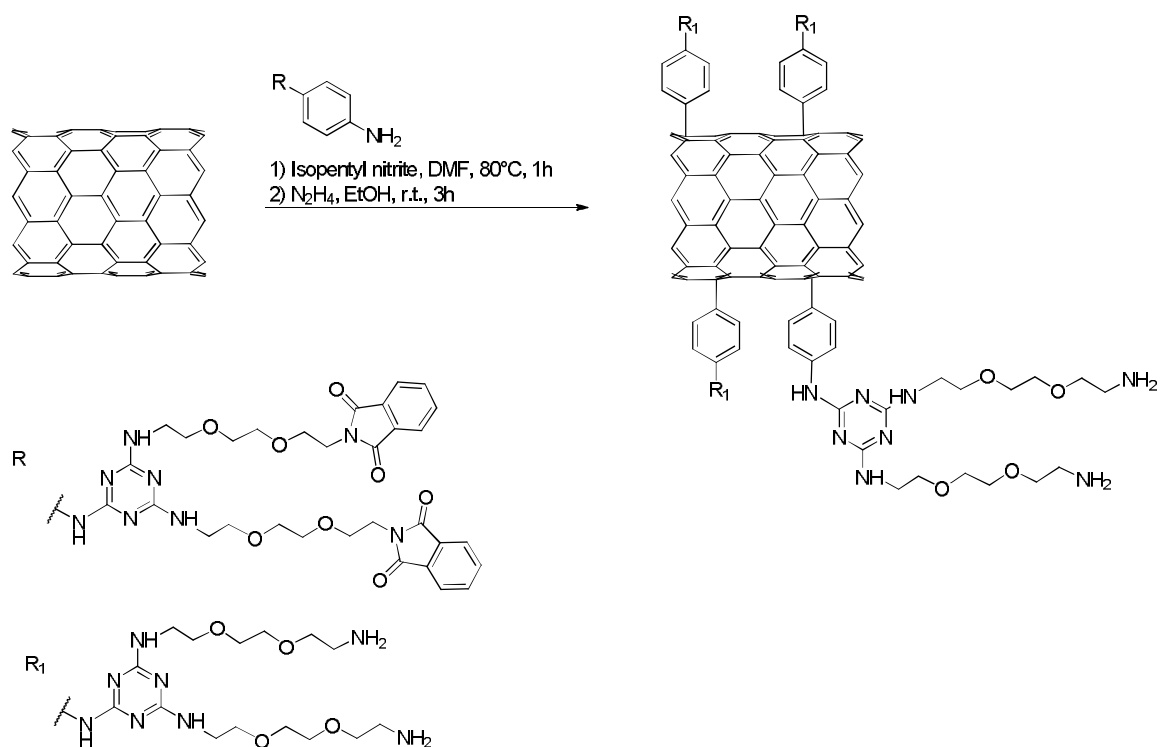
Scheme 26. Synthetic route for the functionalization of CNTs with P12.

In the initial experiments SWCNTs were derivatized with compound **P12** in condition reported by Tour,[33] but also with modified conditions, like shorter reaction time and application of MW. All experiments were carried at 80 °C. The CNTs for the experiment (SWCNTs) were provided by ICMAB from Barcelona. CNTs were previously purified by steam treatment. The functionalized nanotubes were analyzed by TGA, Raman spectroscopy, transmission electron microscope (TEM) and Kaiser Test. Results were compared with pristine SWCNTs (Table 7).

Table 7. Results of functionalization of SWCNTs by P12.

Entry	Excess of P12 to SWCNTs [wt%]	Time [min]	TGA Weight loss [%]	Function al group [µmol/g]	Kaiser test [µmol/g]	Raman [$I_D I_G^{-1}$/ $I_{D0} I_{G0}^{-1}$]	Sample name
1	10	240	20.2	275	125	1.7	**T38**
2	13	240	25.9	318	70	1.7	**T39**
3	13	240	23.9	305	115	1.5	**T40**
4	10	60	21.1	280	137	1.8	**T41**
5	25	60	20.7	276	130	1.9	**T42**
6	10	35 MW	18.2	248	126	1.8	**T43**
7	25	35 MW	21.1	290	145	2.0	**T44**
8	10	20 MW	20.2	276	142	1.9	**T45**
9	10	20 MW	19.3	260	137	2.0	**T46**

The TGA curves of functionalized nanotubes show a weight loss in the region of 200 °C to 500 °C (Figure 15) (in nitrogen atmosphere). The highest weight loss was observed for nanotubes functionalized for 4 h (**T39**). However, the amine groups present after deprotection of phthalimide (Pht) protecting group estimated by Kaiser test shown higher value in the case of SWCNTs functionalized in a shortest time, under MW irradiation (**T44**).
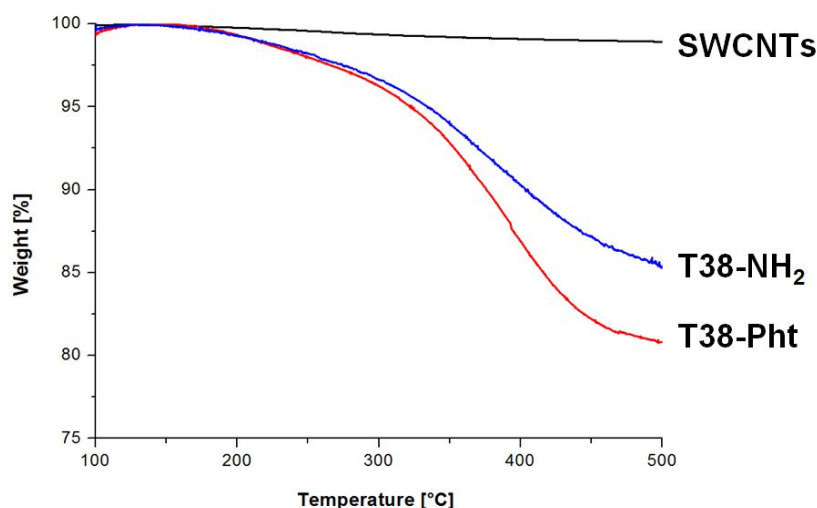

Figure 15. TGA of functionalized SWCNTs (T38) (nitrogen atmosphere).

Analyzing the influence of the excess of **P12** on the functionalization of SWCNTs, we could observed the increased functionalization (entries **5** and **7**)

and also the increased intensity of the D-mode on Raman spectra (Figure 16)when the reaction was carried out in presence of larger excess of aniline.
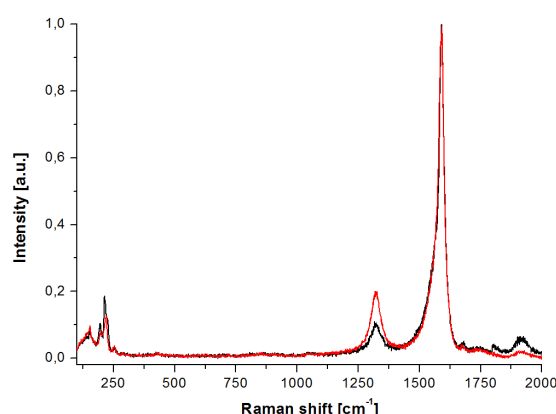

Figure 16. Raman spectra for SWCNTs before and after functionalization (black- pristine SWCNTs; red-T38. Laser excitation - 633 nm.

Starting from these results for SWCNTs we also studied the functionalization of MWCNTs by the aryl diazonium salts generated *in situ* by treatment of **P12** with isopentyl nitrite. Following the same protocol comprehensive purification and characterization (TGA, Raman, Kaiser test) were performed. We investigated the most important parameters to obtain highly functionalized MWCNTs (Table 8).

Table 8. Results of functionalization of MWCNTs by P12.

Entry	Excess of P12 to SWCNTs [wt%]	Time of reaction [min]	TGA Weight loss [%]	Functional group [µmol/g]	Kaiser test [µmol/g]	Raman [$I_D I_G^{-1}$ / $I_{D0} I_{G0}^{-1}$]	Sample name
1	10	60	8.9	122	35	0.81	**T47**
2	20	60	14.3	196	65	0.82	**T48**
3	10	20 MW	15.5	214	41	0.95	**T49**
4	20	20 MW	19.6	264	45	0.86	**T50**

The weight loss of MWCNTs determined by TGA reflects the degree of functionalization (Figure 17). The highest result was for the reaction **T50**, in which the reaction was accelerated by MW treatment. Additionally the higher functionalization yield was observed for MWCNTs functionalized in excess of starting aniline **P12**.
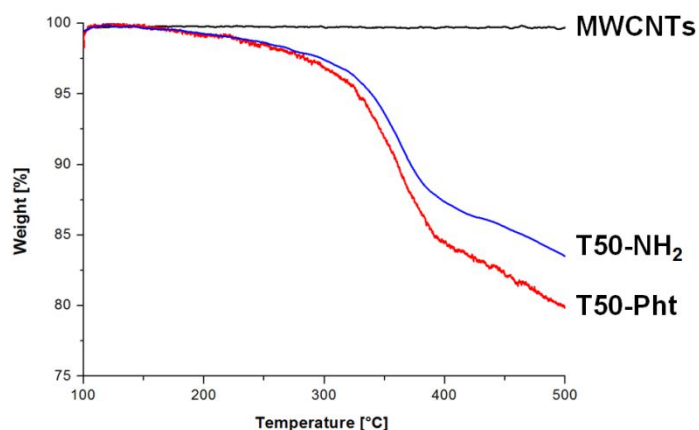
80

Figure 17. TGA of functionalized MWCNTs (T50) (nitrogen atmosphere).

In the Raman spectrum of the product **T47** (Figure 18) we can observe bands characteristic for MWCNTs. The ratio between the intensities of the D and the G peaks of functionalized material was compared to pristine material ($I_D I_G^{-1}$/ $I_{D0} I_{G0}^{-1}$) and listed in Table 8. We observed that this value increases with the higher excess of compound **P12** both in classical heating and MW irradiation.
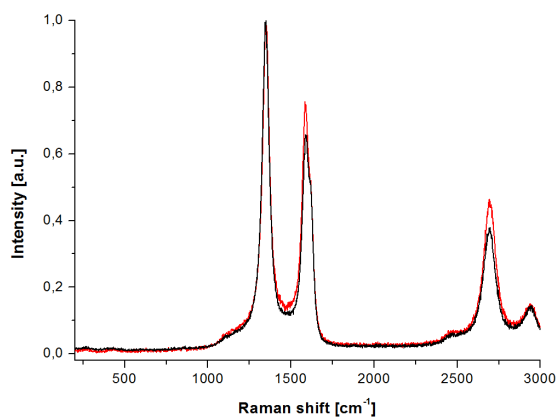

Figure 18. Raman spectra of the pristine (black) and functionalized MWCNTs T47 (red). Laser excitation - 633 nm.

II.3.2 Conclusions

These positive outcomes from the arylation reaction on both types of CNTs are the starting point for the design and controlled processing of novel decorated carbon nanotubes. It would provide an easily and convenient methodology for functionalization of filled nanotubes.

II.4 Experimental part

II.4.1 Synthesis of the organic precursors

***tert*-butyl (2-(2-(2-aminoethoxy)ethoxy)ethyl)carbamate P1**
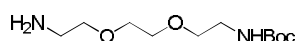
To a solution of 2,2'-(ethylene-dioxy)bis(ethylamine) (50 g, 0.34 mol) in THF (120 mL) a solution of Boc_2O (9.8 g, 0.045 mol) in THF (120 mL), was added dropwise over 40 min at 0 °C. The reaction mixture was stirred overnight at room temperature. Then, the mixture was concentrated under vacuum into white slurry, which was re-dissolved in water (200 mL). Then, to remove not reacted Boc_2O, product was purified by extraction with diethyl ether and then extracted using DCM (3x 50 mL). The combined organic layers were backwashed with water (3x 200 mL), dried with anhydrous $MgSO_4$ and concentrated. Desired product was obtained as colorless viscous oil. Yield: 10.5 g (94%). M/z (ES+) 249 (M+H$^+$, 100%);^{1}H NMR (CDCl$_3$, 400 MHz): δ 1.44 (s, 9H), 2.88 (t, *J*=5.2 Hz, 2H), 3.32 (q, *J*=4.9 Hz, 2H), 3.52 (t, *J*=5.3 Hz, 2H), 3.55 (t, *J*=5.1 Hz, 2H), 3.62 (s, 4H), 5.16 (bs, 1H).Characterization is in agreement with literature.[44]

***tert*-butyl (2,2-dimethyl-7,10-dioxa-4-aza-2-siladodecan-12-yl)carbamate P2**
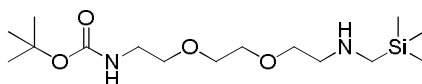
A PIREX tube was charged with **P1** (1.75 g, 7.05 mmol), (chloromethyl)trimethylsilane (491 µL, 3.52 mmol), 12 ml of THF and catalytic amount of KI. The reaction was stirred at 80 °C for 16 h and then the solvent

was evaporated. The residue was dissolved in 0.1 M of NaOH (50 ml) and extracted with Et$_2$O. Chromatographic purification was performed with AcOEt:MeOH:NH$_3$/80:15:5 as eluent. Yield: 350 mg (15 %). M/z (ES+) 335 (M+H$^+$, 100%); ^{1}H NMR (CDCl$_3$, 400 MHz): δ 0.05 (s, 9H), 1.43 (s, 9H), 1.92 (s, 2H), 2.10 (s, 1H), 2.81 (m, 2H), 3.32 (t, 2H), 3.51 (t, 2H), 3.61 (m, 6H) 5.19 (bs, 1H); ^{13}C NMR (CDCl$_3$, 125 MHz, ppm): δ157.4, 80.7, 70.34, 70.10, 69.89, 69.52, 49.4, 40.4, 28.6.

## *N*-hydroxy-2-oxo-2-phenylacetimidoyl chloride P3
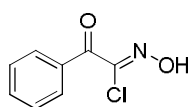
Compound was purchase from CHEMSTEP and used without further purification.

General procedure for oxime synthesis

In a typical procedure for 50 mmol range, the reactants in the molar ratio aldehyde:NH$_2$OHxHCl:NaOH=1:1.2:1.2.A stirred solution of aldehyde (1 mmol) in EtOH (5 ml) was treated with the NaOH (1.2 mmol) solution in water. Than the aqueous solution of NH$_2$OH was added and stirred at room temperature 25 °C overnight. Later the product was concentrated under vacuum and then extracted with ethyl acetate. Than organic layer was dried over anhydrous Na$_2$SO$_4$, filtered and concentrated. Product was recrystallized from ethyl acetate-hexane (1: 2 ratio) afforded the pure oxime products, characterized by melting point comparison and spectroscopic data (IR, ^{1}H NMR, Mass). Characterization is in agreement with literature.[45]

3,4,5-trimethoxybenzaldehyde oxime P4
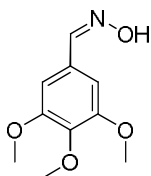
^{1}H NMR (DMSO-d6, 500 MHz, ppm): δ 11.11 (s, 1H), 8.05 (s, 1H), 6.91 (s, 2H), 3.79 (s, 6H), 3.68 (s, 3H); ^{13}C NMR (DMSO-d6, 125 MHz, ppm): δ 153.1, 147.9, 138.4, 128.6, 103.7, 60.1, 55.8; MS m/z: 212 (M$^+$).

2,4-dichlorobenzaldehyde oxime P5
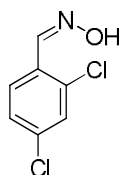
^{1}H NMR (DMSO-d6, 400 MHz): δ 11.80 (s, 1H), 8.32 (s, 1H), 7.82 (d, J= 8.55 Hz, 1H), 7.70 (d, J= 2.1 Hz, 1H), 7.46 (dd, J= 2.25 Hz, J2.25 Hz, 1H); ^{13}C-NMR (DMSO-d6, 125 MHz): δ 150.9, 148.1, 132.0, 127.5, 120.6, 111.9.

anthracene-9-carbaldehyde oxime P6
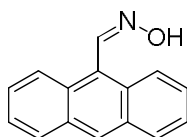
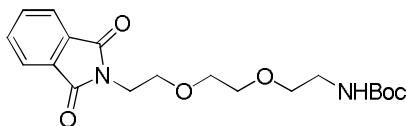^{1}H NMR (DMSO-d6, 500 MHz, ppm): δ 11.74 (s, 1H), 9.21 (s, 1H), 8.65 (s, 1H), 8.44 (d, J= 8.55 Hz, 2H), 8.11 (d, J=8.05 Hz, 2H), 7.62-7.50 (m, 4H); ^{13}C NMR (DMSO-d6, 125 MHz, ppm): δ 146.5, 130.9, 129.5, 128.8, 128.5, 126.7, 125.5, 125.1, 124.8; MS m/z: 222 (M$^+$).

**4-[(N-Boc)aminomethyl]aniline P7**:
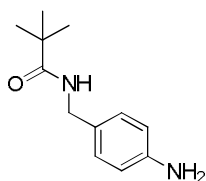
Compound was purchase from Aldrich and used without further purification

P8

A toluene solution (60 mL) of *N*-tert-Butoxycarbonyl-2,2'-ethylenedioxybis(ethylamine) (3 g, 0.012 mol) and phthalic anhydride (1.79 g, 0.012 mol) was stirred at reflux overnight. TLC (toluene:ethyl acetate1:1) indicated the formation of the product (R_f = 0.6). The solvent was removed under reduced pressure. Product was purified by flash chromatography toluene:EtOAc 7:3. Yield: 2.5 g (92%);M/z (ES+) 378 (M+H$^+$,100%);^{1}H NMR (CDCl$_3$, 400 MHz): δ 1.42 (s, 9H), 3.23 (m, 2H), 3.46 (m, 2H), 3.55 (m, 2H), 3.62 (m, 2H), 3.74 (m, 2H), 3.90 (m, 2H), 5.04 (s, 1H), 7.69 (m, 2H), 7.84 (m, 2H). ^{13}C NMR (CDCl$_3$, 125 MHz): δ 168.27, 155.98, 133.95, 132.11, 123.24, 79.12, 70.27, 69.90, 67.93, 40.35, 37.13, 28.41. Characterization is in agreement with literature.[46]
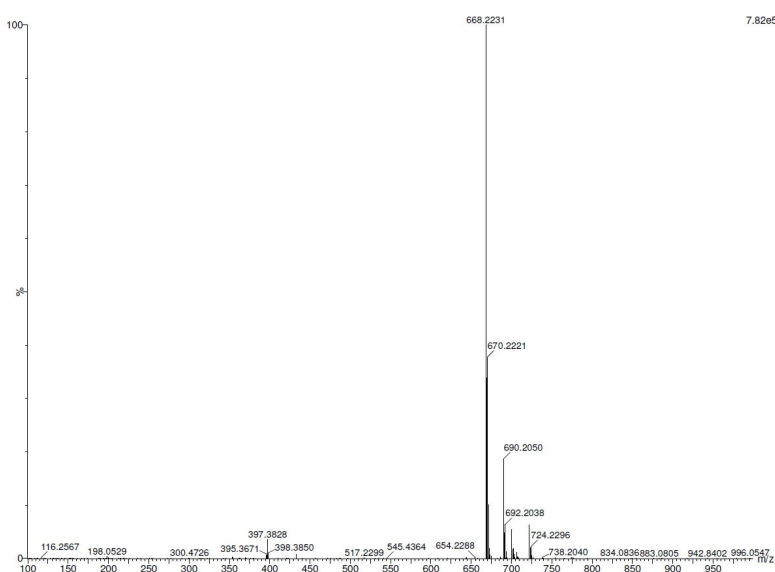
P9
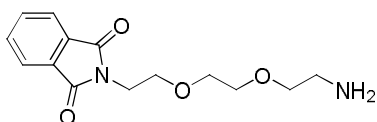
P8 (2.5 g, 6.61 mmol) was dissolved in 5 mL of DCM and the solution was cooled down to 0 °C. Then 5 mL of TFA was added dropwise. The mixture was stirred at room temperature for 24 h. After evaporation of the solvent and precipitation of the product from methanol/cold diethyl ether, white crystals were obtained. After filtration, the product was dried under vacuum to give the pure compound **P9**. Product was stored under vacuum. Yield: 2.5 g (98%). M/z (ES+) 392 (M+H$^+$);^{1}H NMR (CDCl$_3$, 400 MHz): δ 3.21 (m, 2H), 3.60 (s, 4H), 3.72 (m, 4H), 3.88 (m, 2H), 7.71 (m, 2H), 7.84 (m, 2H), 8.22 (m, 2H).^{13}C NMR (CDCl$_3$, 125 MHz): δ 168.54, 161.88, 134.15, 131.88, 123.36, 118.62, 70.05, 69.62, 68.20, 66.52, 39.66, 37.29. Characterization is in agreement with literature.[46]
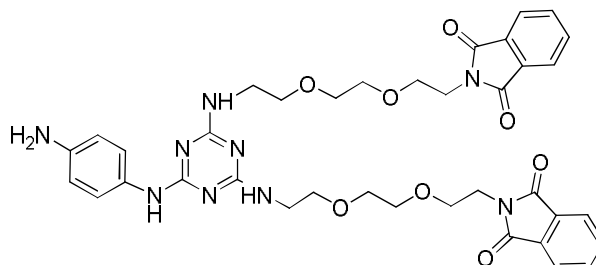
86

P10
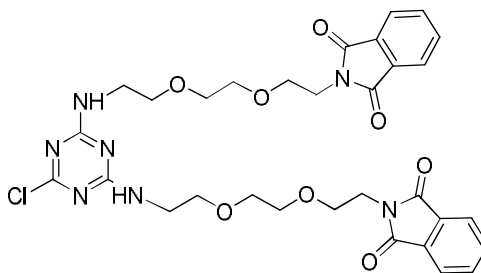
P9 (1.27 g, 3.24 mmol) was dissolved in 30 mL of THF and cooled down to 0 °C. Then DIEA (563 µl, 3.240 mmol) was added. Solution of cyanuric chloride (299 mg, 1.62mmol) in 30 mL of THF was added dropwise. Mixture was warmed to r.t. and stirred overnight. The reaction was monitored by TLC using EtOAc:DCM:MeOH/50:50:3 as eluent. Then the solvent was evaporated and product was purified by flash chromatography using EtOAc:DCM:MeOH/50:50:3 as eluent, affording 1.03 g of yellow oil. The product was stored under vacuum. Yield 1.03 g (90%). M/z (ES+) 669 (M+H$^+$);^{1}H NMR (CDCl$_3$, 400 MHz): δ 3.54 (m, 12H), 3.63 (m, 4H), 3.74 (m, 4H), 3.90 (m, 4H), 5.91 (s, 1H), 6.04 (s, 1H), 7.69 (m, 4H), 7.84 (m, 4H); ^{13}C NMR (CDCl$_3$, 125 MHz, ppm): δ 168.18, 165.43, 133.81, 131.95, 123.16, 123.07, 70.34, 70.10, 69.89, 69.52, 69.31, 67.97, 40.60, 37.09.

P11

P10 (900 mg, 1.35mmol) was dissolved in THF (100 mL), then DIEA (468μl, 2.7mmol) was added. *N*-Boc-*p*-phenylenediamine (270 mg, 1.26mmol) was dissolved in 50 mL of THF and added dropwise to the solution of compound **P10**. Reaction was stirred at 70 °C for 4 h. Product was purified by flash chromatography using EtOAc:DCM:MeOH/50:50:3 as eluent, affording 810 mg of pure product. Yield 810 mg (71%). M/z (ES+) 840 (M+H^{+});^{1}H NMR (CDCl$_3$, 400 MHz): δ 1.51 (s, 9H), 3.52 (m, 4H), 3.59 (m, 8H), 3.65 (m, 4H), 3.76 (m, 4H), 3.92 (t, 4H), 5.98 (s, 2H), 6.55 (s, 1H), 7.31 (m, 2H), 7.50 (m, 2H), 7.68 (m, 4H), 7.83 (m, 4H); ^{13}C NMR (CDCl$_3$, 125 MHz, ppm): δ 168.33, 133.91, 132.06, 123.22, 70.33, 70.00, 67.96, 37.20, 28.36.

P12

Compound **P11** (800 mg, 0.96mmol) was dissolved in 40 mL of DCM and cooled down to 0 °C in ice bath. Then 5 mL of TFA was added drop wise. Reaction mixture was stirred at room temperature for 24 h to cleave of the Boc protecting group. After the solvent was evaporated and the product was triturated few times from toluene and then Et$_2$O to afford a brownish sticky oil. The product was stored under vacuum. Yield 750 mg, yield 88%. M/z (ES+) 740 (M+H$^+$);^{1}H NMR (CDCl$_3$, 100 MHz):δ 3.53 (m, 4H), 3.60 (m, 8H), 3.63 (m, 4H), 3.72 (m, 4H), 3.84 (t, 4H), 7.27 (m, 2H), 7.59 (m, 2H), 7.75 (m, 4H), 7.79 (m, 4H); ^{13}C NMR (CDCl$_3$, 125 MHz): δ 168.31, 162.25, 161.96, 152.82, 134.04, 131.85, 123.23, 121.79, 117.17, 114.87, 70.16, 70.01, 68.70, 68.13, 40.63, 37.37.
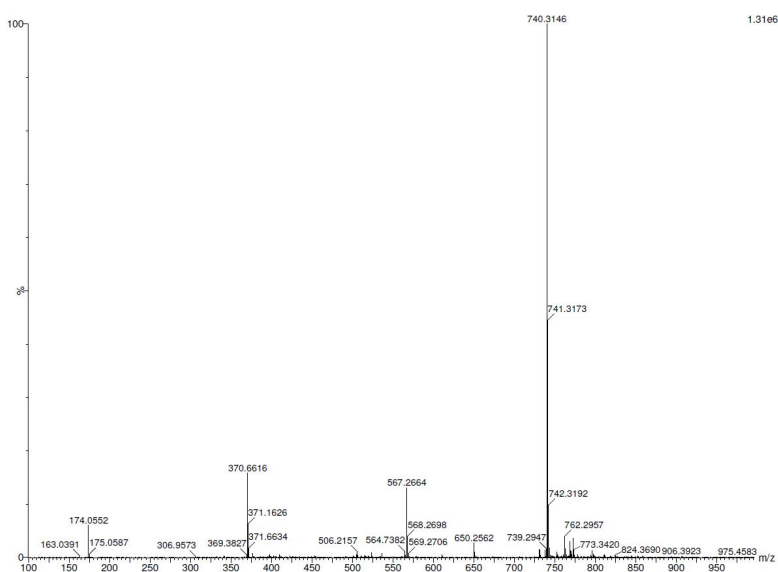
II.4.2 Functionalization

Purification of HiPCO SWCNTs for cycloaddition reactions

The SWCNTs used for cycloaddition study were produced high pressure carbon monoxide method called (HiPCO) purchased from Carbon Nanotechnologies (lot #R0510C). The material was purified by concentrated HCl treatment following a previously reported protocol.[47] In this step the as-received SWCNTs were treated with hydrochloric acid, which is an established method for the removal of impurities. One gram of SWNCTs was placed in a 500 ml round bottom flask and 200 mL of HCl was added. The mixture was stirred using magnetic stirrer for 2 h, then diluted in water, collected by filtration through a 0.2 μm polycarbonate membrane and thoroughly washed with water until neutral pH. The sample was dried under vacuum.

Purification of SWCNTs for diazonium-based functionalization

The SWCNTs used in this investigation were produced by chemical vapor deposition from Thomas Swan & Co. Ltd (Elicarb®). The material was purified by steam treatment following a previously reported protocol.[48] Briefly, SWCNTs were spread inside a silica tube, which was then placed into a furnace alumina tube. The whole system was initially purged with argon for 2 h, to remove atmospheric air. Later on, steam was introduced by bubbling argon through a flask containing hot distilled water and furnace was heated at 900 °C for4 h to allow the purification of the material. The solid powder was collected and treated with 6 M HCl (Panreac) at 110 °C overnight to dissolve the exposed iron nanoparticles (from catalyst). The purified SWCNTs were collected by filtration through a 0.2 μm polycarbonate membrane and thoroughly washed with water until neutral pH. The sample was oven-dried at 80 °C overnight.

Purification of MWCNTs

The MWCNTs were purchased from Thomas Swan & Co. Ltd. As-received MWCNTs were dispersed in fresh piranha solution (H_2SO_4/H_2O_2, 3:1) at a concentration of 1 mg mL^{-1}. The solution was stirred for 2 h at r.t. and the reaction then quenched with distilled water. The pH of the solution was adjusted until neutral. The sample was filtered on a polycarbonate membrane and dried in the oven at 80 °C overnight. Next, the MWCNTs were treated with steam for 1 h at 900 °C and refluxed in 6 M HCl at 110 °C overnight. The solid sample was collected by filtration and rinsed with distilled water until neutral pH.

Oxidation of SWCNTs *T16*
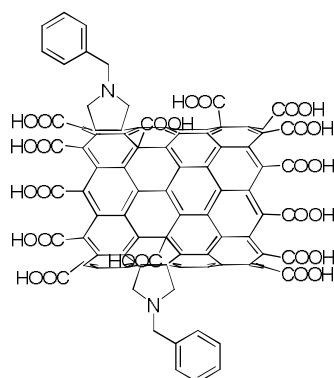
The SWCNTs (HiPCO) purchased from Carbon Nanotechnologies (lot #R0510C) were treated with concentrated H2SO4/HNO3 mixture (3:1). In the experiment, 60 mg of purified SWCNTs was suspended in 50 mL of a 3:1 mixture of concentrated H2SO4 (98 wt %)/HNO3 (16 M) and stirred in a water bath for 24 h. The resultant suspension was then diluted with 250 mL of water, and the SWCNTs were collected on a 0.1 µm-pore membrane filter and washed with deionized water. Then, dried under vacuum.[15]

Functionalization

<u>Synthesis of **T1**-**15**, **T17**</u>

<u>Cycloaddition of azomethine ylide generated from *N*-benzyl-*N*-(methoxymethyl)-*N*-[(trimethylsilyl)methyl]amine</u>
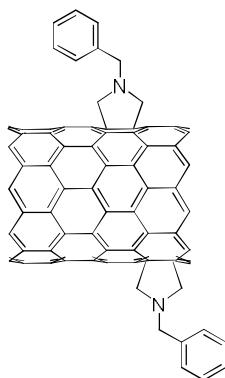
CNTs (10.0 mg) were added to the appropriate solvent (5 mL) and dispersed by sonication for 10 min. Then the *N*-benzyl-*N*-(methoxymethyl)-*N*-[(trimethylsilyl)methyl]amine was added in excess (200 mg) to the dispersion of nanotubes. Then the mixture was degassed with Ar and cooled to 0 °C. The 5mL of solution of TFA (0.18 M) in appropriate solvent was added dropwise. The resultant mixture was allowed to warm to room temperature and react. Then, the product was filtered (membrane MILIPORE, type: JHWP, pore size 0.45 µm). The solid recovered on the filter was dispersed in DMF, sonicated in a water bath until thorough dispersion of the CNTs and again filtered. This sequence was repeated 3 times with DMF, twice with MeOH and once with Et$_2$O and then functionalized CNTs were dried under vacuum.

Synthesis of **T19**

Cycloaddition of azomethine ylide generated from trimethylsilylmethylamine **P2**
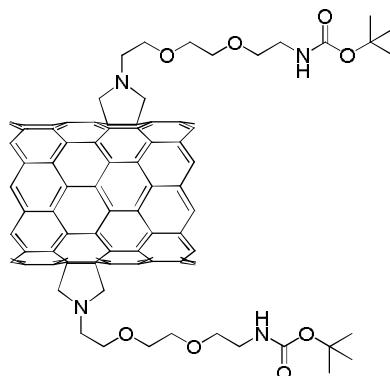
CNTs (10.0 mg) were added to the appropriate solvent (5 mL) and dispersed by sonication for 10 min. Then the paraformaldehyde and trimethylsilylmethylamine **P2** (260 mg) in molar ratio 2:1 were added. Then the mixture was degassed with Ar and cooled to 0 °C. 5mL of solution of TFA (0.18 M) in appropriate solvent was added dropwise. Resultant mixture was allowed to warm to room temperature and react for appropriate time. After, the product was filtered (membrane MILIPORE, type: JHWP, pore size 0.45 µm). The solid recovered on the filter was dispersed in DMF, sonicated in a water bath until thorough dispersion of the CNTs and again filtered. This sequence was repeated 3 times with DMF, twice with MeOH and once with Et$_2$O and then functionalized CNTs were dried under vacuum.

General procedure for deprotection -Boc function (Synthesis of **T20**)
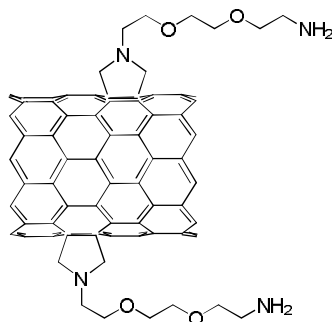
The Boc group was cleaved by treatment with 4 M HCl solution in 1,4-dioxane (1 mL/ 1 g of CNTs) overnight at the room temperature. After reaction, the functionalized SWCNTs were dispersed in1,4-dioxane and filtered. The solid recovered on the filter was dispersed in MeOH, sonicated in a water bath until thorough dispersion of the CNTs and again filtered. This sequence was repeated twice with MeOH and once with Et_2O and then functionalized CNTs were dried under vacuum. The free amine loading was estimated by Kaiser test.

Synthesis of **T21**-**29**

Cycloaddition of nitrile oxide generated from aldoxime chloride (**P3**) with TEA
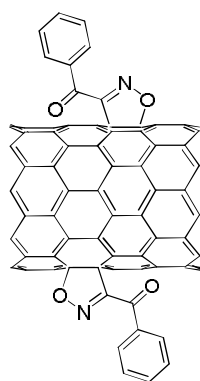
The reaction was performed on CNTs in two aprotic solvents with different polarity (**T21** (DMF) and **T22** (*o*-DCB). Product **P3** was added to the dispersion of CNTs in excess (10 times in weight) and cooled to 0 °C. TEA was added in a molar ratio 3:1 to the aldoxime chloride to generate the nitrile oxide. Reaction was carried out at room temperature for 16 h. After, the product was filtered (membrane MILIPORE, type: JHWP, pore size 0.45 µm). The solid recovered on the filter was dispersed in DMF, sonicated in a water bath until thorough dispersion of the CNTs and again filtered. This sequence was repeated 3 times with DMF, twice with MeOH and once with Et_2O and then functionalized CNTs were dried under vacuum.

Synthesis **T26**-**28**

Microwave-assisted cycloaddition of nitrile oxide generated from aldoxime chloride (**P3**)
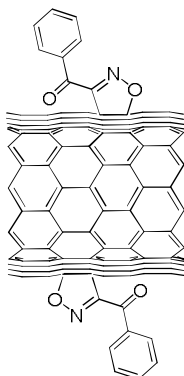
MWCNTs (10.0 mg) were dispersed in 10 mL of solvent by sonication for 10 min. The *N*-hydroxy-2-oxo-2-phenylacetimidoyl chloride (**P3**) was added in excess (10 times in weight) and dissolved by sonication for 5 min. The reaction mixture was stirred at 100 °C for 1 h and then filtered (membrane MILIPORE, type: JHWP, pore size 0.45 μm).The solid recovered on the filter was dispersed in DMF, sonicated in a water bath until thorough dispersion of the CNTs and again filtered. This sequence was repeated 3 times with DMF, twice with MeOH and once with Et$_2$O and then functionalized CNTs were dried under vacuum.
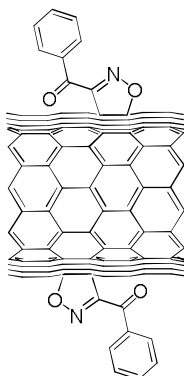
Synthesis **T29**

Microwave-assisted cycloaddition of nitrile oxide generated from aldoxime chloride (**P3**)


MWCNTs (10.0 mg) were dispersed in 20 mL of DCM by sonication for 10 min. The *N*-hydroxy-2-oxo-2-phenylacetimidoyl chloride (**P3**) was added in excess

(10 times in weight) and dissolved by sonication for 5 min. The solvent was evaporated and powder mixture was continually stirred at 100 °C with 200 W of power. Then the powder was dispersed in 100 mL of DMF and filtered (membrane MILIPORE, type: JHWP, pore size 0.45 μm). The solid recovered on the filter was dispersed in DMF, sonicated in a water bath until thorough dispersion of the CNTs and again filtered. This sequence was repeated 3 times with DMF, twice with MeOH and once with Et$_2$O and then functionalized CNTs were dried under vacuum.

Synthesis of **T36**-**37**

Functionalization of CNTs by diazonium-based arylation
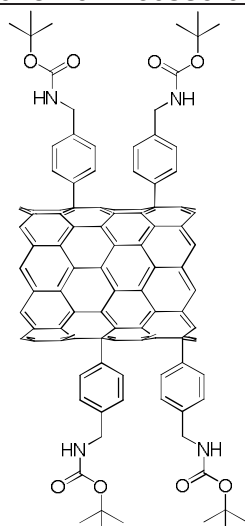
CNTs (10 mg) in 10 mL of DMF were dispersed by sonication for 10 min. Then 4-[(N-Boc)aminomethyl]aniline was added (100 mg, 0.50mmol) and dispersed for another 5 min. The mixture was cooled to 0°C and isopentyl nitrite (173.9 mg, 199.5μL, 1.48 mmol) was added and the mixture was stirred at 80°C for appropriate time(1 or 4 h). Then mixture was cooled down, and filtered (membrane MILIPORE, type: JHWP, pore size 0.45 μm). The solid recovered on the filter was dispersed in DMF, sonicated in a water bath until thorough dispersion of the CNTs and again filtered. This sequence was repeated 3 times with DMF, twice with MeOH and once with Et$_2$O and then functionalized CNTs were dried under vacuum.
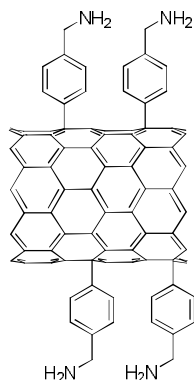
General procedure for deprotection of -Boc function

The Boc group was cleaved by treatment with 4 M HCl solution in 1,4-dioxane (1 mL/ 1 g of CNTs) overnight at the room temperature. After, the functionalized SWCNTs were dispersed in1,4-dioxane and filtered. The solid recovered on the filter was dispersed in MeOH, sonicated in a water bath until thorough dispersion of the CNTs and again filtered. This sequence was repeated twice with MeOH and once with Et_2O and then functionalized CNTs were dried under vacuum. The free amine loading was estimated by Kaiser test.

Synthesis of **T38**-**42**

Diazonium-salt arylation of CNTs with aniline (**P12**)
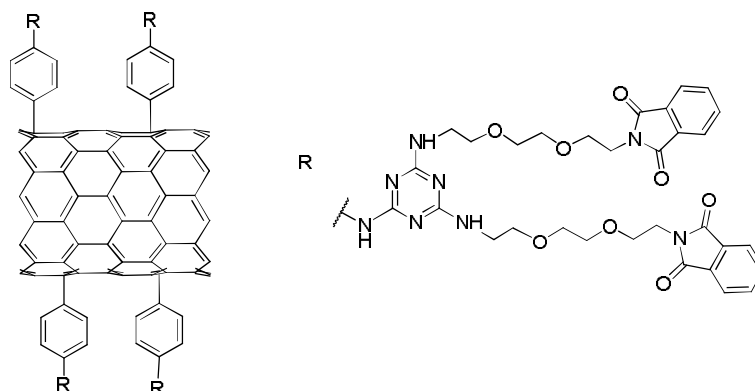
CNTs (10 mg) in 10 mL of DMF were dispersed by sonication for 10 min. Then aniline **P12** was added in appropriate excess (10, 13, 25 times in weight) and dispersed for another 5 min. The mixture was cooled to 0°C and isopentyl nitrite (3:1 molar equivalent to amine) was added and the solution was stirred at 80°C

for appropriate time (1 or 4 h). Then the mixture was cooled down and filtered (membrane MILIPORE, type: JHWP, pore size 0.45 µm). The solid recovered on the filter was dispersed in DMF, sonicated in a water bath until thorough dispersion of the CNTs and again filtered. This sequence was repeated 3 times with DMF, twice with MeOH and once with Et$_2$O and then functionalized CNTs were dried under vacuum.

Synthesis of **T43-46**

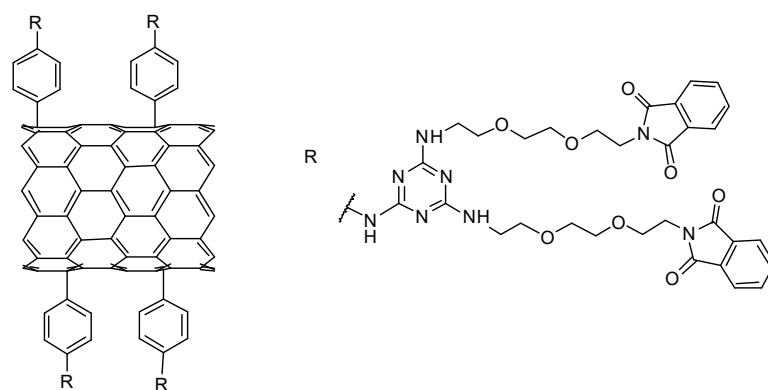Microwave-assisted diazonium-salt arylation of CNTs with aniline (**P12**)

CNTs (10 mg) in 10 mL of DMF were dispersed by sonication for 10 min. Then aniline **P13** was added in appropriate excess (10, 25 times in weight) and dispersed for another 5 min. The mixture was cooled to 0°C and isopentyl nitrite (3:1 molar equivalent to amine) was added and the solution was irradiated for appropriate time (2 min cycles from 75-80°C) with 200 W. Then the mixture was cooled down and filtered (membrane MILIPORE, type: JHWP, pore size 0.45 µm). The solid recovered on the filter was dispersed in DMF, sonicated in a water bath until thorough dispersion of the CNTs and again filtered. This sequence was repeated 3 times with DMF, twice with MeOH and once with Et$_2$O and then functionalized CNTs were dried under vacuum.

General procedure for deprotection of -NPht
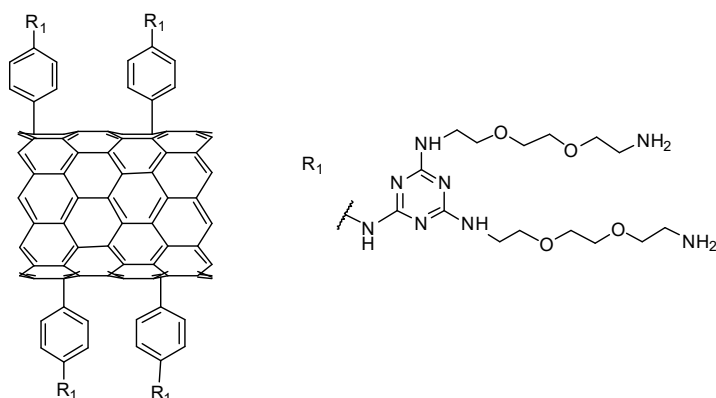
For the deprotection, the CNTs were dispersed in EtOH (1 mg/mL) by sonicating for 5 min, and afterwards treated with hydrazine hydrate (10 mg/mL). The dispersion was stirred at r.t. for 2 h, and then diluted with EtOH and filtered. After filtration, the functionalized CNTs were re-precipitated in EtOH, filtered again (membrane MILIPORE, type: JHWP, pore size 0.45 μm). The solid recovered on the filter was dispersed with 0.1 M HCl solution, sonicated in a water bath until thorough dispersion of the CNTs and again filtered. This sequence was repeated 3 times with water, twice with MeOH and once with Et$_2$O and then functionalized CNTs were dried under vacuum. The free amine loading was estimated by Kaiser test.

Bibliography

[1] V. Georgakilas, K. Kordatos, M. Prato, D. M. Guldi, M. Holzinger, A. Hirsch; *J. Am. Chem. Soc.* **2002**, *124*, 760–761.

[2] G. Pandey, P. Banerjee, S. R. Gadre; *Chem. Rev.* **2006**, *106*, 4484–4517.

[3] R. Huisgen, W. Scheer; *Tetrahedron Lett.* **1971**, *12*, 481–484.

[4] F. G. Brunetti, M. A. Herrero, J. M. Muñoz, S. Giordani, A. Díaz-Ortiz, S. Filippone, G. Ruaro, M. Meneghetti, Maurizio Prato, and Ester Vázquez; *J. Am. Chem. Soc.* **2007**, *129*, 14580–14581.

[5] S. Roy, T. L. S. Kishbaugh, J. P. Jasinski, G. Gribble; *Tetrahedron Lett.* **2007**, *48*, 1313–1316.

[6] V. Georgakilas, K. Kordatos, M. Prato. D. M. Guldi, M. Holzinger, A. Hirsch; *J. Am. Chem. Soc.* **2002**, *124*, 760–761.

[7] Y. Wang, Z. Iqbal, S. Mitra; *Carbon* **2005**, *43*, 1015–1020.

[8] J. Li, H. Grennberg; *Chem. Eur. J.* **2006**, *12*, 386–3875.

[9] Vedejs, E., In Advances in Cycloaddition, Curran, D. P., Ed.; JAI Press: London, **1988**.

[10] E. Laborde; *Tetrahedron Lett.* **1992**, *33*, 6607–6610.

[11] X. Zhang, M. Willems, C. S. Foote; *Tetrahedron Lett.* **1993**, *34*, 8187–8188.

[12] Z. Li, L. Zheng, W. Yan, Z. Pan, S. Wei; *Chem. Phys. Chem.* **2009**, *10*, 2296–2304.

[13] V. Datsyuk, M. Kalyva, K. Papagelis, J. Parthenios, D. Tasis, A. Siokou, I. Kallitsis, C. Galiotis; *Carbon* **2008**, *46*, 833–840.

[14] S. Lee, S. Diab, P. Queval, M. Sebban, I. Chataigner, S. R. Piettre; *Chem. Eur. J.* **2013**, *19*, 7181 – 7192.

[15] J. Zhang, H. Zou, Q. Qing, Y. Yang, Q. Li, Z. Liu, X. Guo, Z. Du; *J. Phys. Chem. B* **2003**, *107*, 3712–3718.

[16] M L. M.alard, M. A. Pimenta, G. Dresselhaus, M. S. Dresselhaus; *Phys. Rep.* **2009**, *473*, 51.

[17] K.B.G. Torssell, Nitrile Oxides, Nitrones and Nitronates in Organic Synthesis, VCH Verlag GmbH, New York **1988**

[18] J. J. Talley, D. L. Brown, J. S. Carter, M. J. Graneto, C. M. Koboldt, J. L. Masferrer, W. E. Perkins, R. S. Rogers, A. F. Shaffer, Y. Y. Zhang, B. S. Zweifel, K. Seibert; *J. Med. Chem.,* **2000**, *43*, 775–777.

[19] D. J Burkhart, B. Twamley, N. R Natale; *Tetrahedron Lett.* **2001**, *42*, 8415–8418.

[20] V. Librando, U. Chiacchio, A. Corsaro, G. Gumina; *Polycydic Aromatic Compounds* **1996**, *11*, 313–316.

[21] M. Alvaro, P. Atienzar, P. de la Cruz, J. L. Delgado, V.Troiani, H. Garcia, F. Langa, A. Palkar, L. Echegoyen; *J. Am. Chem. Soc.* **2006**, *128*, 6626–6635.

[22] M. Popławska, G.Z. Żukowska, S. Cudziło, M. Bystrzejewski; *Carbon* **2010**, *48*, 1318–1320.

[23] R. K. Saini, I. W. Chiang, H. Peng, R. E. Smalley, W. E. Billups, R. H. Hauge, J. L. Margrave; *J. Am. Chem. Soc.* **2003**, *125*, 3617–3621.

[24] A. C. Ferrari, J. Robertson; *J. Phys. Rev. B* **2000**, *61*, 14095–14107.

[25] De-Q. Yang, J.-F. Rochette, E. Sacher; *Langmuir* **2005**, *21*, 8539–8545.

[26] G. Giambastiani, S. Cicchi, A. Giannasi, L. Luconi, A. Rossin, F. Mercuri, C. Bianchini, A. Brandi, M. Melucci, G. Ghini, P. Stagnaro, L. Conzatti, E. Passaglia, M. Zoppi, T. Montini, P. Fornasiero; *Chem. Mater.* **2011**, *23*, 1923–1938.

[27] G. Ghini,a L. Luconi, A. Rossin, C. Bianchini, G. Giambastiani, S. Cicchi, L. Lascialfari, A. Brandi, A. Giannasic; *Chem. Commun.* **2010**, *46*, 252–254.

[28] K.-C. Liu, B. R. Shelton, R. K. Howe; *J. Org. Chem.* **1980**, *45*, 3916–3918.

[29] R. Graupner; *Raman Spectrosc.* **2007**, *38*, 673–683.

[30] J. L. Bahr, J. Yang, D. V. Kosynkin, M. J. Bronikowski, R. E. Smalley, J. M. Tour; *J. Am. Chem. Soc.* **2001**, *123*, 6536–6542.

[31] J. L. Bahr, J. M. Tour; *Chem. Mater.* **2001**, *13*, 3823–3824.

[32] B. K. Price, J. L. Hudson, J. M. Tour; *J. Am. Chem. Soc.* **2005**, *127*, 14867–14870.

[33] B. K. Price, J. M. Tour; *J. Am. Chem. Soc.* **2006**, *128*, 12899–12904.

[34] J. J. Stephenson, J. L. Hudson, S. Azad, J. M. Tour; *Chem. Mater.* **2006**, *18*, 374–377.

[35] X. Chen, J. Wang, W. Zhong, T. Feng, X. Yang, J. Chen; *Macromol. Chem. Phys.* **2008**, *209*, 846–853.

[36] J. Mateos-Gil, L. Rodríguez-Pérez, M. Moreno Oliva, G. Katsukis, C. Romero-Nieto, M. Á. Herranz, D. M. Guldi, N. Martín; *Nanoscale*, **2015**, *7*, 1193–1200.

[37] J. L. Hudson, H. Jian, A. D. Leonard, J. J. Stephenson, J. M. Tour; *Chem. Mater.* **2006**, *18*, 2766–2770.

[38] J. Liu, M. Rodriguez i Zubiri, B. Vigolo, M. Dossot, B. Humbert, Y. Fort, E. McRae; *J. Nanosci. Nanotechnol.* **2007**, *7*, 3519–3523.

[39] M. Burghard, A. Maroto, K. Balasubramanian, T. Assmus, A. Forment-Aliaga, E. J. H. Lee, R. T. Weitz, M. Scolari, F. Nan, A. Mews, K. Kern; *Phys. Stat. Sol. B* **2007**, *244*, 4021–4025.

[40] V. Biju, T. Itoh, Y. Makita, M. Ishikawa; *J. Photochem. Photobiol. A: Chem.* **2006**, *183*, 315–321.

[41] R. A. Graff, T. M. Swanson, M. S. Strano; *Chem. Mater.* **2008**, *20*, 1824–1829.

[42] M. S. Strano, C. A. Dyke, M. L. Usrey, P. W. Barone, M. J. Allen, H. W. Shan, C. Kittrell, R. H. Hauge, J. M. Tour, R. E. Smalley; *Science* **2003**, *301*, 1519–22.

[43] M. R. Heinrich; *Chem. Eur. J.* **2009**, *15*, 820–833.

[44] K. Kordatos, T. Da Ros, S. Bosi, E. Vázquez, M. Bergamin, C. Cusan, F. Pellarini, V. Tomberli, B. Baiti, D. Pantarotto, V. Georgakilas, G. Spalluto, and M. Prato; *J. Org. Chem.* **2001**, *66*, 4915–4920.

[45] J. Yua, M. Lu; *Adv. Synth. Catal.* **2015**, *357*, 1175–1180.

[46] W. Wu, S. Wieckowski, G. Pastorin, M. Benincasa, C. Klumpp, J. P. Briand, R. Gennaro, M. Prato, A. Bianco; *Angew. Chem. Int. Ed. Engl.* **2005**, *44*, 6358–6362

[47] V. Datsyuk, M. Kalyva, K. Papagelis, J. Parthenios, D. Tasis, A. Siokou, I. Kallitsis, C. Galiotis; *Carbon* **2008**, *46*, 833–840.

[48] B. Ballesteros, G. Tobias, L. Shao, E. Pellicer, J. Nogués, E. Mendoza, M. L.H. Green; *Small* **2008**, *4*, 1501–1506.

III. Functionalization of filled CNTs for radioactivity delivery

III.1 Introduction

Among all carbon nanostructures there is a growing interest to combine carbon nanotubes with foreign materials to explore their properties in potential biological application. Taking advantage of CNTs' ability to cross many biological barriers with a small cytotoxic effect, the internal part of CNTs provides an excellent host matrix for several therapeutic agents. Filling of both SWCNTs and MWCNTs were reported in the literature[1] and the activity of such system in a biological media was reported, for the first time, on SWCNTs filled with NaI. Hong *et al.* presented single-walled CNTs filled with Na^{125}I (Auger and γ-emitter), functionalized and glycosylated for *in vitro* and *in vivo* study (Figure 1).[2]
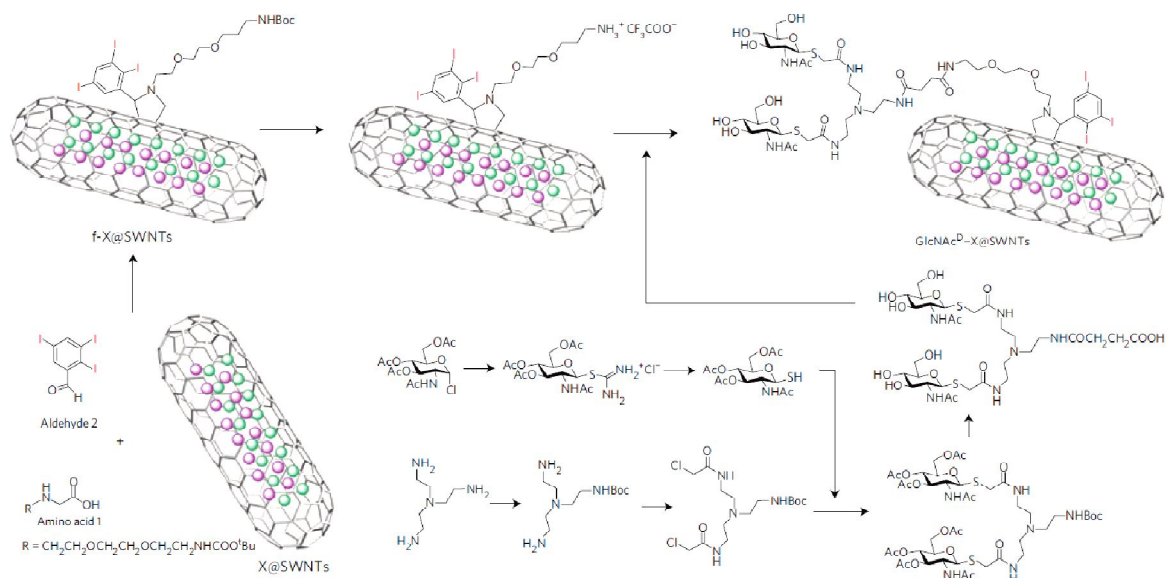
Figure 1. Synthesis of glycosylated– Na^{125}I @SWCNTs.

These radioactive, functionalized nanotubes showed very high natural affinity to lungs. Moreover no leakage of the filling was observed and this allowed their use as a precise tool for imaging. This system, in comparison to CNTs externally bounded with radioisotopes such as ^{86}Y, ^{125}I, ^{14}C, ^{64}Cu or ^{99m}Tc,[3] revealed much higher potential radiodose.

Among several isotopes used in radiotherapy,[4] Bianco and coworkers tested two radionuclide analogues (SmCl$_3$ and LuCl$_3$) encapsulated in SWCNTs (Figure 2) for targeted anticancer therapy.[5]
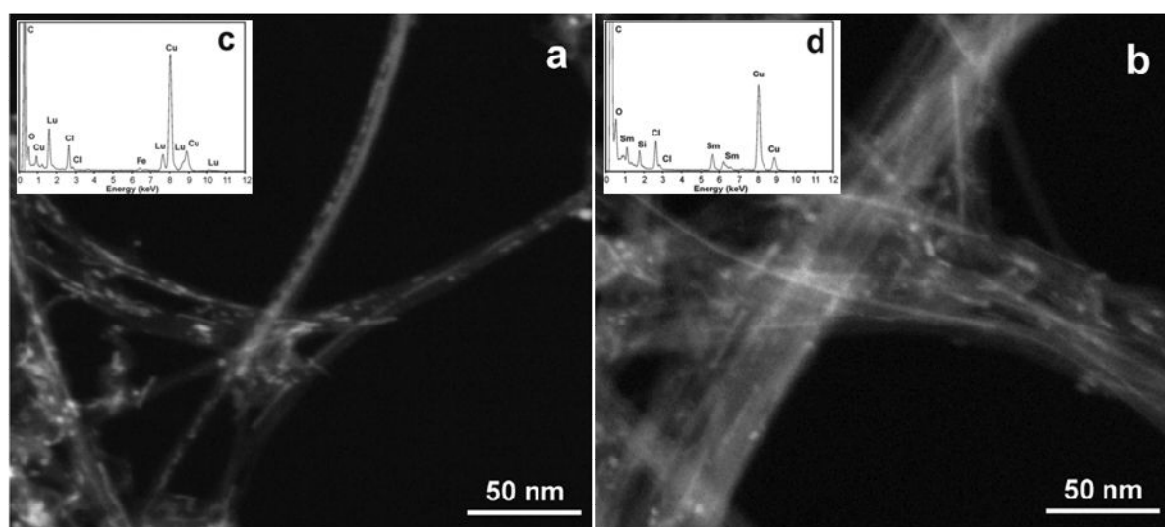

Figure 2. HAADF-STEM images of (a) LuCl$_3$@SWCNTs and (b) SmCl$_3$@SWCNTs; EDX spectrum of (c) LuCl$_3$@SWCNTs and (d) SmCl$_3$@SWCNTs. The Cu peaks arise from the grid employed for the analysis.

The preparation method of the loading and washing was previously optimized by Tobias and co-workers.[6] Nanotubes were filled with metal halides and sealed, then functionalized by nitrene cycloaddition and bound to monoclonal antibody (Cetuximab) for *in vitro* targeting cancer cells (Figure 3). For both filled SWCNTs, it was observed that the antibody functionalization allowed for the active endocytosis and "nanoneedle" mechanism, a passive translocation into the cytoplasm, previously reported by Markovic *et al.*[7] No significant reduction of viability was observed for the different compounds at 10, 50 and 100 µg mL^{-1}, confirming that the filled metal chlorides are not released from capsulated tubes.
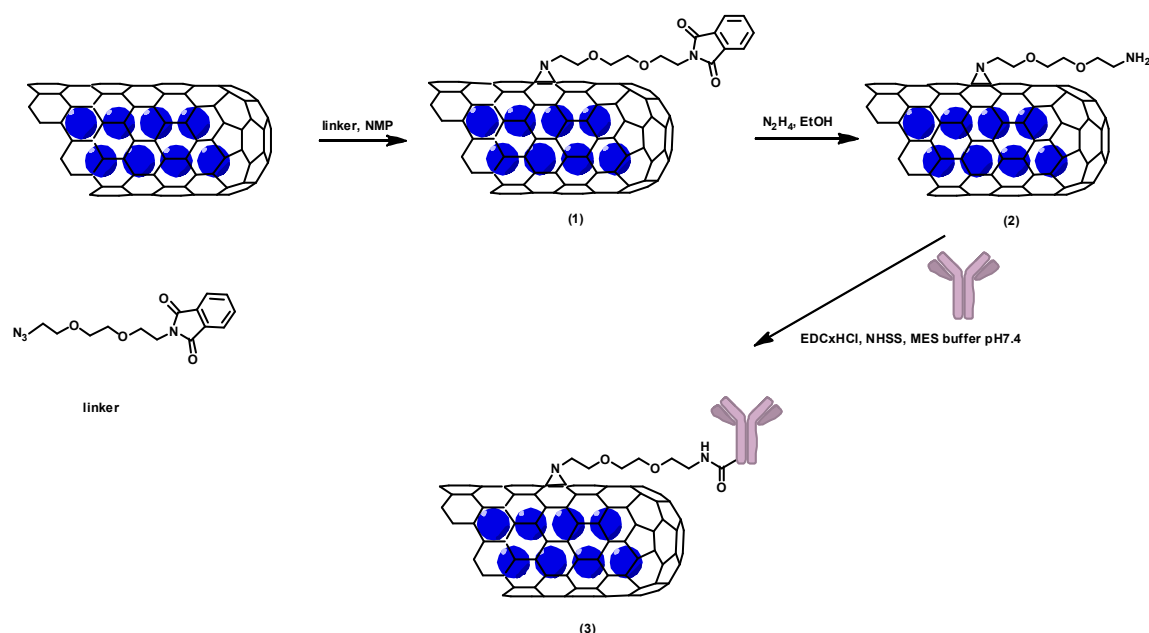
Figure 3. Nitrene reaction on SmCl$_3$@SWCNT (1) and cleavage of the phthalimide group to afford the amino functionalized SmCl$_3$@SWCNT-NH$_2$ (2); Covalent derivatization of SmCl$_3$@SWCNT-NH$_2$ with Cetuximab forming SmCl$_3$@SWCNT-mAb (3).

This finding is very promising for the application of radioactive metals inside of nanocapsules. They would not be released for uncontrolled distribution in the organism. Also after sealing of radionuclides, the external walls of the closed-ended filled carbon nanotubes can be decorated with active molecules for specific targeting enhancing their biocompatibility.

One limitation of this approach is due to the long reaction time necessary to functionalize the tubes (96 h of 1,3-dipolar cycloadditions of azomethine ylides and 12 h of nitrene cycloadditions) and we develop a faster method of functionalization of the nanocapsules, which would be suitable for radioactivity delivery.

III.2 Result and discussion

III.2.1 Functionalization of filled SWCNTs

The first attempt of functionalization of filled carbon nanotubes was performed on SWCNTs encapsulated with NaI. This study of functionalization by arylation method, was performed in comparison to the one, reported in the literature[2] where filled tubes were functionalized by 1,3-dipolar cycloaddition. NaI@SWCNTs were treated with aryl diazonium salts generated *in situ* from aniline derivatives.[8] The direct treatment was used to avoid the necessity of isolation and storage of unstable and light-sensitive aryl diazonium salts. In the first trial, the commercially available *N*-Boc-*p*-phenylenediamine was used for the functionalization. Reaction was carried out at 80 °C for 1 h in the presence of isopentyl nitrite to obtain the diazonium salt. The achieved functionalized material was purified by dispersion/filtration method in order to remove unreacted material. After the treatment with a solution of hydrochloric acid in 1,4-dioxane, the resulted material was characterized by TGA and Raman spectroscopy.
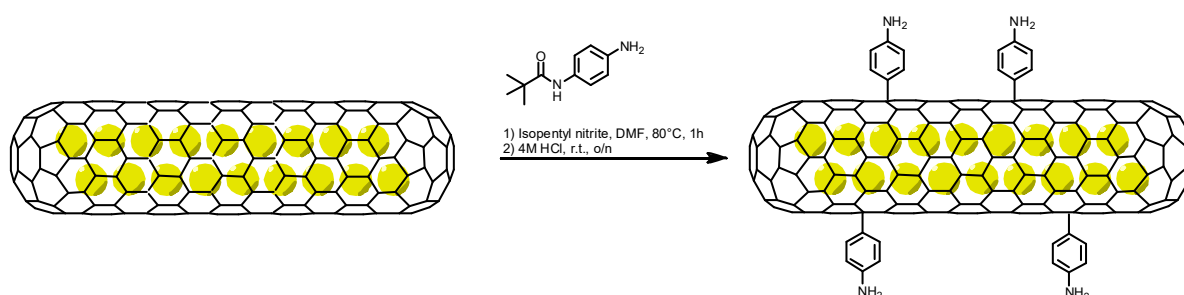
Scheme 1. Synthetic scheme of the functionalization of NaI@SWCNTs with N-Boc-*p*-phenylenediamine.1) DMF, 80°C, 1 h; 2) 4M HCl in dioxane, r.t., overnight.

The thermogravimetric analysis of the pristine NaI@SWCNTs (Figure 4a) displayed a significant weight loss, which corresponded to the removing of associated amorphous carbon. By comparing the weight loss of functionalized NaI@SWCNTs (NaI@SWCNTs-NH$_2$) with staring material, we estimated that the functionalization was around 560 µmol g^{-1} (one functional group per 125 of carbon atoms, taking into account the filling yield). Where, the example mentioned from literature[2] was only 170 mmol g^{-1}.
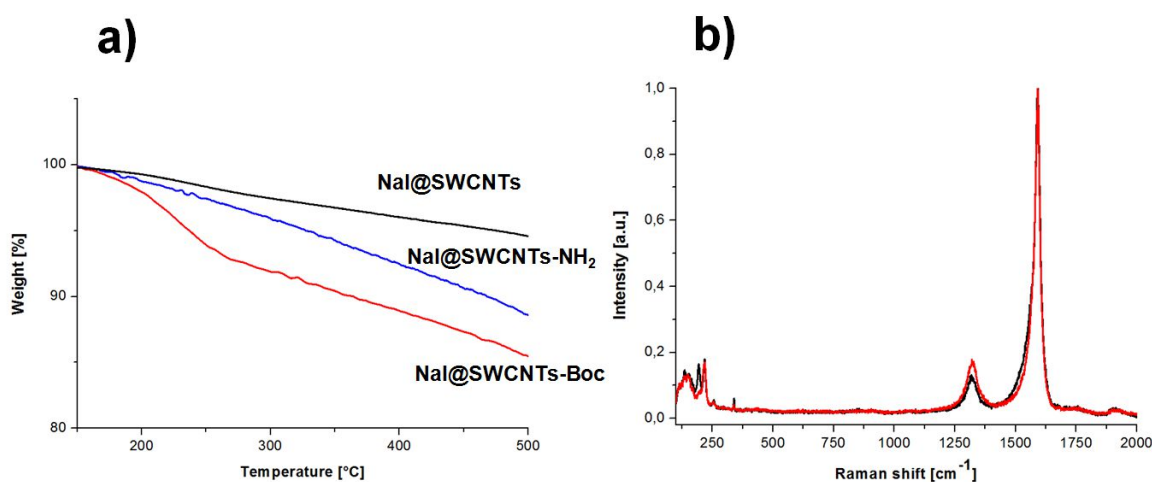

Figure 4. a) TGA profiles of pristine NaI@SWCNTs(black), functionalized NaI@SWCNTs before (red) and after (blue) deprotection of amine groups (N$_2$ atmosphere); b) Raman spectra of pristine NaI@SWCNTs (black), and functionalized NaI@SWCNTs (red).

The comparison of pristine and functionalized material's Raman spectra is presented (Figure 4) and it clearly shows the typical resonant Raman peaks for SWCNTs.[9] The NaI@SWCNTs exhibit a tangential mode at 1586 cm^{-1} (G-band) and the band centered at 1325 cm^{-1}, the disorder mode (D-band). The D-band increased in intensity once functional groups were introduced to sp^2 hybridized carbons and made them sp^3 hybridized.[10] The ratio of the intensity of the D-band and the intensity of the tangential mode (G-band) at 1586 cm^{-1} provides a good indication of the relative degree of functionalization. After the arylation of the pristine NaI@SWCNTs the I$_D$/I$_G$ ratio changed significantly, indication significant sidewall derivatization for NaI@SWCNTs.

Hence, following the studied arylation method for the functionalization of filled nanotubes, we decided to modify SWCNTs filled with $LuCl_3$ with two filling yield - 20% ($LuCl_3$20%@SWCNTs) and 30% ($LuCl_3$30%@SWCNTs) -to understand how/if different internal loading can affect the functionalization (Scheme 2). The tubes were covalently modified by arylation with commercially available 4-[(*N*-Boc)aminomethyl]aniline to introduce primary aliphatic amino groups on the nanotube sidewall.
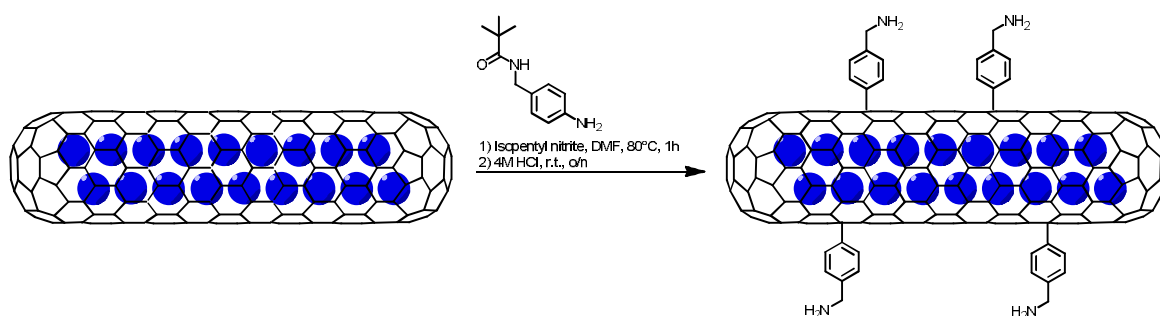
Scheme 2. Synthetic scheme of the functionalization of LuCl$_3$@SWCNTs with 4-[(*N*-Boc)aminomethyl]aniline. 1) DMF, 80°C, 1 h; 2) 4M HCl in dioxane, r.t., overnight.

The amount of amine functions was assessed by Kaiser test and TGA. Raman spectroscopy was also used to assess the functionalization.

Thermogravimetric analysis under nitrogen atmosphere revealed the decomposition of the material along with the temperature increasing. The weight loss at 500 °C was taken as the final temperature of degradation of covalently bound material. The thermogravimetric profiles obtained in nitrogen of the carbon nanotubes filled with two different amounts of halides, functionalized with the same procedure and deprotected by the same HCl treatment, showed a good degree of functionalization 790 and 850 µmol g^{-1} respectively for $LuCl_3$20%@SWCNTs and $LuCl_3$20%@SWCNTs (Figure 5). These values were obtained taking into account the different amount of filling.
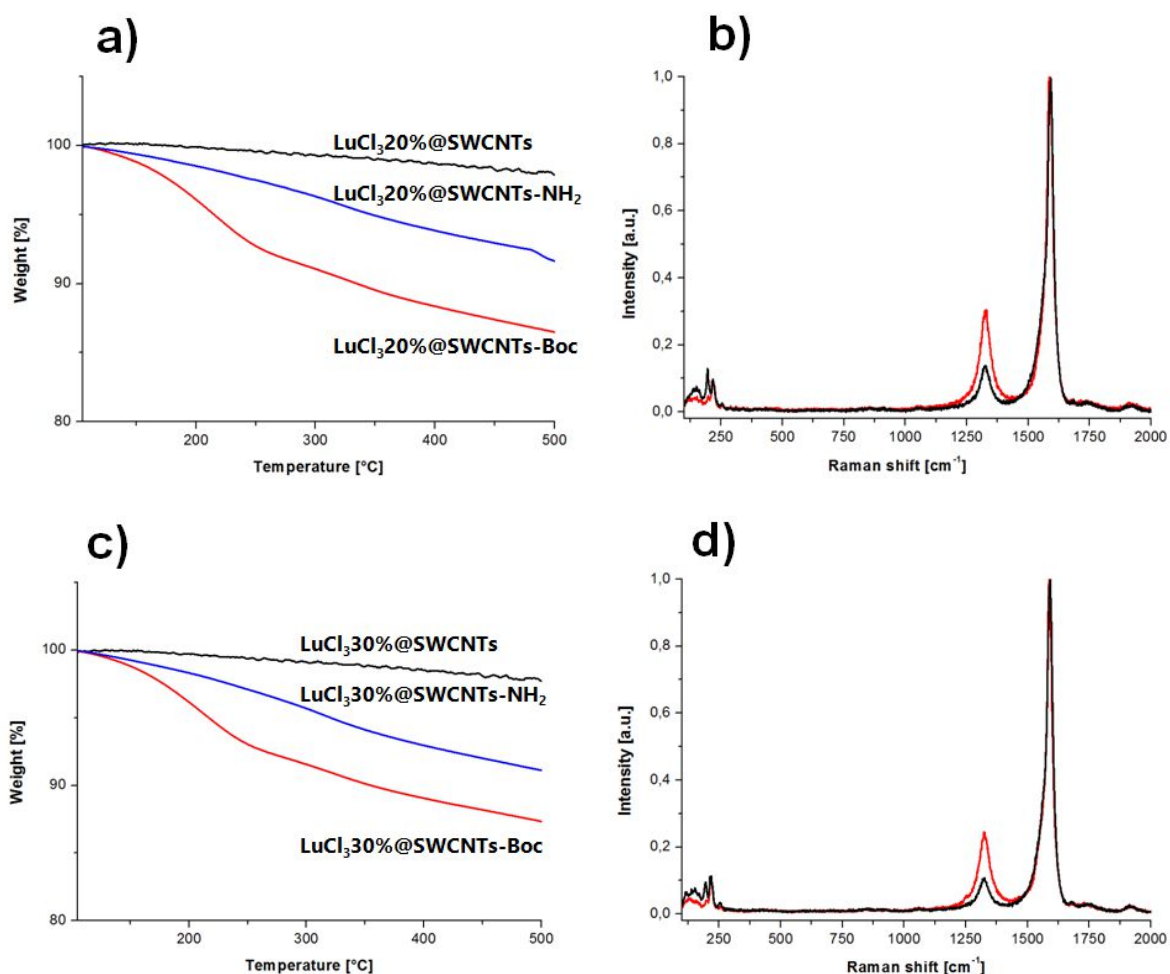
Figure 5.TGA profiles of pristine (black) and functionalized LuCl₃20%@SWCNTs (a) and LuCl₃30%@SWCNTs(b) respectively, before (red) and after (blue) deprotection of amine groups (N₂ atmosphere); Raman spectra of pristine LuCl₃@SWCNTs (black), and functionalized LuCl₃@SWCNTs (red) for LuCl₃20%@SWCNTs (b) LuCl₃30%@SWCNTs (d).

Kaiser test was used to estimate the amount of free primary amino groups on the surface of the nanocapsules. It was performed after the deprotection reaction with 4M HCl. Intensive blue color was generated by reaction of ninhydrin with free primary amines. The values of free amines in two samples were calculated according to the initial filling of the tubes, obtaining 315 and 360 µmol g^{-1} respectively for 20% and 30% filled SWCNTs.

Raman spectra for all tubes showed a strong peak around 1586 cm^{-1} (G-band) and additional band around 1325 cm^{-1} (D-band). All peaks were visible before and after functionalization of all LuCl₃@SWCNTs. For SWCNTs with 20% and 30% of LuCl₃ with 633 nm laser excitation wavelength, significant changes

in the intensity of D-band after functionalization with respect to the staring material (Figure 5) were observed. The increasing intensity of this band is attributed to the introduction of defects as functional groups on the CNTs surface. The ratio between D- and G-band for filled nanotubes before and after functionalization was compared: $I_D I_G^{-1}/I_{D0} I_{G0}^{-1}$ for LuCl$_3$20%@SWCNTs was equal to 2.14 and for LuCl$_3$30%@SWCNTs to 2.20.

The obtained results showed that the tubes with higher filling had slightly higher reactivity in arylation reaction. What can suggest that amount of foreign material, encapsulated inside the nanotubes, can have the influence on their chemical properties. In conclusion, it can be stated that the payload has an influence on the reactivity of the tubes.

The following step was the application of the arylation for the functionalization of filled SWCNTs with the linker previously applied on empty SWCNTs (**P12**). Branched linker was built on cyanuric chloride core, containing two hydrophilic chains ended with a protected amine and *p*-phenylenediamine for diazonium salt formation (Scheme 3).
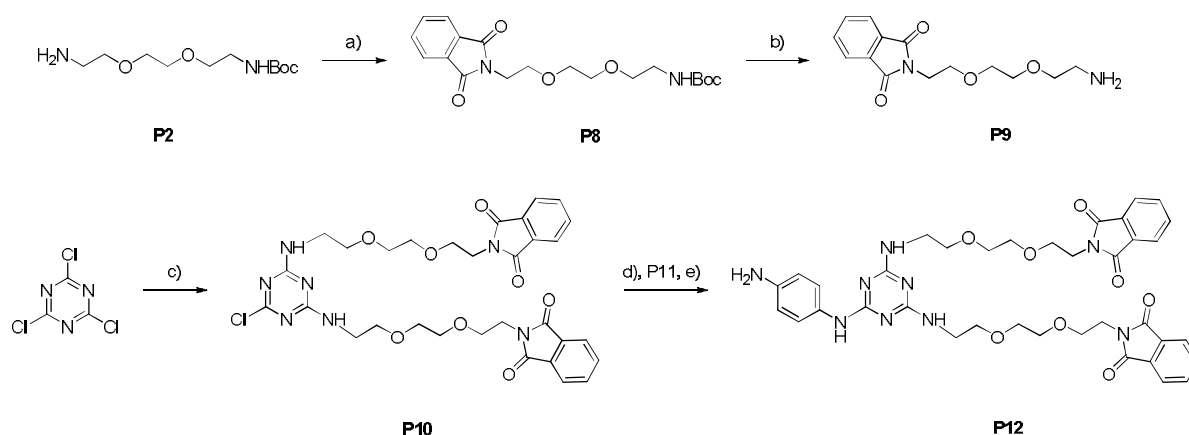
Scheme 3. General scheme for the preparation of compound P12. a) phthalic anhydrite, toluene, reflux, overnight, 92%; b) TFA, DCM, 4h, r.t., 98%; c) DIEA, THF, 0 °C to r.t., 90%; d) *N*-Boc-*p*-phenylenediamine, THF, 80°C, 4h, 71%; e) TFA, DCM, 4h, r.t., 88%.

The functionalization was performed on LuCl$_3$20%@SWCNTs. The aryl diazonium salt was generated *in situ* from aniline derivative **P12** (Scheme 4) and the reaction was carried out at 80 °C for 4 h in the presence of isopentyl nitrite. The achieved functionalized material was purified by dispersion/filtration method to remove unreacted material. The phthalimide-protected amino groups on the LuCl$_3$20%@SWCNTs-Pht were cleaved by treatment with ethanol solution of hydrazine. The products were analyzed by TGA, Raman spectroscopy and Kaiser test.
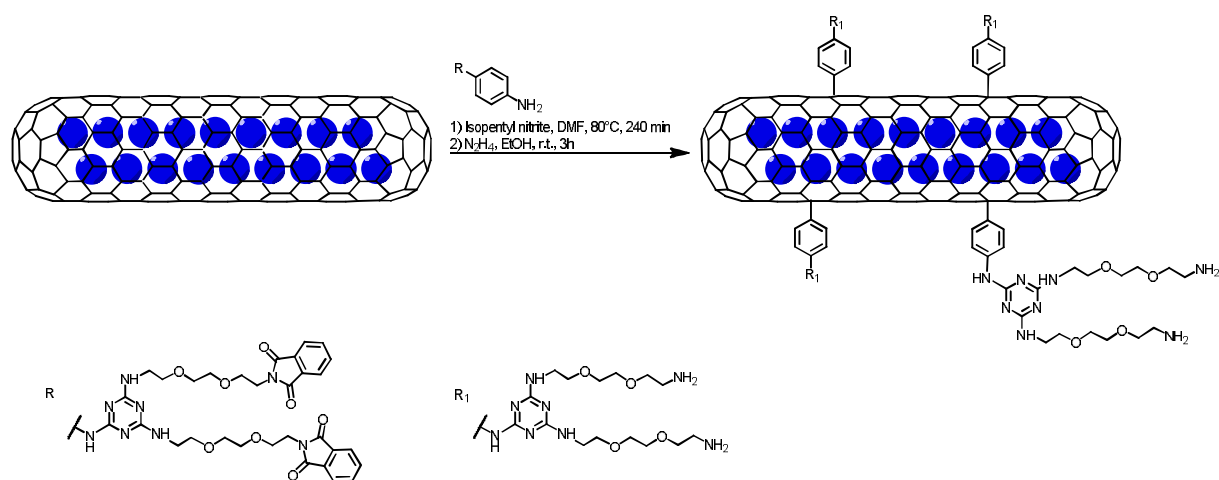
Scheme 4. Functionalization of LuCl$_3$@SWCNTs with the linker.

Thermogravimetric analysis of functionalized nanotubes showed a weight loss in region between 200 °C and 500 °C (Figure 6 a, c). This loss was attributed to the decomposition of the organic material covalently attached to the nanotubes structure. From TGA of functionalized, filled LuCl$_3$@SWCNTs, the amount of external material was calculated as a 245 µmol g^{-1} respect to 20% of filling. After deprotection of amine groups, the presence of amine groups on the functionalized material was estimated with Kaiser test at the level of 75 µmol g^{-1}.

Raman spectra (Figure 6 b, d) for all tubes showed a strong peak around 1585 cm^{-1} (G-band), band around 1315 cm^{-1} (D-band). All peaks were visible before and after functionalization and the ratio in the intensity of D-band and G-band after functionalization with respect to the staring material $I_D I_G^{-1} / I_{D0} I_{G0}^{-1}$

(Figure 6c) was calculated as a 1.21.
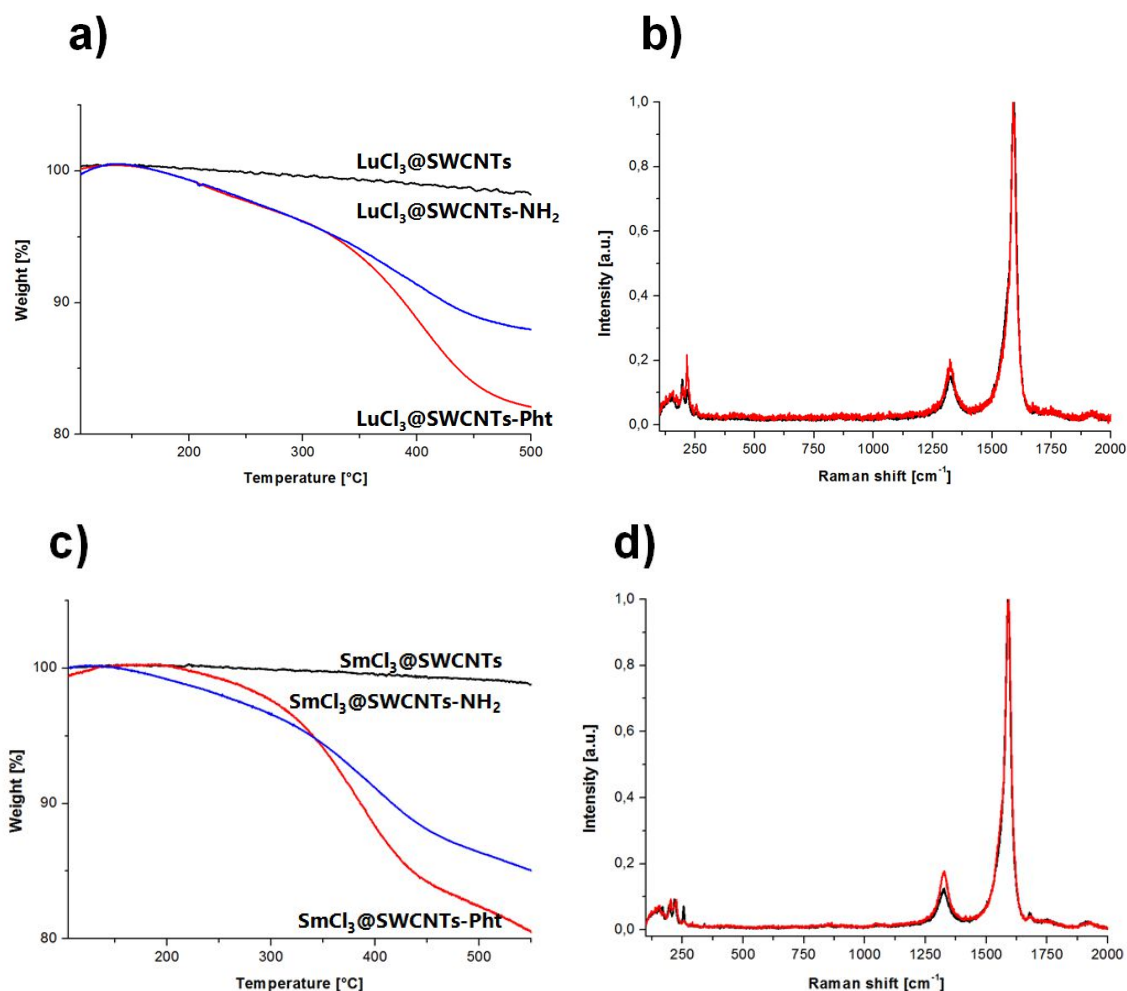
Figure 6.TGA profiles of pristine (black) and functionalized filled SWCNTs, before and after deprotection of amine groups for a)LuCl$_3$@SWCNTs c) SmCl$_3$@SWCNTs (N$_2$ atmosphere); Raman spectra of pristine (black), and functionalized (red) filled SWCNTs with b) LuCl$_3$, d) SmCl$_3$;.

The same experiment was performed also on SWCNTs filled with samarium (III) chloride (SmCl$_3$@SWCNTs). TGA and Kaiser test values were processed to obtain the degree of functionalization for every filled and functionalized SWCNTs, showing a good agreement between the two filling (Table 1).

Table 1.Results of functionalization of SWCNTs with deferent payload.

Entry	Tubes Type	Reaction Time [min]	TGA [μmol/g]	Kaiser Test [μmol/g]	Raman $[I_D I_G^{-1} / I_{D0} I_{G0}^{-1}]$
1	LuCl$_3$@SWCNTs	240	245	50	1.21
2	SmCl$_3$@SWCNTs	60	220	60	1.68

The morphology of the materials was observed by HRTEM, confirming the unchanged lattice of the carbon nanotubes after the chemical treatments (Figure 7). The SmCl$_3$ nanowires are visible inside SWCNTs as high (bright) contrast areas.

Figure 7. HRTEM images of SmCl$_3$@SWCNTs before and after functionalization. The HAADF-STEM images confirmed the presence of the filling after functionalization.

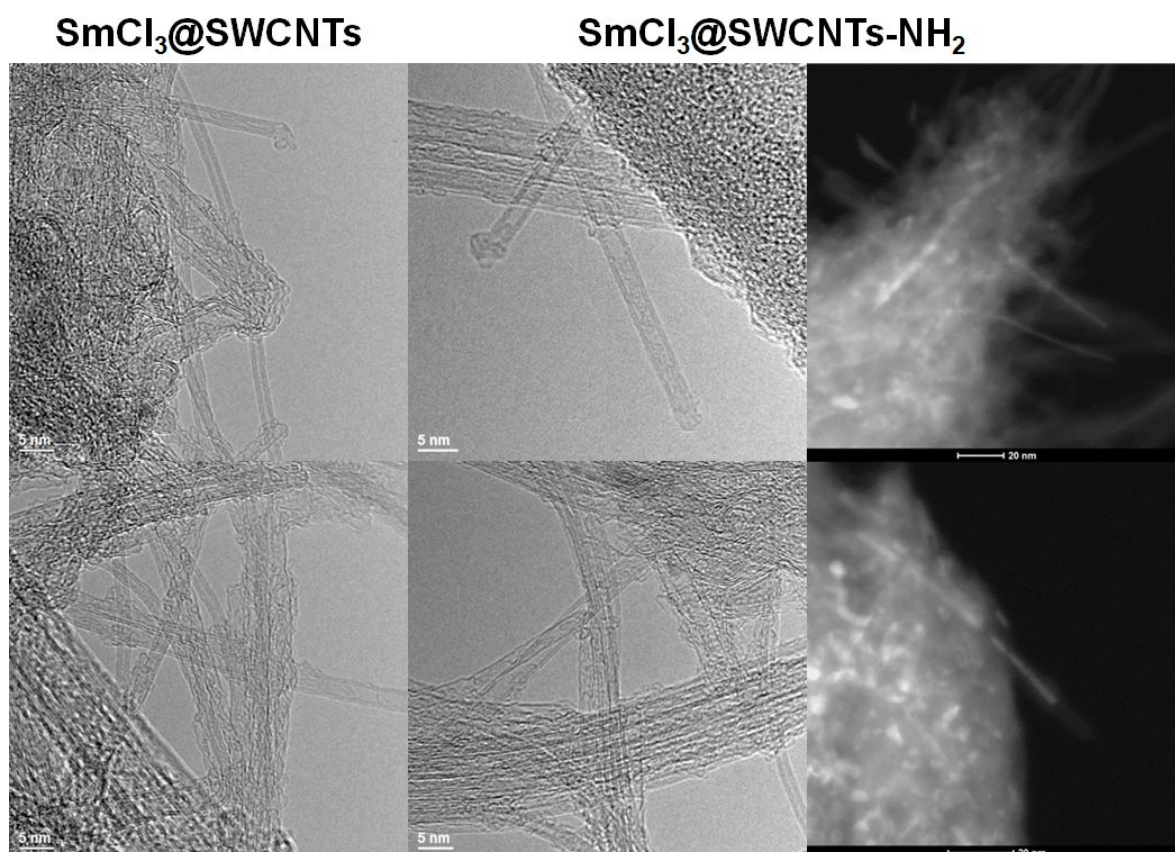To conclude, all experiments on filled nanotubes were successfully performed, and the proposed functionalization method has been applied to modify all types of tubes filled with lanthanide salts.

III.2.2 Functionalization of filled MWCNTs

The same strategy was applied for the functionalization of multi walled carbon nanotubes filled with several metal halides (Scheme 5) as $LuCl_3$ and $SmCl_3$.

Considering filled MWCNTs as analogues of empty MWCNTs, in first trials we applied the same reaction conditions as for the empty MWCNTs for which the optimization of the conditions was described in previous chapter. In this way we could understand the influence of the filling on the final effect of the functionalization. In this experiment, the functionalization calculation was always addressed to the filing yield of the tubes. For this reaction we applied the linker **P12** which was used before (Scheme 3).
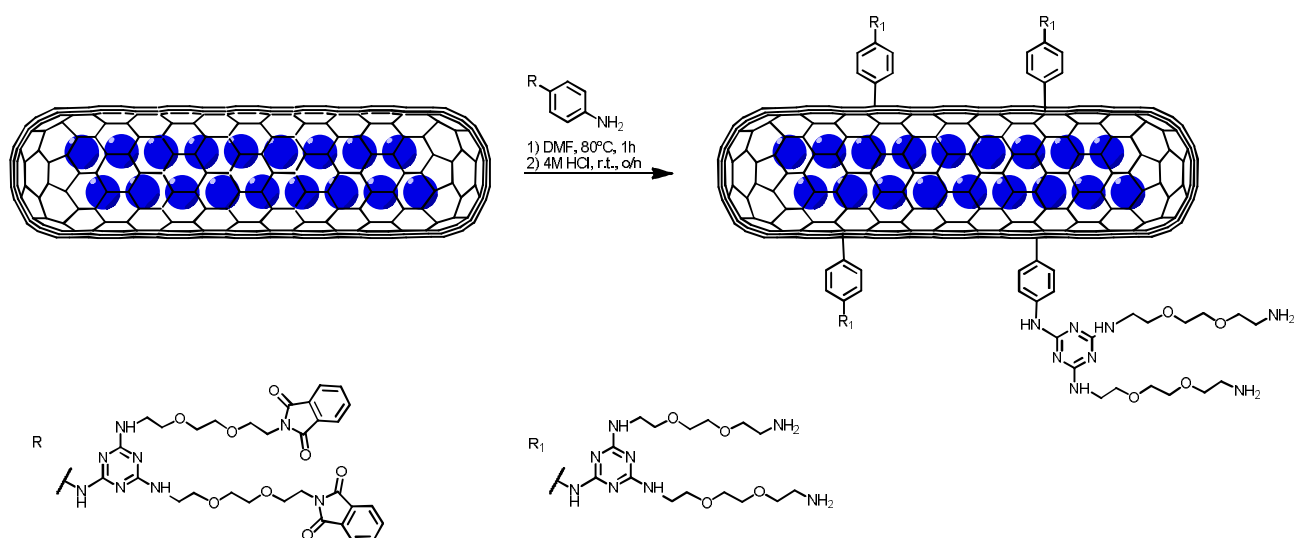
Scheme 5. Functionalization of LuCl$_3$@MWCNTs with the linker.

In a typical experiment, DMF was used as solvent and a 10 wt% fold excess of amine was employed for the diazonium generation. The curve of thermal analysis in air (Figure 8a) presents the behavior of filled MWCNTs. At 800 °C 30% of the filling is still preserved as a solid residue whereas for pristine

114

empty material, this behavior is not observed (data not shown). In both cases the internal material was preserved as a solid residue after functionalization.
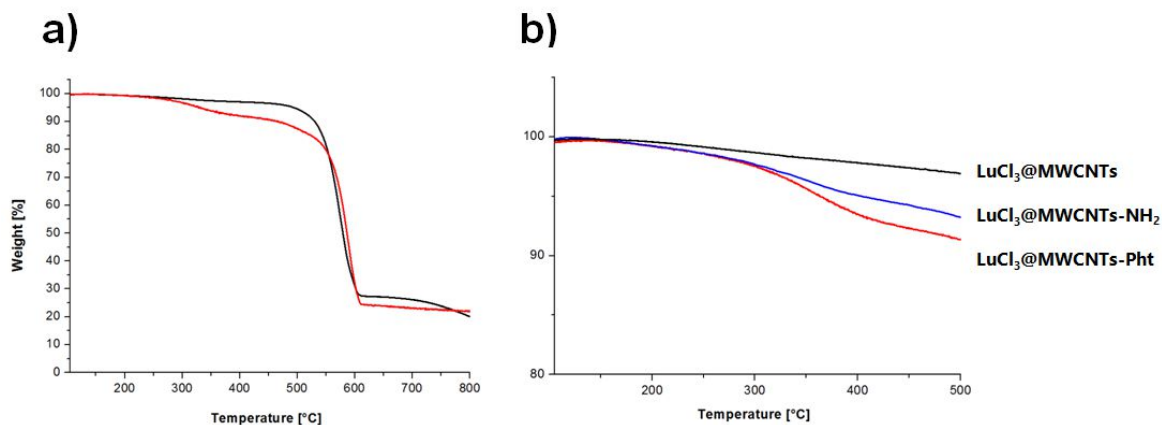
Figure 8. TGA profiles of: a) pristine (black) and functionalized LuCl$_3$@MWCNTs (red) (in air atmosphere); b) before and after deprotection of the amine groups for LuCl$_3$@MWCNTs (in N$_2$ atmosphere).

From the TGA profile in nitrogen, the functionalization level was calculated taking into account the percentage of the filling (Table 2).

Table 2.Results of functionalization of MWCNTs with deferent payload.

Entry	Tubes Type	Reaction Time [min]	TGA[a] [µmol/g]	Kaiser Test [µmol/g]
1	LuCl$_3$@MWCNTs	60	120	50
2	SmCl$_3$@MWCNTs	60	90	40

[a]TGA performed in nitrogen.

In both experiments, filled MWCNTs were functionalized with a good yield and the Kaiser test proved that primary amines are present on the surface. The TGA profiles in air confirmed that the internal filling is present and leaves a solid residue after the analysis in air at 800°C while all the organic portion undergoes degradation (Figure 8a).

HRTEM analyses were performed only for SmCl$_3$@MWCNTs-NH$_2$. The images revealed no visible difference in the integrity of SmCl$_3$@MWCNTs, before and after the functionalization and HAADF-STEM analyses confirmed the

presence of the filling after functionalization of SmCl$_3$@MWCNTs (Figure 9). The SmCl$_3$ nanowires are visible inside MWCNTs as high (bright) contrast areas.

Figure 9. HRTEM images of SmCl$_3$@MWCNTs, before and after the functionalization. HAADF-STEM images of filled and functionalizedSmCl$_3$@MWCNTs.
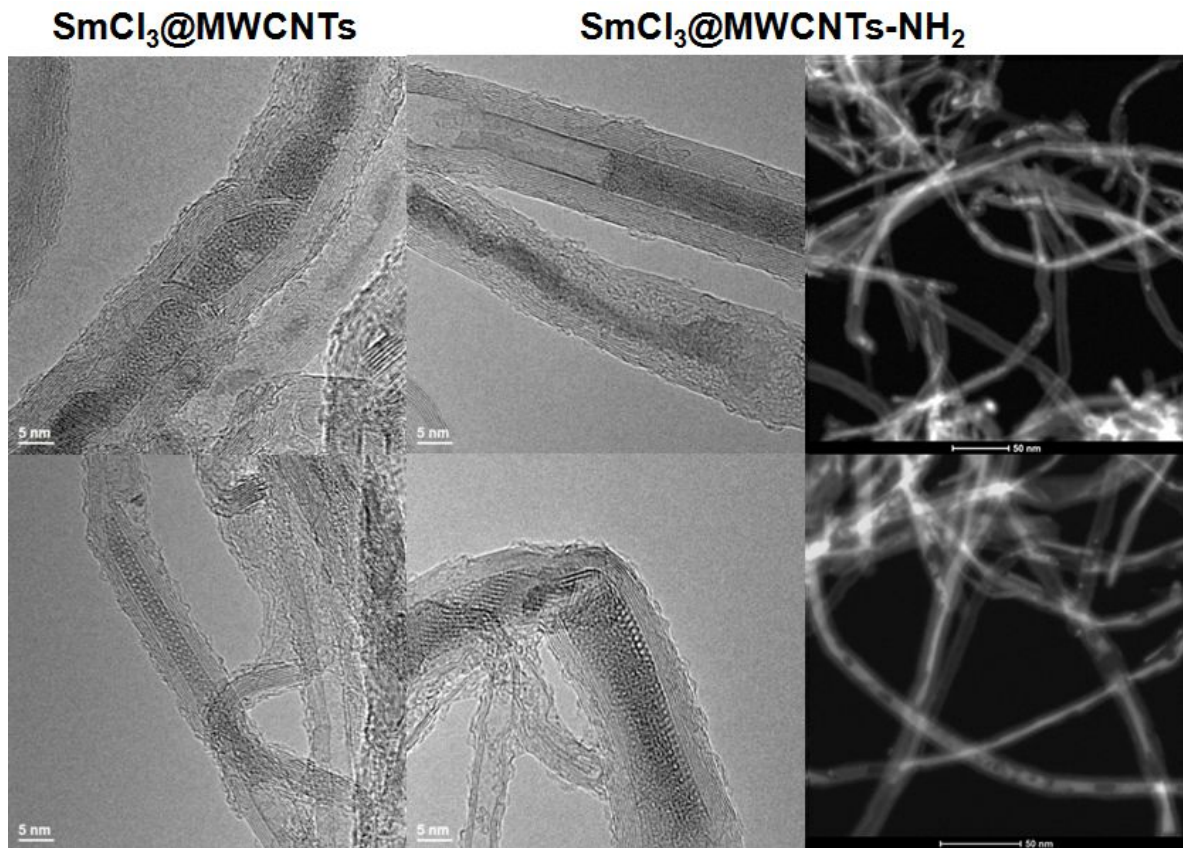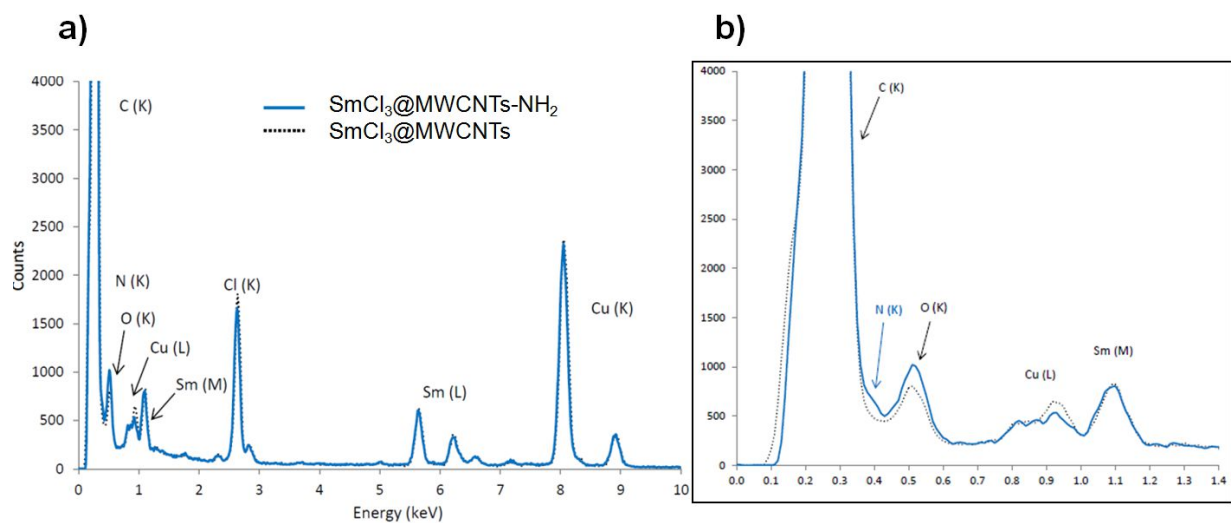

Figure 10.a) EDX spectrum of the area represented on HRTEM image b) the magnified range 0 - 1.4 keV of the spectrum.

The EDX spectrum of the area represented on HRTEM image is reported in Figure 10. Carbon peak corresponds to the MWCNTs and the lacey carbon film (TEM grid). Copper peaks correspond to the TEM grid and the content of samarium is stable.

III.2.3 Microwave accelerated functionalization of filled CNTs

The application of microwaves (MW) in organic synthesis is widely used as an effective tool to accelerate reactions, to increase the yields under milder reaction conditions, and to obtain higher product purity.[11] The value of this technique was recognized both in the academic and industrial sectors, and was successfully applied to numerous organic transformations, also including chemistry of CNTs. Starting from the first pioneering studies developed by the microwave-assisted covalent sidewall functionalization of carbon nanotubes microwave irradiation rapidly rose as an efficient and effective implement for CNTs surface modification.[12] In the case of arylation reactions, application of MW could increase the *in situ* generation of diazonium salts from the anilines, providing an efficient approach suitable for the CNTs modification.

In our research, we developed a fast methodology for the derivatization of CNTs by means of the MW-assisted arylation, with a sort of "one shot" procedure, which would allow the surface functionalization of filled SWCNTs and MWCNTs.

The MW-assisted synthetic trials were optimized on empty nanotubes and reported in the previous chapter (chapter II). By the application of microwave we were able to decrease the reaction time to just 10 minutes, without decreasing the yield of functionalization. We decided to apply previously optimized conditions on filled nanotubes, by adapting the protocol taking into account the weight of the filling. This fast methodology would be a

promising way to functionalize nanotubes filled with radioactive material with short live-time, providing an efficient platform to bind biological molecules and to deliver internal materials for various theranostic applications.

In a typical experiment with microwaves heating, arylation reaction was performed employing 10 fold wt% excess of amine (**P12**) calculated with respect to amount of carbon of CNTs. Reaction was carried out in DMF at 80 °C under microwave irradiation for 10 min (200 W). All reactions were carried out in a 0.5 to 1 mmol scale in closed pressure-resistant (due to nitrogen evolution in the course of arylation reaction) vessels. The so introduced phthalimide-protected amino groups were cleaved by treatment with hydrazine in ethanol. The samples were analyzed by TGA and Raman spectroscopy and the amount of amine functions was assessed by Kaiser test (Table 3).

As mentioned, the experiments with the assisted microwave irradiation were performed on filled SWCNTs and filled MWCNTs. As a model for SWCNTs, we have chosen $LuCl_3$@SWCNTs. By Raman spectroscopy, we could follow the changes in the D-mode.
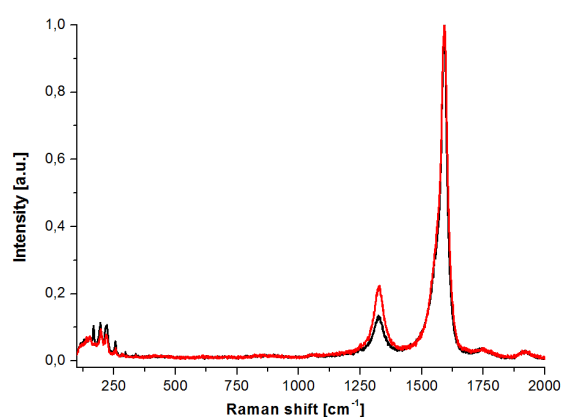
Figure 11. RAMAN spectra of $LuCl_3$@SWCNTs-Phtfrom MW irradiation (red) and of pristine $LuCl_3$@SWCNTs (black).

As it presented on Figure 11, after 10 min of the reaction we could observe the increasing of D-band intensity. Compared to $LuCl_3$@SWCNTs functionalized in the reaction with traditional heating we could also see the slightly higher $I_D I_G^{-1}/I_{D0} I_{G0}^{-1}$ratio [1.57]. Results from TGA and Kaiser test indicate

that MW-assisted reaction exhibited higher values of functionalization, what undoubtedly proved higher reactivity under MW conditions.

Following this idea we also functionalized MWCNT filled with gadolinium chloride. These tubes were also successfully decorated with the linker **P12** (Table 3).

Table 3. Results of functionalization of filled CNTs with MW irradiation.

Tubes Type	Reaction Time [min]	TGA [μmol/g]	Kaiser Test [μmol/g]	Raman [$I_D I_G^{-1} / I_{D0} I_{G0}^{-1}$]
LuCl$_3$@SWCNTs	10	120	85	1.57
GdCl$_3$@MWCNTs	10	130	50	0.90

By HRTEM we revealed no visible difference in the integrity of GdCl$_3$@MWCNTs, before and after the functionalization (Figure 12). The filling was preserved inside the MWCNTs and HAADF-STEM images confirmed the presence of the filling in GdCl$_3$@MWCNT-NH$_2$ as visible from the high (bright) contrast areas due to GdCl$_3$ nanowires.

GdCl$_3$@MWCNTs　　　　　**GdCl$_3$@MWCNTs-NH$_2$**
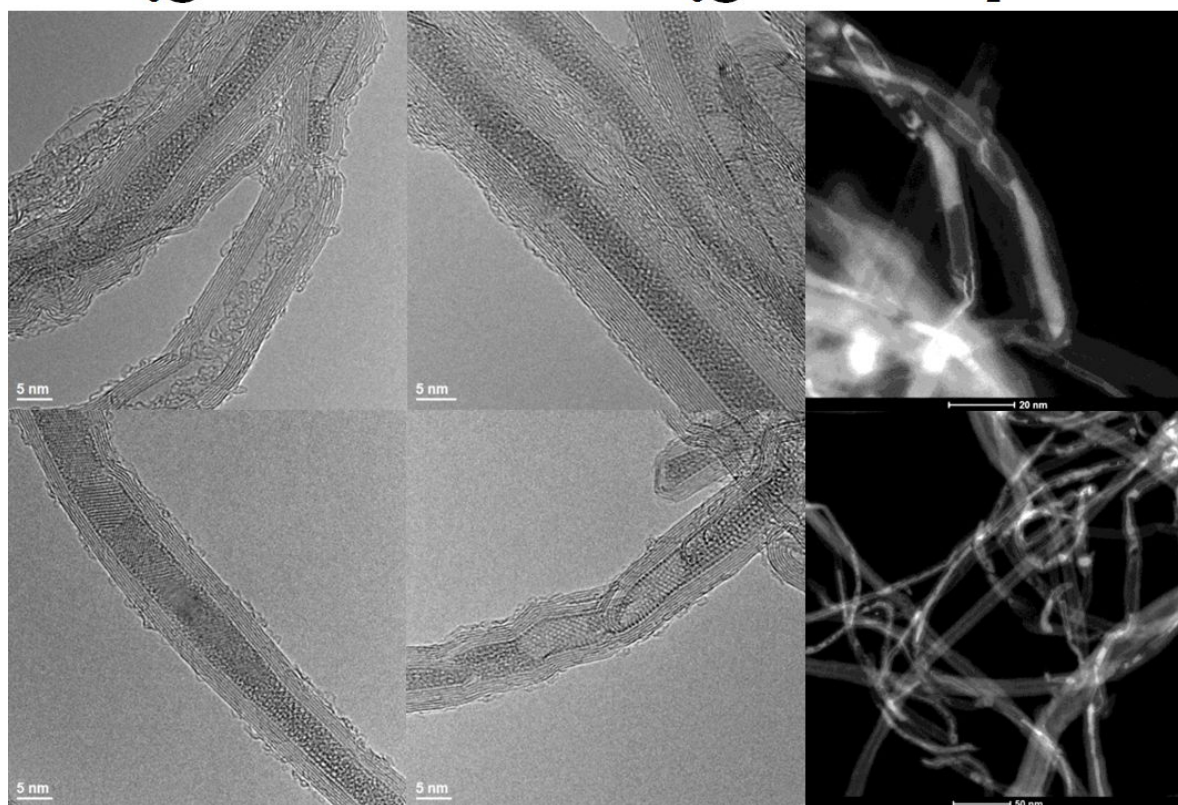
Figure 12. HRTEM images of GdCl$_3$@MWCNTs, before and after the functionalization. HAADF-STEM images (on the right) confirmed the presence of the filling after functionalization of GdCl$_3$@MWCNTs.

We successfully found an efficient way to functionalize filled carbon nanotubes through a microwave-assisted reaction and the results obtained with filled SWCNTs and MWCNTs functionalized by arylation through both a classical thermal reaction and a microwave assisted reaction were compared. The sidewall modification is increased with the microwave application. It facilitated by shortening the reaction time and allowing an effective modification of CNTs without breaking the internal structure of resultant X@CNTs-NH$_2$.

III.3 Conclusions

The increasing application of nanotechnology in the biomedical field and the current development of nanoscience and biomedicine are encouraging to search for new nanoscale drug delivery systems with multiple functions and advanced applications. The main advantage of nanocarriers is the possibility of their versatile modification with different functionality. Indeed, multimodal nanosystems with targeting, imaging, and drug delivery capabilities within a single nanoscale construct, hold incredible promise in the treatment of different types of diseases and in particular for cancer therapy. Theranostic, which combines simultaneous diagnostics and therapeutics, represents a new modality that utilizes therapy and real-time non-invasive *in vivo* imaging. This specific combination of functions can provide biodistribution information, opportunities to study therapeutic mechanisms, and strategies for improving therapeutic efficacy and reducing side effects. The unique structural properties of carbon nanotubes make this material a promising tool for nanoscience, in particular nanomedicine.

The exploitation of different covalent functionalization reactions permits the surface modification, which will be available for binding several cargos such as bioactive compounds (small molecules or proteins), and the increase of CNTs dispersibility. Following our research in this area, CNTs can be further conjugated with therapeutic or tracking molecules. In particularly this short time of reaction and convenience of covalent functionalization is suitable for delivery of radioisotopes which could be closed inside the tubes. The biological study, toxicity and first trials *in vivo* of such a system will be described in next chapter.

III.4 Experimental Part

III.4.1 Chemical Synthesis

Synthesis of the organic precursors
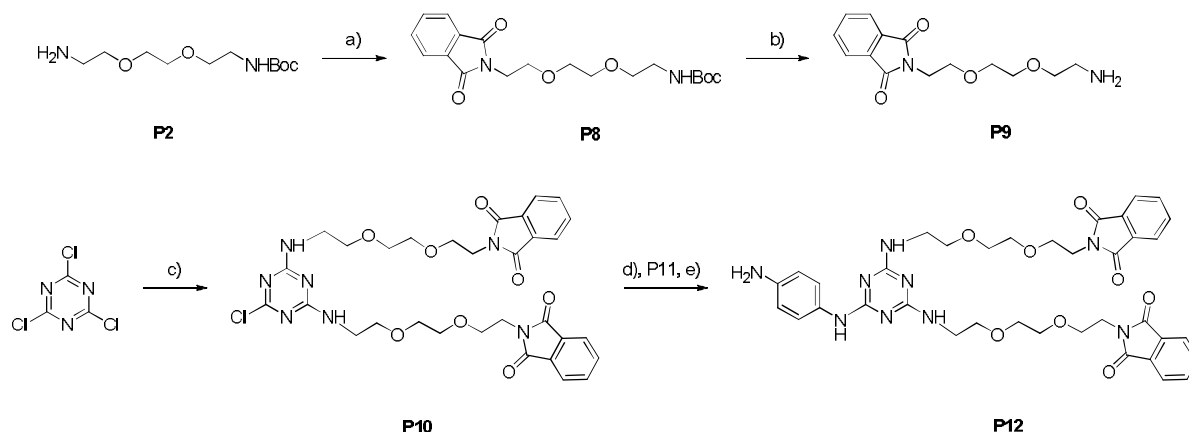
General scheme for the preparation of compound P12. a) phthalic anhydrite, toluene, reflux, overnight, 92%; b) TFA, DCM, 4h, r.t., 98%; c) P9, DIEA, THF, 0 °C to r.t., 90%; d) N-Boc-p-phenylenediamine, THF, 80°C, 4h, 71%; e) TFA, DCM, 4h, r.t., 88%.

Syntheses were reported in previous chapter.

III.4.2 Preparation of filled CNTs (X@CNTs)

For all experiments, the samples were provided by ICMAB from Barcelona where the CNTs were previously purified and filled with the payload. In all experiment the time of dispersion of the filled CNTs in the solvent was decreased to 5 min to avoid the damages of the tubes.

Purification of SWCNTs

The SWCNTs used in this investigation were produced by chemical vapor deposition from Thomas Swan & Co. Ltd (Elicarb®). The material was purified by steam treatment following a previously reported protocol.[13] Briefly, SWCNTs were spread inside a silica tube which was then placed into a furnace alumina tube. Steam was introduced by bubbling argon through a flask containing hot

distilled water. The whole system was initially purged with argon, to remove atmospheric air, before heating the furnace to 900 °C during 4 h to allow the purification of the material. The solid powder was collected and treated with 6 M HCl (Panreac) to dissolve the exposed metal nanoparticles. The purified SWCNTs were collected by filtration through a 0.2 µm polycarbonate membrane and thoroughly washed with water until neutral pH. The sample was oven-dried at 80 °C overnight.

Purification of MWCNTs

The MWCNTs were purchased from Thomas Swan & Co. Ltd. As-received MWCNTs were dispersed in fresh piranha solution (H_2SO_4/H_2O_2, 3:1) at a concentration of 1 mg mL^{-1}. The solution was stirred for 2 h at r.t. then the reaction was quenched with distilled water. The pH of the solution was adjusted until neutral. The sample was filtered on a polycarbonate membrane and dried in the oven at 80 °C overnight. Next, the MWCNTs were treated with steam for 1 h at 900 °C and refluxed in 6 M HCl at 110 °C overnight. The solid sample was collected by filtration and rinsed with distilled water until neutral pH.

Filling of CNTs

NaI@SWCNTs

Purified SWCNTs and aq. solution of sodium iodide were transferred into a silica ampoule and heated to 70 °C overnight to remove water. The ampoule was sealed under vacuum and annealed at 900 °C for 4 h. The mixture was then washed with water to remove external material. Sample was filtered and dried to afford NaI@SWCNTs.

LuCl₃@CNTs

LuCl₃ mixed with SWCNTs and grinded with an agate mortar in an argon-filled glovebox. The mixture was sealed under vacuum inside a silica tube. The sample was then annealed in a horizontal furnace at 960 °C during 12 h. The resulting

sample contained filled closed-ended nanotubes and external crystals of $LuCl_3$. The non-encapsulated material was removed by washing the sample in hot water. From the performed TGA in air it was possible to determine the filling yield of the encapsulated materials employing a reported formula (Appendix). In the presented case, the two samples were prepared, one with about the 20 % of filling yield ($LuCl_3$20%@SWCNTs) and 30 % ($LuCl_3$30%@SWCNTs).

$SmCl_3$@CNTs

For encapsulation of samarium chloride, previously purified CNTs were mixed with samarium (III) chloride (w/w 1:10 respectively) and grinded with an agate mortar and pestle inside a glovebox until the mixture presented a homogeneous color. The resulting mixture was then vacuum sealed inside a silica ampoule and annealed at 900 °C for 12 h. After cooling down the sample, the silica tube was opened and the material was stirred in water at 80 °C to remove the non-encapsulated $SmCl_3$. The filling yield of $SmCl_3$@SWCNTs was 18.1 wt% and 19.5 wt% for $SmCl_3$@MWCNTs.

$GdCl_3$@MWCNTs

For encapsulation of gadolinium chloride previously purified MWCNTs were then mixed with gadolinium (III) chloride (w/w 1:10 respectively) and grinded with an agate mortar and pestle inside a glovebox until the mixture presented a homogeneous color. The resulting mixture was then vacuum sealed inside a silica ampoule and annealed at 900 °C for 12 h. After cooling down the sample, the silica tube was opened and the material was stirred in water at 80 °C to remove the non-encapsulated $GdCl_3$ external to the CNTs.

III.4.3 Functionalization of CNTs

General functionalization using traditional heating functionalization

10 mg of CNTs in 5mL of DMF were dispersed by sonication for 10 min. Then the corresponding aniline derivative was added in 25 fold wt% excess respect to CNTs to in 5 mL of DMF was added, dispersed for another 5 min and cooled to 0°C. Isopentyl nitrite (5 fold molar excess with respect to the amine) was added and reaction mixture was heated up to 80 °C and stirred for 1-4 hours. Then the mixture was cooled to room temperature. The CNTs were filtered (membrane MILIPORE, type: JHWP, pore size 0.45 μm) and washed with DMF until the solvent eluted colorless, washed with DMF, water, MeOH, EtOAc, Et_2O and dried.

General microwave-assisted functionalization

In a typical reaction of arylation, DMF dispersion of pristine filled CNTs were loaded into a microwave vessel, along with DMF solution of amine **P12** (25 fold wt% excess respect to CNTs), cooled to 0°C and injected with isopentyl nitrite (5 fold molar excess respect to amine) for the generation of diazonium salt. The microwave power was set to 200 W, the pressure at 125 psi, and the reaction was carried out in ten cycles from 75 to 80 °C for 10 min in total. After cooling to room temperature, the mixture was filtered (membrane MILIPORE, type: JHWP, pore size 0.45 μm), washed with DMF, re-dispersed/filtered with water, MeOH, dried with EtOAc and Et_2O.

General procedure for deprotection of -Boc

For the deprotection, X@CNTs-Boc (10 mg) were dispersed in 4 M HCl solution of dioxane (10mL) by sonication for 5 min. The dispersion was stirred at r.t. for overnight, and then diluted with dioxane (50 mL) and filtered. After filtration, the functionalized X@CNTs-NH_2 were re-precipitated in water, filtered (membrane MILIPORE, type: JHWP, pore size 0.45 μm), washed with water, MeOH, diethyl

ether finally dried under vacuum to afford functionalized material (X@CNTs-NH$_2$. The free amine loading was estimated by Kaiser test.

General procedure for deprotection of -NPht

For the deprotection, X@CNTs-Pht (30 mg) were dispersed in EtOH (30mL) by sonicating for 5 min, and afterwards treated with hydrazine hydrate (3 mL). The dispersion was stirred at r.t. for 2 h, and then diluted with EtOH (15 mL) and filtered. After filtration, the functionalized SmCl$_3$@MWCNTs-NH$_2$ were re-precipitated in EtOH, filtered(membrane MILIPORE, type: JHWP, pore size 0.45 µm), washed with 0.1 M HCl solution, water, MeOH, diethyl ether finally dried under vacuum to afford functionalized X@CNTs (X@CNTs-NH$_2$). The free amine loading was estimated by Kaiser test.

Bibliography

[1] R. Klingeler, R. B. Sim "Carbon Nanotubes for Biomedical Applications"; Springer, Berlin, Heidelberg, **2011**.

[2] S. Y. Hong, G. Tobias, K. T. Al-Jamal, B. Ballesteros, H. Ali-Boucetta, S. Lozano-Perez, P. D. Nellist, R. B. Sim, C. Finucane, S. J. Mather, M. L. H. Green, K. Kostarelos, B. G. Davis; *Nature materials* **2010**, *9*, 485–490.

[3] J. T. Wang, L. Cabana, M. Bourgognon, H. Kafa, A. Protti, K. Venner, A. M. Shah, J. Sosabowski, S. J. Mather, A. Roig, X. Ke, G. V. Tendeloo, R. T. de Rosales, G. Tobias, K. T. Al-Jamal; *Adv. Funct. Mater.* **2014**, *24*, 1880–1894.

[4] M. K. Bakht, M. Sadeghi, M. Pourbaghi-Masouleh, C. Tenreiro; *Current Cancer Drug Targets* **2012**, *12*, 998–1015.

[5] C. Spinato, A. P. Ruiz de Garibay, M. Kierkowicz, E. Pach, M. Martincic, R. Klippstein, M. Bourgognon, J. Tzu-Wen Wang, C. Ménard-Moyon, K. T. Al-Jamal, B. Ballesteros, G. Tobias, A. Bianco; *Nanoscale* **2016**, Doi:10.1039/C5NR07923C.

[6] M. Martincic, E. Pach, B. Ballesteros, G. Tobias; *Phys. Chem. Chem. Phys.* **2015**, *17*, 31662–31669.

[7] L. Lacerda, J. Russier, G. Pastorin, M. A. Herrero, E. Venturelli, H. Dumortier, K. T. Al-Jamal, M. Prato, K. Kostarelos, A. Bianco; *Biomaterials*, **2012**, *33*, 3334–3343.

[8] J. L. Bahr, J. M. Tour; *Chem Mater* **2001**, *13*, 3823–3824.

[9] R. Graupner; *Journal of Raman Spectroscopy*, **2007**, *38*, 673–683.

[10] R. Sharma, J. Hyun B. Chrisantha, J. Perera, M. S. Strano; *Nano Letters*, **2010**, *10*, 398–405.

[11] V. Polshettiwar, R. S. Varma; *Pure Appl. Chem*. **2008**, *80*, 777–790.

[12] Y. Wang, Z. Iqbal, S. Mitra; *Carbon* **2005**, *43*, 1015–1020.

[13] B. Ballesteros, G. Tobias, L. Shao, E. Pellicer, J. Nogués, E. Mendoza, M. L.H. Green; *Small*, **2008**, *4*, 1501–1506.

IV. Biomedical application of functionalized, filled CNTs for radioactivity delivery

IV.1 Introduction

Up to now, the hypothesis of CNTs clinical administration is strongly limited by multiple factors such as low solubility, impurity content, reproducibility in the preparation of the pristine materials, toxicity and pharmacokinetics, among the others.

The conjugation of pharmacological agents with nanoparticles has met great interest from the medical point of view[1] and there are many examples of current application of these systems in clinical practice and also at various stages of clinical development.[2,3] Versatile agents attached to the particles show improved pharmacological and toxicological properties against their non-conjugated form. The circulating half-life of the conjugates, maximal tolerated dose (MTD), and target selectivity are the important factors affecting the high therapeutic index. Typically conjugates are attached to the surface of nanoparticles, or encapsulated and protected inside the core. The nanoparticle

can also be designed to provide either controlled or triggered release of the therapeutic molecule.[4] Then, the surface of the particle can be properly functionalized by various methods to increase the circulating half-life, and by reducing nonspecific distribution in some cases by targeting tissue with specific cell surface antigens with a specific ligand (peptide, aptamer, antibody, small molecule). Surface functionalization can address the major limiting factor of long-circulating nanoparticles, notably protein absorption. Proteins adsorbed on the surface of the nanoparticle promote opsonization, leading to aggregation with subsequent rapid clearance from the bloodstream.[5] The resultant rapid clearance is due to phagocytosis by the mononuclear phagocyte system (MPS) in conjunction with the liver and spleen filtration network. Typically, the majority of opsonized particles are cleared by a receptor-mediated mechanism within minutes due to the high concentration of phagocytic cells in the liver and spleen or alternatively they may be excreted.[6] Several biological barriers are applied to defend the human body from invasion by foreign particles. The biodistribution of any nanoparticle is primarily ruled by their ability to penetrate biological barriers.[7] These barriers consist of: - the reticuloendothelial system (RES), - endothelial/epithelial membranes, - complex networks of blood vessels, - abnormal flow of blood and interstitial gradients. Endothelia composing the blood vessels have been classified as continuous, fenestrated, or discontinuous, depending on the morphological features and organ location.

The first *in vivo* study on functionalized CNTs biodistribution was reported by Wang et al. using mice treated with intraperitoneally (i.p.) administered short hydroxylated SWCNTs. The tubes were shown to accumulate mainly in the liver and kidney, and, in a lower degree, in the spleen and lung, and excreted mainly by the kidney within 18 days.[8] Functionalized SWCNTs, labeled with indium [^{111}In] thanks to the presence of a chelating molecule(diethylenetriaminepentaaceticacid- DTPA) on the surface were demonstrated to not been retained in the reticuloendothelial system (liver or

spleen) after intravenous administration (i.v.), and were rapidly cleared from the systemic blood circulation again via renal excretion.[9] This studied was performed tracing the indium radioactivity by gamma scintigraphy. It was also possible to compare the biodistribution of two types of functionalization: the first with no free amino groups and a second one with 40% free amino groups resulting in charged surface. Both derivatized SWCNTs were found in kidney, muscle, skin, and blood after 30 min. However the charged SWCNTs led to a higher affinity for kidney, muscle, skin, and lung, leading to their rapid clearance from all tissues. In 3 h the nanotubes were cleared from all organs down to levels of 1–2% (relative to the 30 min time point). TEM analysis of urine samples indicated high levels of intact functionalized CNTs, demonstrating that they are rapidly cleared from the systemic circulation via the kidney.[9] Later on, Lacerda et al. presented an elimination mechanism for CNTs, using [^{111}In] DTPA-MWCNTs. After tail vein injection, CNTs fast distributed in the systemic blood followed by rapid urinary clearance through via the kidney glomerular filtration (Fig. 3).[10] The reason for the more rapid elimination observed herein, in comparison to derivatives functionalized with surfactants, is that in the latter case once in the blood these surfactants desorbed from the CNTs with subsequent circulation of bundles and accumulation in the liver tissue. It is important to note that [^{111}In] DTPA-MWCNTs complexes used in this study were considerably longer than the dimensions of the glomerular capillary wall. Hence, the length does not appear to be a critical parameter in their renal clearance. The mechanism by which CNTs pass through the glomerular filtration system is believed to involve the acquisition of a conformation in which the longitudinal dimension of the nanotube is perpendicular to the glomerular fenestrations (cross section is between 20 and 30 nm) and small enough to allow permeation through the glomerular pores.[10] This hypothesis was later confirmed by TEM imaging, where individualized, well-dispersed MWCNTs were observed in the renal capillary lumen. During their translocation through the glomerular filtration barrier, their

longitudinal axis was shown to be vertically oriented to the endothelial fenestrations.[11] Moreover, histological examination of the different tissues confirmed that those MWCNTs complexes did not induce any physiological abnormality 24 h after the injection.[12]

The findings described above have domostrated that CNTs can be designed in many ways to form system, which allow them to enter blood circulation, target cells, deliver pay-loads, be exocytosed and finally eliminated from the body. As a nanoparticle for medical applications, the carbon nanotubes need to achieve good biodistribution and good target specificity in order to have therapeutic efficacy.
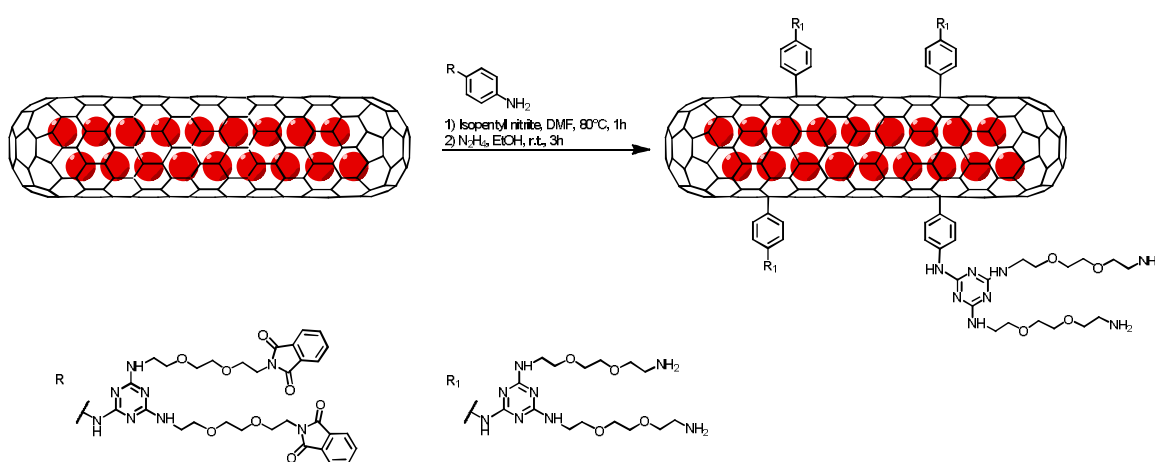
In a previous chapter, we reported functionalization on two types of CNTs encapsulated with several metal halides like NaI, $SmCl_3$, $LuCl_3$, $GaCl_3$. Filled CNTs were successfully functionalized by covalent bounding with solubilizing linkers. In all steps of processing the leakage of the internal cavities was not observed.

In this chapter we showed the interactions between functionalized $SmCl_3$@CNTs and *in vitro* cellular models in order to understand their potential mechanisms of toxicity.

We also used isotope of ^{153}Sm encapsulated in functionalized MWCNTs to follow exposure via tail vein injection, to discuss their biodistribution as models for imaging and theranostic application.

IV.2 Results of *in vitro* study

The aim of this study was to assess the cytotoxicity of functionalized SmCl₃@CNTs. Two types of nanotubes (SmCl₃@SWCNTs and SmCl₃@MWCNTs) were covalently functionalized by the Tour reaction. The reaction was performed through *in situ* generation of diazonium salt from aniline precursors on the linker **P12** (as reported in chapter III) Scheme 1. The linker was designed to provide solubility to the system, and create a flexible platform for an eventual further binding of targeting molecules.

Scheme 1. Functionalization of SmCl₃@CNTs with the linker.

All samples used in this work were presented and characterized in previous chapter. Raman spectroscopy and thermogravimetric analysis proved high degree of functionalization on the surface of the tube. The degree of functionalization for SmCl₃@SWCNTs was 220 µmol g^{-1} and 90 µmol g^{-1} for SmCl₃@MWCNTs.

The solubilizing functionalities on covalently modified SmCl₃@SWCNTs (SmCl₃@SWCNTs-NH₂) and SmCl₃@MWCNTs (SmCl₃@MWCNTs-NH₂) were resulting in stable suspension in water without the use of surfactants. However, to assess the toxicity, the water suspensions of functionalized SmCl₃@CNTs were compared to the functionalized samples and pristine SmCl₃@CNTs in 1%

solution of Pluronic F127. It is known that CNTs in 1% Pluronic F127 results in non toxic, individualized suspended nanotubes.[13]

The uptake was determined by optical microscopy and then correlated with the cytotoxicity results obtained by the modified LDH assay. Cells were incubated with 10, 50 and 100 µg mL^{-1} for 24 h and 72 h. 10% DMSO was used as positive control in order to test potential cytotoxicity.[14] So the cytotoxicity of the CNTs before and after functionalization (in water or Pluronic suspension) was determined for two cell lines as reported in Figure 2.

In the case of J774, cells exhibited the dose-depended cytotoxic response, lower for covalently functionalized SmCl$_3$@CNTs than for non-functionalized CNTs dispersed in Pluronic F127. It can be observed that cells J774 were less resistant to pristine (dispersed in 1% Pluronic solution) and functionalized SmCl$_3$@MWCNTs (dispersed in water) compare to all SmCl$_3$@SWCNTs.

The explanation for this behavior could be the low uptake of small SWCNTs. Perhaps larger structures are better recognized and internalized by macrophages and therefore more capable in giving in a toxic response than the smaller structure. On theFigure 1 Figure 1 were showed the untrated J774 cells a); after incubation with functionalized SmCl$_3$@SWCNTs b) and SmCl$_3$@MWCNTs c).
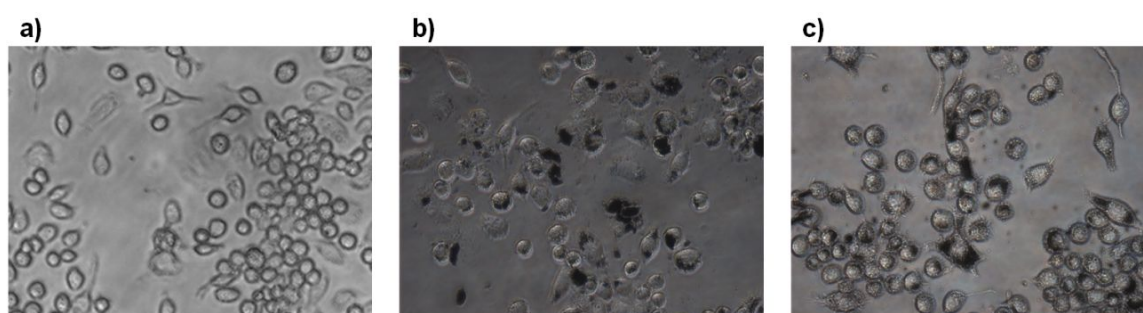

Figure 1. Images represent J774 cell line - a) untreated; incubated for 24 h with pluronic solution of 50 µg mL^{-1} of SmCl$_3$@SWCNTs-NH$_2$ b) and SmCl$_3$@MWCNTs-NH$_2$ c). Images were captured at 40×magnification.
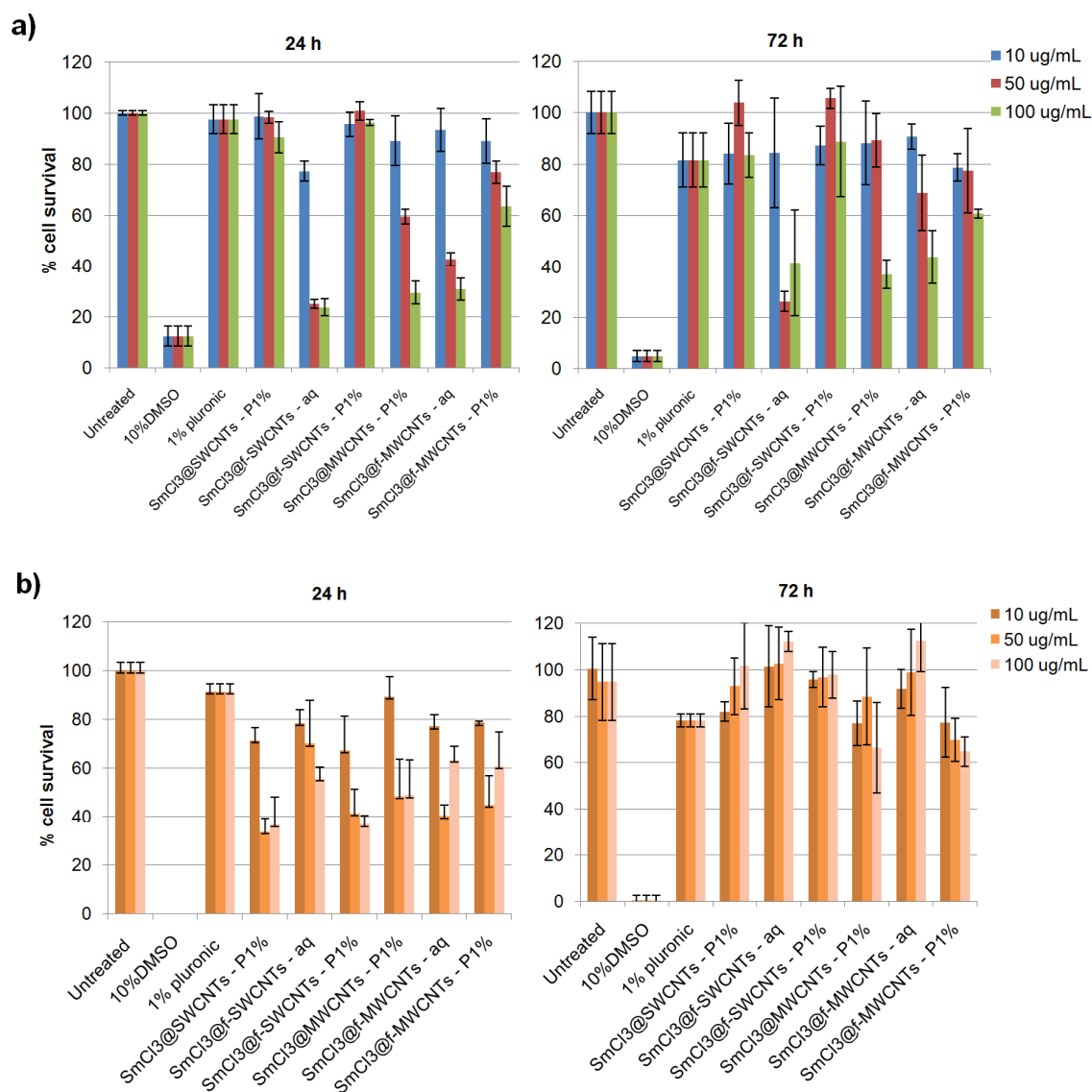
Figure 2. Cytotoxicity of pristine and functionalized SmCl₃@CNTs on two cell lines. a) J774; b) B16F10.

The cytotoxicity study of SmCl$_3$@CNTs on B16F10 cells were shown in Figure 2b. The cell viability remained above 60% even at higher concentrations (100 μg mL^{-1}). This result indicated that SmCl$_3$@CNTs-NH$_2$ had moderate toxicity to B16F10 cells after 24 h incubation. In both cell lines exposure to a 1% Pluronic F127 solution control exhibited only a 10% decrease in viability.

Results obtained in this work demonstrated that functionalization methodology of introducing solubilizing linker with the free amine groups onto CNTs filled with SmCl$_3$ was highly effective to increasing the survival compare to

pristine, non-functionalized SmCl$_3$@CNTs. The linker, successfully introduced on SmCl$_3$@SWCNTs and SmCl$_3$@MWCNTs provide the best-possible dispersion of the system. The high effective dose for to the *in vitro* system was showed without causing reduced viability.

IV.3 Results of *in vivo* study

Applications of carbon nanotubes (CNTs), as a vehicle for radioisotopes was proposed recently, and great progress has been achieved in *in vitro* studies.[15] However, the use of this material in animals and humans are strongly limited, because the knowledge about their behavior *in vivo* still needs to be explored.

Most of the studies so far were carried out by using radioisotopes, including ^{125}I, ^{111}In, ^{64}Cu, ^{99m}Tc and ^{14}C. Indubitably, radioisotope tracing is an effective and indispensable technique to study the *in vivo* absorption, distribution, metabolism, excretion and toxicity of foreign material. Here we reported the biodistribution study of functionalized MWCNTs filled with $^{152}SmCl_3$ and irradiated to isotope of samarium ^{153}Sm as a model of radioisotope with application to radiotherapy ($^{153}SmCl_3$@MWCNTs-NH$_2$).[16] The radioactive $^{153}SmCl_3$@MWCNTs were obtained in reactor in Saclay. The half-life of ^{153}Sm is 46.3 hours. It emits both medium-energy beta particles and a gamma photon.

The sample of multi-walled CNTs filled with $^{153}SmCl_3$ ($^{153}SmCl_3$@MWCNTs) with radioactivity of 1GBq was diluted to final activity 100MBq with the MWCNTs already filled with isotope enrich with $^{152}SmCl_3$. Then, the same protocol of functionalization (chapter III, experimental part for SmCl$_3$@CNTs functionalization) was used to attach the solubilizing linker **P12**. The ready $^{153}SmCl_3$@MWCNTs-NH$_2$ were re-suspended in 1% Pluronic F127 solution for injection to mice. 250µL of $^{153}SmCl_3$@MWCNTs-NH$_2$ with the final activity of 1 MBq/mouse were injected intravenously in mice via the tail vein.

To obtain the excretion profile major organs including skin, liver, spleen, heart, lung, muscle, bone, brain, stomach and intestine were recovered post mortem at 1, 4 and 24 h after injection of $^{153}SmCl_3$@MWCNTs-NH$_2$. Tissues were weighed and the radioactivity was measured by γ-scintigraphy (Figure 3).
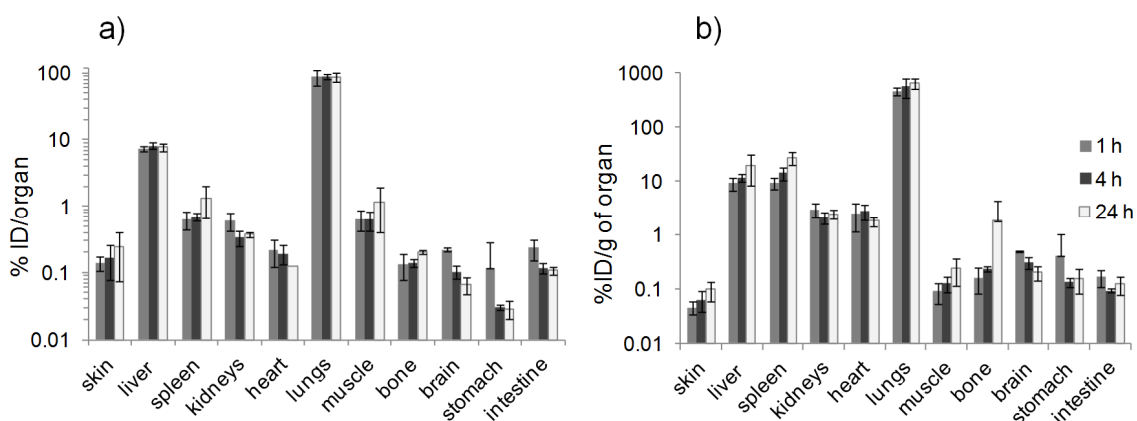
Figure 3. Organ biodistribution of SmCl₃@MWCNTs-NH₂ in C57/Bl6 mice. Radioactivity was measured in selected major organs by γ-scintigraphy at each time point. Data are presented in a) % ID/organ and b) % ID/g of organ of as mean ± S.D.

Biodistribution graphs (Figure 3) presented the values from every each organ indicated high affinity to lung for up to 24 hours almost 100 %ID/organ while 10% ID/ organ and 1.2% ID/ organ go to the liver and spleen respectively and less than 1% to the other organs, i.e. brain, stomach, muscle, bone and intestine.

Low radioactivity (c.a. 4% ID/ g of organ of ^{153}SmCl₃@MWCNTs-NH₂) was detected in blood after injection with complete clearance after one hour (Figure 4a). The absence of isotope in blood and faeces (Figure 4b) after 24h could be attributed to the no-leakage of the radioisotope from the tubes and to their high affinity to the organs.

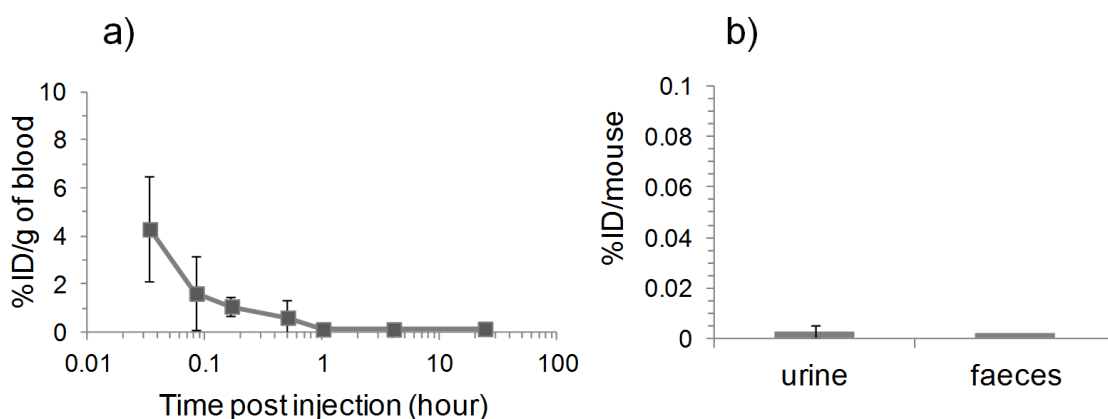**Figure 4. a) Blood clearance profile of SmCl₃@MWCNTs-NH₂; b) Profile of elimination of SmCl₃@MWCNTs-NH₂ to urine and faeces were in C57/Bl6 mice. Samples were collected after 24 h post-administration followed by γ-scintigraphy. The values are presented as mean ± S.D.**

138

The similar results for biodistribution of MWCNTs with free amino groups were found in the work of Wang et al. where investigated the biodistribution profile of functionalized MWCNTs with two different size and diameter.[17] In that work the biodistribution studies were evaluated for tubes functionalized with 1,3-dipolar cycloaddition, with the chain terminated with free amino groups and then bounded to an antibody. However, it can be assumed that free amine groups, present on the surface of MWCNTs could affect interaction with biological membranes. Also the diameter can be the main factor that impacts organ biodistribution *in vivo*.

IV.4 Conclusions

In concussions, SWCNTs and MWCNTs were functionalized by endohedral and exohedral method and used as a model for radioactivity delivery. No significant reduction of viability was observed in *in vitro* tests, for two different cell lines at different compounds concentration: 10, 50 and 100 µg mL^{-1}.

Then, we have developed a convenient and general method to use ^{153}Sm inside the MWCNTs for *in vivo* biodistribution study. Among the radioisotopes used in the tracing studies, samarium is the most convenient and it can be sealed in MWCNTs easily and directly irradiated to samarium-153 (^{153}Sm). It emits beta particles what makes it highly therapeutic component and the gamma rays for straightforward tracing.

By molten phase high temperature method, MWCNTs were filled with metal halide (SmCl$_3$). The larger diameter of MWCNTs allowed us to increase the yield of filling respect to already reported work on SWCNTs.[1] Thanks to this fact, the final specific activity of the irradiated system reached almost 1 GBq. After fast functionalization via alternative aryl diazonium chemistry (1 hour of reaction suitable for half-life time of isotope ^{153}Sm) an adequate level of functionalization was achieved. In spite of the modification of the sp^2 carbon network of SmCl$_3$@CNTs by the covalent attachment of the aniline modified with triazine derivative, the internal part of the tubes was intact and the leakage of the internal material was not observed after the functionalization or during the biological study.

Our results suggest that the application of diazonium based arylation of filled MWCNTs can be generally adoptable as an efficient and convenient technique for functionalization, without breaking and opening the tubes. The functionalized nanocapsules filled with ^{153}Sm can be in this way, *in vivo* delivery for long-term tracing studies.

IV.5 Experimental Part

IV.5.1 Preparation of samarium filled CNTs (SmCl₃@CNTs) was described in Chapter III

IV.5.2 Preparation of radioactive ^{153}SmCl₃@MWCNTs

For encapsulation of samarium chloride, previously purified MWCNTs were mixed with enrich 152-samarium (III) chloride (w/w 1:10 respectively) and grinded with an agate mortar and pestle inside a glovebox until the mixture presented a homogeneous color. The resulting mixture was then vacuum sealed inside a silica ampoule and annealed at 900 °C for 12 h. After cooling down the sample, the silica tube was opened and the material was stirred in water at 80 °C to remove the non-encapsulated SmCl₃. The filling yield of SmCl₃@MWCNTs was 19.5 wt%.

Then the radioactive ^{152}SmCl₃@MWCNTs was irradiated in reactor in Saclay and provided as ^{153}SmCl₃@MWCNTs in a solution of DMF with final activity of 1 GBq.

IV.5.3 Functionalization of SmCl₃@CNTs for *in vitro* study was the same as in Chapter III for filled nanotubes.

IV.5.4 Functionalization of ^{153}SmCl₃@MWCNTs

6 mg of ^{152}SmCl₃@MWCNTs in 4 mL of DMF were dispersed by sonication for 10 min. Then the 100 µL of ^{153}SmCl₃@MWCNTs dispersion in DMF, with the activity 100 MBq, were injected. Then the **P12** was added in excess (25 times in weight) with respect to CNTs in 2 mL of DMF, dispersed for another 5 min and cooled to 0°C. Isopentyl nitrite (5 fold molar excess with respect to amine) was added and reaction mixture was heated up to 80 °C and stirred was continued for one hours. Then the mixture was cooled to room temperature. The CNTs were filtered (membrane MILIPORE, type: JHWP, pore size 0.1 µm) and washed

with DMF until the solvent eluted colorless, washed with DMF, water, MeOH, EtOAc, Et_2O and dried to afford $^{153}SmCl_3$@MWNTs-Pht.

Deprotection of -NPht

For the deprotection, $^{153}SmCl_3$@MWNTs-Pht (6 mg) were dispersed in EtOH (6 mL) by sonicating for 5 min, and afterwards treated with hydrazine hydrate (1 mL). The dispersion was stirred at r.t. for 3 h, and then diluted with EtOH (50 mL) and filtered. After filtration, the functionalized $SmCl_3$@MWCNTs-NH_2 were re-precipitated in EtOH, filtered (membrane MILIPORE, type: JHWP, pore size 0.45 μm), washed with 0.1 M HCl solution, water, MeOH, diethyl ether finally dried under vacuum to afford functionalized $SmCl_3$@MWCNTs ($SmCl_3$@MWCNTs-NH_2).

IV.5.5 Cell toxicity assays

Reagents

RPMI-1640 media, fetal bovine serum (FBS), penicillin/streptomycin, Trypsin/EDTA, and phosphate buffered saline (PBS) were obtained from Gibco, Invitrogen (UK). Cytotoxicity assay (LDH kit) was purchased from Promega UK Ltd. B16F10 melanoma cells were cultivated in DMEM supplemented with 10% fetal bovine serum, 100 IU/mL penicillin, and100 μg/mL streptomycin at 37 °C in 20% CO_2 atmosphere. Culture of J774 macrophage cells were cultivated in DMEM-HG supplemented with 10% heat-inactivated bovine fetal serum, 100 IU/mL of penicillin, 100 μm/mL of streptomycin, and 2 mM L-glutamine at 37° C in 20% CO_2.

Cell culture

Cells were seeded at a density of 8000 cells per well in flat-bottomed 96-well plates and left to adhere overnight at 37° C and 20% CO_2. Cells were then

treated with the CNTs dispersed in 1% of Pluronic F127 and or in water for 24 h and 72 h. Dispersions were diluted in complete media at three concentrations: 10, 50, 100 µg/mL. Healthy control cells were incubated with complete media while positive controls were treated with 10% DMSO.

$$\%\text{Cell Survival} = \frac{A_{490nm} \text{ of treated cells}}{A_{490nm} \text{ of untreated cells}} \times 100$$

IV.5.6 Biodistribution study of ^{153}SmCl$_3$@MWCNTs-NH$_2$ in mice by gamma scintigraphy

Tissue biodistribution of SmCl$_3$@MWCNTs-NH$_2$ in mice was performed by gamma scintigraphy. All *in vivo* experiments were conducted under the authority of project and personal licences granted by the UK Home Office and the UKCCCR Guidelines (1998). The blood circulation and the excretion profiles of radio-labeled SmCl$_3$@MWCNTs-NH$_2$, as well as the biodistribution in major organs were carried out using normal C57/Bl6 mice. The ^{153}SmCl$_3$@MWCNTs-NH$_2$ were centrifuged and re-suspended in 1% Pluronic F127 solution for injection. Mice were injected intravenously via the tail vein with 250µL of 0.5 mg mL^{-1} solution of ^{153}SmCl$_3$@MWCNTs-NH$_2$ presenting the final activity of 1 MBq/mouse. To obtain the excretion profile, mice were housed singly in metabolic cages in which animals had free access to water and food. After 24 h, urine and faeces were collected from individual cages and counted by γ-scintigraphy. For tissue biodistribution study, blood samples were collected in heparinised capillaries from 4 min up to 24 h after injection and counted by γ-scintigraphy (LKB Wallac 1282 Compugamma, PerkinElmer). Then the animal was flushed with 10 mL of normal saline via the heart to clear any blood remaining in the organs. Major organs including skin, liver, spleen, heart, lung, muscle, bone, brain, stomach and intestine were obtained post mortem at 1, 4 and 24 h after injection of ^{153}SmCl$_3$@MWCNTs-NH$_2$. Tissues were weighed and

the radioactivity was measured by γ-scintigraphy. The percentage injected dose per gram of tissue was calculated for each organ. Four animals were used for each time point for every compound.

Bibliography

[1] L. Zhang, F. X. Gu, J. M. Chan, A. Z. Wang, R. S. Langer, O. C. Farokhzad; *Clin. Pharmacol. Ther.* **2008**, *83*, 761–769.

[2] Hua He, L. Ai Pham-Huy, P. Dramou, D. Xiao, P. Zuo, C. Pham-Huy; *Biomed. Res. Int.* **2013**, 578290–578302.

[3] G. Seeta Rama Raju, L. Benton, E. Pavitraa, J. S. Yu; *Chem. Commun.* **2015**, *51*, 13248–13259.

[4] Z. Liu, S. Tabakman, K. Welsher, H. Dai; *Nano Research* **2009**, *2*, 85-120.

[5] N. Kotagiri, J.-W. Kim; *International Journal of Nanomedicine* **2014**, *9*, 85–105.

[6] S. M. Moghimi, A. C. Hunter, J. C. Murray; *Pharmacol. Rev.* **2001**, *53*, 283–318.

[7] M. Ferrari; *Nat. Rev. Cancer* **2005**, *5*, 161–171.

[8] H. Wang, J. Wang, X. Deng, H. Sun, Z. Shi, Z. Gu, Y. Liu, Y. Zhaoc; *J. Nanosci. Nanotechnol.* **2004**, *4*, 1019–1024.

[9] R. Singh. *Proc. Natl. Acad. Sci. USA* **2006**, *103*, 3357–3362.

[10] L. Lacerda, et al.; *Adv. Mater.* **2008**, *20*, 225–230.

[11] L. Lacerda, M. A. Herrero, K. Venner, A. Bianco, M. Prato, K. Kostarelos; *Small* **2008**, *4*, 1130–1132.

[12] L. Lacerda, H. Ali-Boucetta, M. A. Herrero, G. Pastorin, A. Bianco, M. Prato, K. Kostarelos; *Nanomedicine* **2008**, *3*, 149–161.

[13] M. S. Strano, V. Moore, M. K. Miller, M. J. Allen, E. H. Haroz, C. Kittrell, R. H.Hauge; Smalley, R. E.; *J. Nanosci. Nanotechnol.* **2003**, 3, 81–86.

[14] H. Ali-Boucetta, K. T. Al-Jamal, K. H. Müller, S. Li, A. E. Porter, A. Eddaoudi, M. Prato, A. Bianco, K. Kostarelos; *Small* **2011**, *7*, 3230–3238.

[15] C. Spinato, A. P. Ruiz de Garibay, M. Kierkowicz, E. Pach, M. Martincic, R. Klippstein, M. Bourgognon, J. Tzu-Wen Wang, C. Ménard-Moyon, K. T. Al-Jamal, B. Ballesteros, G. Tobias, A. Bianco; *Nanoscale* **2016**, Doi:10.1039/C5NR07923C.

[16] M. K. Bakht, M. Sadeghi, M. Pourbaghi-Masouleh, C. Tenreiro; *Current Cancer Drug Targets*, **2012**, *12*, 998–1015.

[17] J. T.-W. Wang, C. Fabbro, E. Venturelli, C. Ménard-Moyon, O. Chaloin, T. Da Ros, L. Methven, A. Nunes, J. K. Sosabowski, S. J. Mather, M. K. Robinson, J. Amadou, M. Prato, A. Bianco, K. Kostarelos, K. T. Al-Jamal; *Biomaterials* **2014**, *35*, 9517–9528.

V. Appendix

V.1 Chemicals and Solvents

Chemicals were purchased from, Aldrich, Acros, Alfa Aesar and used as received. Solvents were purchased from Aldrich, Acros, and Alfa Aesar. Deuterated solvents from Aldrich and Cambridge Isotope Laboratories. All solvents used for synthesis were analytical grade. When anhydrous conditions were required, high quality commercial solvents were used (THF, DCM, o-DCB, toluene, DMF). Water was purified using a Millipore filter system MilliQ®.

V.2 Characterization Methods and Instrumentation

Nuclear magnetic resonance spectroscopy (NMR) - NMR spectra were recorded on a Bruker 400 or on a Varian 500 spectrometer (500 MHz for 1H, 125 MHz for ^{13}C). All the spectra were run at ambient temperature and chemical shifts were reported in ppm according to tetramethylsilane using as internal reference. Deuterated solvents (d-chlorophorm: δ_H = 7.26 ppm, δ_C = 77.16 ppm; d-methanol: δ_H = 3.31). Resonance multiplicity was described as s (singlet), d (doublet), t (triplet), m (multiplet) and br (broad signal).

Thermogravimetric analysis (TGA) - All TGAs were performed using Q500 (TA Instruments) to record TGA analysis under N_2 and air, by equilibrating from room temperature to 100°C, and following a thermal ramp 10 °C/min up to 800 °C with a flow rate of 90 mL/min. The loss of weight was extracted as a difference by the weight % and evaluated at the plateau of the curve for each derivative. About 0.7 mg of sample per each analysis was required. Reported graphs are an average of at least two separate measurements.

Determination of the filling yield:

The filling yield (FY) was calculated consider the amount of TGA residues in air: from empty nanotubes (R_1), clean filled nanotubes (R_2) and bulk material (R_A):

$$FY \text{ (wt\%)} = \frac{100 \cdot (R_2 - R_1)}{R_A - R_1} \quad (1)$$

R_A was calculated basing on stoichiometry of the oxidative reaction which was taking place during TGA analysis. Where M_A and M_B are molecular weights of A and B; x and y are stoichiometric coefficients of reaction. Thus residue was calculated according to following formula (2):

$$R_A = \frac{100 \cdot y \cdot MW_B}{x \cdot MW_A} \quad (2)$$

High Resolution Transmission Electron Microscopy (HRTEM) - TEM analyses were performed on Hitachi H7500 microscope (Tokyo, Japan) with an accelerating voltage of 80 kV, equipped with an AMT Hamamatsu camera (Tokyo, Japan). HAADF-STEM images were acquired at 20 kV on a FEI Magellan XHR 400L SEM equipped with a dedicated STEM detector. HRTEM micrographs and EDX spectra were acquired on a FEI Tecnai G2 F20 operated at 200 kV and equipped with an EDAX super ultra-thin window (SUTW) X-ray detector. Samples were dispersed in ethanol and deposited on lacey carbon Cu TEM grids (Agar).

Thin Layer Chromatography (TLC) - was conducted on pre-coated aluminium plateswith 0.25 mm *Macherey-Nagel* silica gel with fluorescent indicator UV254.

Column Chromatography - Chromatographic purifications were carried out with silicagel (Merck Kieselgel 60 - 200 mesh ASTM).

Infrared spectra (IR) were recorded on Varian 660-R, FT-IR spectrometer using KBrplates or on a Perkin Elmer Spectrum One ATR-FT-IR spectrometer.

Mass spectra Both ESI and MALDI HR were performed on a Waters Synapt G2-Si

UV-VIS-NIR spectroscopy - Spectra were recorded on Cary 5000 spectrophotometer (Varian) using 1 cm path quartz cuvettes.

Microwave - Microwave assisted reactions were carried out in a CEM Discover.

Kaiser test - Kaiser test (Kaiser test kit, Sigma Aldrich) was performed to determine the degree of amine groups on the synthesized CNTs constructs. In a typical test, 0.3-0.5 mg of CNTs were dispersed in a mixture of phenol (75 μL, 80% in ethanol) and KCN (100 μL in H_2O/pyridine) solution and sonicated for 2 min in an ultrasonic bath. Subsequently, 75 μL of ninhydrin solution (6% in ethanol) were added, and the mixture was heated at 120 °C for 10 min. It was then cooled and diluted with 60% ethanol in water to a final volume of 3 mL. After centrifugation (3000 rpm, 10 min), the absorption spectrum of the supernatant was measured, using as blank a solution obtained in the same way but without CNTs. The absorbance maximum at 570 nm was used to calculate the amine loading in the CNTs samples (molar extinction coefficient ε=15000 $M^{-1} cm^{-1}$). Reported values are an average of at least two separated measurements.

$$\frac{\mu mol}{g} = \frac{[Abs_{sample}\text{-}Abs_{blanc}]\cdot dilution\ (mL)\cdot 10^6}{\varepsilon \cdot sample\ weight\ (mg)}$$